Experimental and CFD Analyses of Cuttings Transport in Horizontal Annuli and A Study on Isotropic Rocks for Strength Correlations

By

© Golam Rasul

A Thesis submitted to the School of Graduate Studies
In partial fulfillment of the requirements for the degree of

Master of Engineering

Department of Process Engineering
Faculty of Engineering and Applied Science
Memorial University of Newfoundland

October 2021

St. John's Newfoundland

Abstract

The research activities performed in this study focused on the cuttings transport process in horizontal annuli that represents the horizontal drilling phenomenon. Both experimental and numerical approaches have been adopted to investigate the efficient hole cleaning process. Numerous flow conditions were examined in laboratory conditions and the subsequent visualization was performed with the help of a high-speed camera. The effects of drilling parameters such as drill pipe's rotational speed (RPM), eccentricity and flow rate were scrutinized throughout the experimental and computational fluid dynamics (CFD) analyses. The common findings indicate enhanced hole cleaning ability at increased RPM and eccentricity. On the other hand, an increasing trend for pressure drop across the annulus section is identified with the enhanced drill pipe's rotation (RPM), eccentricity and flow rate. The last part of this study examined tensile and shear fracture examination to find out different strengths of isotropic rock samples and establish strength correlations among them. This study will contribute to an ongoing investigation to predict cuttings size distribution from rock formation properties and drilling parameters. Unconfined compressive strength and indirect tensile strength (UCS-ITS) and unconfined compressive strength and point load strength index (UCS-PLSI) correlations were developed. Additionally, the ultrasonic pulse wave measurement was performed to establish the unconfined compressive strength and primary wave velocity (UCS-V_P) relationships for sandstone and medium strength rock like material (RLM). Ultimately, all fitted relationships were analyzed through a comparative study with published correlations. This study on isotropic rocks is a part of an investigation to predict cuttings size distribution and future research will take the lead from this current thesis.

Acknowledgement

First, I would like to take the opportunity to thank my supervisor, Dr. Stephen Butt and co-supervisor, Dr. Aziz Rahman for accepting me as a graduate student. Dr. Stephen Butt not only supervised my research work but also taught me the basic drilling and rock mechanics concepts, which were new to me since my background was in Mechanical Engineering. Dr. Aziz Rahman introduced me to the wonderful experimental environment at Texas A&M University at Qatar and gave me the complete freedom to work in his laboratory. Moreover, their thoughtful suggestions helped me to improve my analytical thinking and technical writing skill. It is my pleasure to express the deepest gratitude to them for their continuous support and guidance during my whole course and research work.

I am also grateful to the research groups that I worked with at the Memorial University of Newfoundland (MUN) and Texas A&M University at Qatar (TAMUQ). I also acknowledge the high-performance computing support provided by Compute Canada and Memorial University.

Moreover, I appreciate the financial support that I received from the funding sources through my supervisor and co-supervisor.

I would also love to thank my family members, who continuously supported me and encouraged me throughout this journey. My heartfelt gratitude to my beloved father, who always inspired me despite his illness and last but not least, I dedicate this work to the departed soul of my dear mother.

Contents

List of Tables

List of Figures

Abbreviations and Symbols

e	Eccentricity
P_g	Gas pressure, Pa
DP	Drill pipe
C_w	Solid concentration
R_e	Reynolds number
V_{SL}	Liquid superficial velocity, m/s
V_{SG}	Gas superficial velocity, m/s
g	Gravitational acceleration, m/s^2
D_H	Hydraulic diameter, m
ρ_L	Liquid density, kg/m^3
ρ_G	Gas density, kg/m^3
CFD	Computational Fluid Dynamics
ID	Inner Diameter, m
OD	Outer Diameter, m
ROP	Rate of Penetration
RPM	Revolution Per Minute
v	Velocity, m/s
α	Volume fraction
μ	Dynamic viscosity, Pa.s
ρ	Density, kg/m^3
ω	Angular velocity, rad/s

Chapter 1. Introduction

1.1. Background

The most important function of the drilling fluid is to transport cuttings from the drill bit zone through the annulus to the surface facility. The inefficiency of this procedure causes drilling problems and depending on the amount and position of cuttings accumulation; the intensity may vary from stuck pipe issue to the lost circulation. Since the beginning of the 1980s, the experimental analysis of cuttings transport for deviated wellbores has been studied, which signifies various hole cleaning mechanisms. Findings argue that the high fluid flow rate is desired but hard to maintain through the annulus because of the limitation of pump capacity and high dynamic pressure. This fact becomes more evident for high-angle or horizontal drilling and so the effect of rotational speed comes into play when such a high flow rate cannot be achieved [1].

After a certain period, around the mid-1980s, a basic understanding of cuttings transport in highly inclined wellbores was developed through experimental analyses. However, the requirement of new experimental data was also soaring up because of increasing demand in horizontal wells with longer lateral reaches. Therefore, in partnership with several companies, The University of Tulsa Drilling Research Projects (TUDRP) constructed a longer flow loop consisting of a 100-ft long and 8-inch diameter annulus test section. Similarly, new flow loops at British Petroleum, Heriot-Watt U., Southwest Research, etc., were constructed with transparent annular sections to observe cuttings movement mechanism through the annuli. These newly developed flow loops were helpful to collect the required experimental data for cuttings transport at different drilling conditions [1]. Newly developed flow loops performed hundreds of tests at critical and subcritical flow conditions considering different drilling parameters. From these analyses, the critical fluid velocity concept was developed below which the cuttings start to accumulate in a bed. Moreover, the hole cleaning data indicated that the impact of the drill pipe's rotation depends on the cuttings' size and the mud rheology. The rotational impact was reported more effective on smaller cuttings with viscous fluid [2]. The complete study on hole cleaning in inclined wellbore signified the combined effect of cuttings' size, fluid rheology, flow rate and dynamic behavior of drill pipe for enhanced cuttings removal process [3].

Moreover, the drilling hydraulics studies based on computational fluid dynamics [4], modelling [5] and experimental analysis [6] for single phase flow have been reported in a pipe geometry without considering annulus configurations, eccentricity and rotation. Additionally, wellbore hydraulics were analyzed for both single phase flow [7], [8] and two phase flow [9]–[16] for the single tubing configuration. Literature also reports the two phase flow mechanisms in the tubing geometry [17]–[21] as well as the three phase solid-liquid-gas flow for the same configuration [22]–[24]. On the other hand, recent studies for annulus configuration have been performed considering different hydrodynamics and drilling operating conditions for two phase flow [25]–[27] and three phase flow [28]–[31]. All of these studies have performed in segregated ways, either performed experimentally or numerically. In this thesis, in the first part, we have combined both experimental and numerical studies.

On the other hand, the remaining part of the thesis deals with isotropic rock strengths and subsequent correlations establishment. The unconfined compressive strength (UCS) is required to evaluate numerous geomechanical factors that influence wellbore instability as well as sand production capability [32], [33]. However, the UCS test requires exact measurement and specimen preparation, which is a time-consuming and expensive procedure to follow. Sometimes, it is impossible to get the core specimen's desired dimension, especially in highly jointed rock masses. Therefore, the point load strength index is considered for estimating the UCS of rocks considering its simplicity and flexibility of testing specimens in both field and laboratory applications. Since the 1970s, researchers have developed several correlations between the UCS and point load index and the majority of them shows linear relationship. The correlation may vary depending on the textural, mineralogical factors as well as chemical composition and anisotropic behavior of the rocks [34].

Moreover, The UCS and indirect tensile strength correlation is helpful to determine essential rock characteristics as well. A number of studies in finding the relation between UCS and indirect tensile strength have reported linear relationships, whereas some investigations also suggested the non-linear relationships between them [35], [36].

Additionally, the dynamic measurement of rock specimen performed by ultra-sonic pulse wave velocity assessment is another method to evaluate elastic properties of rocks and develop subsequent strength correlation with primary wave velocity (V_P). Therefore, a complete analysis of rock strength and the corresponding correlations were established based on static and dynamic measurements.

In the next section the objective outlines the ultimate research goals of this current study based on the background discussed in this section.

1.2. Objectives

The purposes of this study were to find out the optimum cuttings transport process in horizontal annulus section and evaluate drilling performance for isotropic rocks through strength test of the samples. The cuttings transport analyses were divided into experimental and numerical assessments. On the other hand, the isotropic rock samples were tested in geomechanics frame for strength tests. The overall objective of this study can be articulated as follows:

- Analyzing the cuttings transport process and finding out the corresponding flow patterns at different drilling conditions based on experimental data derived from the fully instrumented flow loop system.
- Developing a CFD based model to simulate cuttings transport in horizontal annulus showing prior validation with experimental results.
- Performing several strength tests and establishing correlation among them to evaluate optimal drilling performance for isotropic rock samples.

1.3. Co-authorship Statement

This manuscript-based thesis contains four manuscripts (already published or accepted or submitted in the proceedings) in separate chapters. These manuscripts are the results of collaborative efforts from several individuals. As the first author of all manuscripts, I performed a significant portion of experimental and CFD analyses and played the lead role in writing the manuscripts. The contributions of co-authors are outlined below.

Chapter three represents a published journal article. Among the co-authors, M. Fahed Qureshi and Hicham Ferroudji were directly involved in data interpretation, especially flow regime analysis. They also contributed to the manuscript writing and revision process. The rest of the co-authors conceptualized and supervised the experimental work and provided technical feedbacks during manuscript writing.

Chapter four embodies a presented and published conference proceeding, where the co-authors helped planning the test matrix ensuring experimental facilities and supervised the experimental work. They also shared thoughtful suggestions during manuscript writing.

Chapter five is a CFD-based conference manuscript, which is already presented in the proceeding and accepted for publication. The two co-authors, M. Azizur Rahman and Stephen Butt, directly supervised the work, ensured the high-performance computing facility and shared their critical feedbacks during manuscript writing.

Chapter six represents a submitted manuscript in a conference proceeding. Among the co-authors, W. Quan and A. Abugharara were directly involved in experiments and data collection in the laboratory. The other co-authors supervised the work and participated with technical feedbacks during manuscript writing.

1.4. Thesis Organization

The thesis contains seven chapters altogether. The first chapter provides the introduction to the thesis having a proper background of the study. It also includes the objective of this research work, defining the purposes and motives. Additionally, the first chapter outlines the co-authors' contributions to prepare the manuscripts. Lastly, the outline of the thesis is discussed chapter-by-chapter in this ongoing section. The second chapter contains a comprehensive literature review, where a detailed discussion is presented with appropriate data and references. The third chapter comprises a published journal article representing an experimental work on cuttings transport and subsequent flow pattern analysis at different flow conditions. The chapter contains the schematic of the experimental facility, including a full specification of the flow loop used for the experiments. The chapter also reports the conclusive findings regarding cuttings bed height and flow patterns at different conditions. The fourth chapter of this thesis reports cuttings transport mechanism for aerated drilling. The chapter outlines the experimental facility, including testing conditions and details the findings at the end. Chapter five articulates a CFD analysis on cuttings accumulation trend in the horizontal annulus. This study reports model validation with mesh sensitivity analysis and finally illustrates the findings in charts with appropriate contours. Chapter six contains a manuscript based on isotropic rock strength analysis, where two different rock types, namely sandstone and medium strength rock-like material (RLM), are tested in a fully calibrated geomechanics frame. Chapter 6 represents a part of an investigation to predict cuttings size distribution from rock formation properties and drilling parameters; however, this work continues as future research from this thesis. Lastly, chapter seven concludes the whole thesis with an appropriate conclusion and recommends future research prospects that could be continued from the current study. In summary, the primary outcomes of the research activities can be listed as follows:

1. The experimental analysis on cuttings transport and flow pattern in nearly horizontal extended reach well is published in an article in the Journal of Advanced Research in Fluid Mechanics and Thermal Sciences in 2020. The article outlines the schematic of the experimental facility, including a detailed specification of the flow loop. The research reports the conclusive findings regarding cuttings bed height and flow patterns at different drilling conditions.
2. The experimental findings regarding aerated drilling for cuttings transport in the horizontal well are presented and published in the proceedings of 4th Thermal and Fluids Engineering Conference (TFEC) at Las Vegas, NV, USA in 2019. The results indicate the cuttings bed height variation with air injection and drill pipe rotation.
3. A CFD-based analysis of cuttings accumulation tendency at different drilling conditions is presented and accepted for publication in the proceedings of ASME 40th International Conference on Ocean, Offshore and Arctic Engineering, OMAE 2021. Confirming mesh

sensitivity and validation, the developed model indicates the impact of several drilling parameters on cuttings accumulation in the annulus.

4. To evaluate the isotropic rock strengths and establish relationships among them, an experimental study is summarized, submitted and accepted in the proceedings of 74th Canadian Geotechnical Conference, GeoNiagara 2021. Several correlations are developed along with the ultrasonic pulse wave measurement for sandstone and medium strength RLM samples. Eventually, all fitted relationships are analyzed through a comparative study with published correlations. However, this is an ongoing investigation to predict cuttings size distribution from rock formation properties and drilling parameters. The study is continuing for future research, taking the lead from this current thesis.

References

[1] Petrowiki, "Cuttings Transport," 2015. [Online]. Available: https://petrowiki.spe.org/Cuttings_transport.

[2] T. R. Sifferman and T. E. Becker, "Hole cleaning in full-scale inclined wellbores," *SPE Drill. Eng.*, 1992, doi: 10.2118/20422-PA.

[3] A. . Bassal, "Study of the Effect of Drill Pipe Rotation on Cuttings Transport in Inclined Wellbores," U. of Tulsa, Tulsa, Oklahoma, 1995.

[4] X. Xiong, M. A. Rahman, and Y. Zhang, "RANS Based Computational Fluid Dynamics Simulation of Fully Developed Turbulent Newtonian Flow in Concentric Annuli," *J. Fluids Eng. Trans. ASME*, 2016, doi: 10.1115/1.4033314.

[5] A. Amin, S. Imtiaz, A. Rahman, and F. Khan, "Nonlinear model predictive control of a Hammerstein Weiner model based experimental managed pressure drilling setup," *ISA Trans.*, 2019, doi: 10.1016/j.isatra.2018.12.008.

[6] A. Ihmoudah, M. A. Rahman, and S. D. Butt, "CFD and experimental studies of yield power-law fluids in turbulent pipe flow," in *Proceedings of the International Conference on Offshore Mechanics and Arctic Engineering - OMAE*, 2018, doi: 10.1115/OMAE2018-77996.

[7] M. A. Rahman, S. Mustafiz, M. Koksal, and M. R. Islam, "Quantifying the skin factor for estimating the completion efficiency of perforation tunnels in petroleum wells," *J. Pet. Sci. Eng.*, 2007, doi: 10.1016/j.petrol.2006.11.012.

[8] M. A. Rahman, S. Mustafiz, J. Biazar, M. Koksal, and M. R. Islam, "Investigation of a novel

perforation technique in petroleum wells-perforation by drilling," *J. Franklin Inst.*, 2007, doi: 10.1016/j.jfranklin.2006.05.001.

[9] M. Morshed, A. Amin, M. A. Rahman, and S. Imtiaz, "Experimental and computational analysis of pressure response in a multiphase flow loop," in *AIP Conference Proceedings*, 2016, doi: 10.1063/1.4958370.

[10] M. A. Rahman, J. Gomez, T. Heidrick, B. A. Fleck, and J. McMillan, "Correlations of the droplet size-velocity of the two-phase, air/liquid spray using a particle-dynamic-analyzer," in *2008 Proceedings of the ASME Fluids Engineering Division Summer Conference, FEDSM 2008*, 2009, doi: 10.1115/FEDSM2008-55330.

[11] M. A. Rahman, J. McMillan, T. Heidrick, and B. A. Fleck, "Characterizing the two-phase, air/liquid spray profile using a phase-doppler-particle-analyzer," *IOP J. Physics–conference Ser.*, no. 147, pp. 1–15.

[12] M. A. Rahman, "Scaling of Effervescent Atomization and Industrial Two-Phase Flow," University of Alberta, 2011.

[13] C. Ejim, M. Rahman, A. Amirfazli, and B. Fleck, "Scaling analysis of nozzle size on atomization in two-phase, gas-liquid nozzles. Multiphase Science and Technology," *Multiph. Sci. Technol.*, vol. 22, no. 2, pp. 133–155, 2010.

[14] M. Rahman, J. McMillan, T. Heidrick, and B. Fleck, "Horizontal two-phase flow regimes and bubble size distribution prediction using high speed image analysis," in *Proceedings of the 13th International Symposium on Flow Visualization*, 2008.

[15] M. Rahman, T. Heidrick, and B. Fleck, "A critical review of two-phase gas/liquid industrial

spray systems. International Review of Mechanical Engineering," *Int. Rev. Mech. Eng.*, pp. 110–125, 2009.

[16] M. J. Ahammad, M. A. Rahman, L. Zheng, J. M. Alam, and S. D. Butt, "Numerical investigation of two-phase fluid flow in a perforation tunnel," *J. Nat. Gas Sci. Eng.*, 2018, doi: 10.1016/j.jngse.2017.10.016.

[17] K. Manikonda, A. R. Hasan, O. Kaldirim, N. Rahmani, and M. A. Rahman, "Estimating swelling in oil-based mud due to gas kick dissolution," in *Proceedings of the International Conference on Offshore Mechanics and Arctic Engineering - OMAE*, 2020, doi: 10.1115/OMAE2020-18115.

[18] A. K. Sleiti, G. Takalkar, M. H. El-Naas, A. R. Hasan, and M. A. Rahman, "Early gas kick detection in vertical wells via transient multiphase flow modelling: A review," *Journal of Natural Gas Science and Engineering*. 2020, doi: 10.1016/j.jngse.2020.103391.

[19] K. Manikonda, A. R. Hasan, O. Kaldirim, J. J. Schubert, and M. A. Rahman, "Understanding gas kick behavior in water and oil-based drilling fluids," in *Society of Petroleum Engineers - SPE Kuwait Oil and Gas Show and Conference 2019, KOGS 2019*, 2019, doi: 10.2118/198069-ms.

[20] K. Manikonda, A. R. Hasan, A. Barooah, M. El-Naas, A. K. Sleiti, and M. A. Rahman, "A mechanistic gas kick model to simulate gas in a riser with water and synthetic-based drilling fluid," in *Society of Petroleum Engineers - Abu Dhabi International Petroleum Exhibition and Conference 2020, ADIP 2020*, 2020, doi: 10.2118/203159-ms.

[21] M. M. Huque, S. Imtiaz, A. Rahman, and M. Hossain, "Kick detection and remedial action in managed pressure drilling: a review," *SN Applied Sciences*. 2020, doi: 10.1007/s42452-

020-2962-2.

[22] R. A. Sultan, M. A. Rahman, S. Rushd, S. Zendehboudi, and V. C. Kelessidis, “Validation of CFD model of multiphase flow through pipeline and annular geometries,” *Part. Sci. Technol.*, 2019, doi: 10.1080/02726351.2018.1435594.

[23] D. Herath, F. Khan, S. Rathnayaka, and M. A. Rahman, “Probabilistic estimation of hydrate formation,” *J. Pet. Sci. Eng.*, 2015, doi: 10.1016/j.petrol.2015.08.007.

[24] M. A. Rahman, K. F. Adane, and R. S. Sanders, “An improved method for applying the lockhart-martinelli correlation to three-phase gas-liquid-solid horizontal pipeline flows,” *Can. J. Chem. Eng.*, 2013, doi: 10.1002/cjce.21843.

[25] R. A. Sultan, M. A. Rahman, S. Rushd, S. Zendehboudi, and V. C. Kelessidis, “CFD Analysis of Pressure Losses and Deposition Velocities in Horizontal Annuli,” *Int. J. Chem. Eng.*, 2019, doi: 10.1155/2019/7068989.

[26] M. M. Huque, S. Imtiaz, S. Zendehboudi, S. Butt, M. A. Rahman, and P. Maheshwari, “Experimental study of cuttings transport with non-Newtonian fluid in an inclined well using visualization and ERT techniques,” in *Proceedings - SPE Annual Technical Conference and Exhibition*, 2020, doi: 10.2118/201709-MS.

[27] H. Ferroudji, A. Hadjadj, T. N. Ofei, and M. A. Rahman, “The effect of orbital motion and eccentricity of drill pipe on pressure gradient in eccentric annulus flow with Newtonian and non-Newtonian fluids,” *Prog. Comput. Fluid Dyn.*, vol. 20, no. 4, pp. 238–247, 2020, doi: 10.1504/PCFD.2020.108520.

[28] M. F. Qureshi *et al.*, “Measuring solid cuttings transport in Newtonian fluid across

horizontal annulus using electrical resistance tomography (ERT)," *Flow Meas. Instrum.*, vol. 77, no. October 2019, 2021.

[29] A. A. Zahid, S. R. ur Rehman, S. Rushd, A. Hasan, and M. A. Rahman, "Experimental investigation of multiphase flow behavior in drilling annuli using high speed visualization technique," *Front. Energy*, 2020, doi: 10.1007/s11708-018-0582-y.

[30] S. R. Ur Rehman, A. A. Zahid, A. Hasan, I. Hassan, M. A. Rahman, and S. Rushd, "Experimental investigation of volume fraction in an annulus using electrical resistance tomography," in *SPE Journal*, 2019, doi: 10.2118/194211-PA.

[31] M. F. Qureshi, M. Ali, M. A. Rahman, I. Hassan, G. Rasul, and R. Hassan, "Experimental Investigation of Multi-Phase Flow in an Annulus Using Electric Resistance Tomography," 2019, doi: 10.2118/198011-ms.

[32] D. Moos, P. Peska, T. Finkbeiner, and M. Zoback, "Comprehensive wellbore stability analysis utilizing Quantitative Risk Assessment," *J. Pet. Sci. Eng.*, 2003, doi: 10.1016/S0920-4105(03)00024-X.

[33] F. J. Santarelli, J. L. Dctienne, and J. P. Zundel, "Determination of the mechanical properties of deep reservoir sandstones to assess the likelyhood of sand production," in *ISRM International Symposium, IS 1989*, 1990, doi: 10.1016/0148-9062(90)91096-p.

[34] T. N. Singh, A. Kainthola, and A. Venkatesh, "Correlation between point load index and uniaxial compressive strength for different rock types," *Rock Mech. Rock Eng.*, 2012, doi: 10.1007/s00603-011-0192-z.

[35] R. Nazir, E. Momeni, D. J. Armaghani, and M. F. M. Amin, "Correlation between

unconfined compressive strength and indirect tensile strength of limestone rock samples," *Electron. J. Geotech. Eng.*, 2013.

[36] R. Altindag and A. Guney, "Predicting the relationships between brittleness and mechanical properties (UCS, TS and SH) of rocks," *Sci. Res. Essays*, 2010.

Chapter 2. Literature Review

2.1. Cuttings Transport in Horizontal Annulus

Cuttings bed tends to form in the annulus as the inclination angle increases more than 35^0 and as the wellbore deviates towards horizontal from the vertical position, the problem gets intensified with increasing eccentricity at the bottom part of the annulus [1]. The investigation on mud rheology for cuttings transport indicates that the high-viscosity mud could be beneficial for vertical well drilling; however, it has the opposite impact on high-angle wellbores if the drill string's rotation is negligible. The study opines that the low-viscosity mud can accelerate turbulence, which is more advantageous to cuttings transport in directional drilling [2]. Therefore, the dependency of cuttings transport on inclination angle, fluid rheology, hydraulics and eccentricity was evidently confirmed.

However, further studies developed several cuttings transport models for highly inclined wellbores. Based on their laboratory investigations and field experiments, Zamora and Hanson proposed 28 rules of thump for improved cuttings transport process at high-inclination drilling [3]. On the other hand, Luo and Bern developed empirical charts based on their flow loop data to predict critical flow rate that will not allow cuttings bed formation in the deviated well. They further extended their study by comparing the prediction with field data [4].

However, the previous discussion referred to the empirical models developed based on laboratory or field data. Therefore, a comprehensive mechanistic cuttings transport model was required to be developed that could be verified with experimental data afterward. In that regard, a two-phase (fluid-solid) interaction model that would be coupled and combined with a fluid flow model to simulate the complete cuttings transport technique was required. Considering this requirement, a numerical model was proposed based on the field and laboratory data set [5]. A further study reported cuttings transport model based on fluid mechanics relationship, where three different transport modes: rolling, lifting and settling, were assumed and each of them was considered for a specific range of hole angle [6]. Moreover, the predicted model was compared with experimental data derived from the university of Tulsa drilling research projects (TUDRP) flow loop. Another mechanistic model was developed to predict cuttings bed height and critical flow velocity at subcritical flow conditions [7]. Eventually, a solid foundation on the cuttings transport process was laid based on the combined analysis of empirical and mechanistic models. The below table has summarized some existing literatures on the discussed models.

Table 2.1. Cuttings transport models with considered parameters and targets of the analyses.

Model Type	**Authors**	**Considered Factors**	**Target**
Empirical	Wang et al. [8]	Flow rate, cuttings injection rate, mud rheology, eccentricity, pipe rotation.	cuttings bed height
	Ozbayoglu et al. [9]	Flow rate, ROP, annuli size, inclination, mud rheology, pipe rotation, eccentricity	cuttings bed area
	Loureiro et al. [10]	Annuli size, cuttings density, local gravity, mud rheology, rotational speed	ratio between mass of suspended particles

			and initial mass of deposited cuttings
	Ozbayoglu et al. [11]	Flow rate, ROP, annuli size, inclination, mud density and rheology	cuttings bed area
Mechanistic	Duan et al. [12]	Static force, drag force, lift force and Van der Waals force	Critical resuspension velocity
	Larsen et al. [13]	Mass generated by drill bit transported by mud	critical transport fluid velocity
	Peden et al. [14]	Drag force, friction force, gravity force and lift force	minimum transport velocity
	Clark and Bickham [6]	Buoyancy force, the plastic force, gravity force, lift force, drag force and pressure force	minimum transport velocity

2.1.1. Multiphase Flow Mechanism in the Horizontal Annulus

The multiphase flow confronted during the drilling operations could be the combination of three phases, including solid, liquid and gas [15]. The presence of such multiphase flow is a hard nut to crack for the petroleum industry, since the different phases constitute with different phase behaviors that are extremely complex to understand [16]. Moreover, these factors make it hard to predict the relationships among the flow rate, pipe configuration and pressure drop for multiphase flow formed in offshore fields and onshore processing facilities [17]. Hence, the study of cuttings transport is important to understand this complicated mechanism to ensure proper cleaning of the annulus section. Because cuttings accumulation may cause several issues, including lost circulation, differential sticking, flow impediments and eventually leads to inefficient hole cleaning [18].

In solid-liquid two phase flow, the traveling particles influence the adjacent fluid to manifest several flow patterns [19]. When the flow velocity ranges between moderate to low, the stationary bed is formed and the corresponding liquid phase flows over the bed leaving it at the bottom of the annulus. If the flow rate increases the stationary bed tends to disintegrate into moving dunes and the further enhancement of flow velocity causes the scouring effect in the annulus [20]. In the meantime, few particles are found to travel over the dunes, while most of them gather at the bottom of the dune. However, the high flow rate of the liquid phase demonstrates dispersed flow regimes in the horizontal annulus section [21].

The cuttings bed forms when the fluid flow rate is insufficient to avoid the cuttings accumulation in the annulus. If the cuttings bed increases in height, the flow area reduces, therefore, the annular speed enhances with increasing pressure drop until the equilibrium state is achieved [22]. The majority of cuttings transport models and correlations are also set up under equilibrium conditions or steady-state conditions. In order to ensure effective drilling operations and efficient transport of cuttings, it is essential to know about different types of multi-phase flow regimes patterns that occur in the horizontal or vertical systems. However, slug flow is identified as the most effective flow regime for efficient cuttings transport process [22].

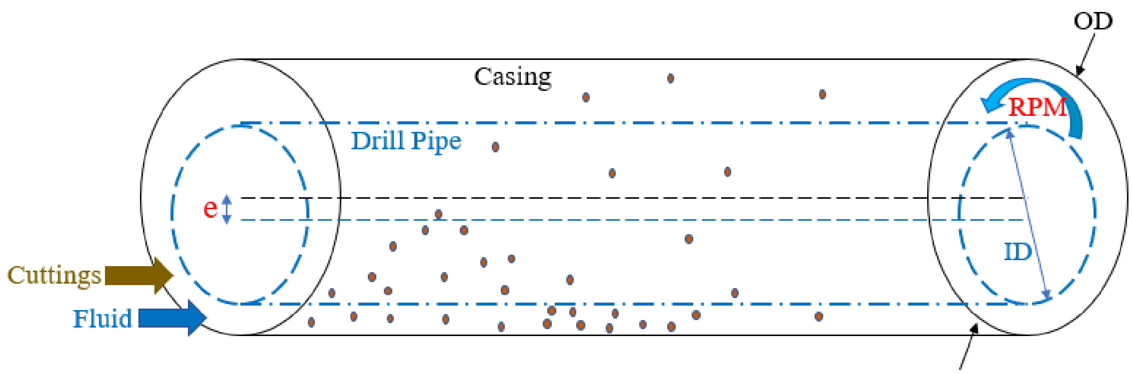

Figure 2.1. Cuttings transport through horizontal annulus section.

2.1.2. Effect of Drilling Parameters and Conditions on Cuttings Transport

The effect of rotational speed of the drill pipe is a proven mechanism for cuttings transport process. The rotation suspends the particles asymmetrically along the cross section of the annulus. Such impact is dominant on the cuttings transport process until the critical fluid velocity is achieved [23]. However, the impact of rotation on the pressure drop across the annulus shows an interesting finding while representing both increasing and decreasing trends of pressure gradient with changing RPM [51–54]. While determining the effect of drill pipe's rotation in deviated wells, the presence of orbital motion is found effective for cuttings transport process [28]. It is found that the drill pipe's orbital motion may appear within the range between 80 RPM to 110 RPM [29]. However, separate study confirmed the significant variation in frictional pressure drop in the annulus due to the orbital motion with increasing Reynolds number [30]. The impacts of drill pipe's rotational speed and orbital motion are shown by the summary table below.

Table 2.2. Drill pipe's rotation and orbital motion’s impact on cuttings transport.

Authors	**Rotational Speed Range**	**Findings**
Bassal [31]	--	Rotational speed improves hole cleaning process with a higher mud viscosity and smaller cuttings
Sifferrman and Becker [32]	0-60 RPM	Rotational speed shows the greatest impact on small cuttings and low ROP at near horizontal position
Sorgun [33]	0-120 RPM	The orbital motion reduces the critical velocity required to wipe out stationary cuttings bed. However, drill pipe’s rotation has no additional impact on hole cleaning after a certain RPM
Sanchez et al. [28]	0-175 RPM	Orbital motion can provide a better hole cleaning with high rotary speed at 90^0 inclination and low flow rate

Bilgesu et al. [34]	0-60 RPM	Rotation provides with improved cuttings transport for smaller particles
Li et al. [35]	0-200 RPM	Rotation between 80-120 RPM has significant impact on cuttings transport process

The impact of eccentricity on the cuttings transport is another point of interest while examining the particles accumulation tendency in the horizontal annulus. Several studies have confirmed the impact of drilling parameters while varying the eccentricity up to 75% from concentric position [36]. The findings addressed that the cuttings tend to accumulate after a certain point of eccentricity as well as the drill pipe's rotational speed has barely any influence on the particles transport process after a certain RPM. On the other hand, the experimental study on the pressure drop proposed that the pressure drop across the annulus may completely disappear with increasing eccentricity of the drill pipe [37]. On the other hand, the study on cuttings size reported the impact of pipe's rotation on cuttings transport and indicated the improvement of efficiency up to twofold for smaller particles [38]. A summary table is provided here to indicate the particle size effect on the cuttings transport process.

Table 2.3. Impact of particles size on cuttings transport process.

Authors	Particles Size Range	Findings
Sanchez et al. [28]	2 to 7 mm	At high rotational speed, the smaller cuttings are easier to transport with high viscosity mud
Duan et al. [39]	0.45 to 3.3 mm	Pipe rotation improves the transport efficiency of smaller cuttings compared with larger-sized cuttings
Walker and Li [21]	0.15 to 7 mm	Particles having average size of 0.76 mm is the most difficult ones to be removed by the water
Mishra [40]	3 to 8 mm	If water is the drilling fluid, larger particles are easier to transport
Martins et al. [41]	2 to 6 mm	Smaller particles are easier to transport than larger ones

2.1.3. Effect of Annulus Configuration on Multiphase Flow

The annulus configuration plays a vital role in cuttings transport mechanism. Two different annulus configurations having radius ratio of 0.76 and 0.94 were investigated for two-phase flow mechanism. The experimented flow portrayed some hybrid regimes, including the common shapes, such as slug, plug, bubble and dispersed bubble [42]. Another experimental study was performed in horizontal and marginally diverged fully eccentric annuli with 0.5 radius ratio [43]. The mixtures of water-air and nitrogen-diesel were tested in that annulus. The flow patterns observed out in this investigation were comprised of stratified, dispersed bubble, annular and intermittent flows. Moreover, the conducted experiments on two phase flow in a larger size anulus (8.34-in×3.50-in) section identified stratified wavy, stratified-smooth, stratified to slug, slug, slug to annular and slug to dispersed bubble flow patterns [44].

An interesting experimental study was performed on the flow obstructing geometry to investigate pressure drop in horizontal annulus section. In that study, some obstacles were positioned centrally and tangentially inside a 1-inch horizontal pipe to evaluate the pressure drop across the obstacles for two phase flow [45]. Another study reported flow regimes alterations in horizontal annulus originated by concentrically positioned central rod having different diameters inside a 2-inch acrylic pipe. Moreover, experimental analysis performed on a specially designed flow loop having a horizontal annulus of variable outer (3.67-inch, 4.5-inch) and inner diameters (1.92-inch, 2.25-inch) depicted intermittent flow regimes for the setup restrictions [46].

2.2. Rock Strengths and Subsequent Correlations

Rock strength evaluation is an essential primary step for drilling performance assessment that is also applicable for the activities, such as tunnel boring and mining. The unconfined compressive strength (UCS) of rocks provides valuable information regarding wellbore instability and sand production capability while drilling is performed [73-74]. Moreover, such information derived form UCS is somehow more significant than the mud weight or azimuth angle determination during drilling [49]. However, there is an internationally recognized standard to evaluate UCS of rock samples [50]. The ASTM standard has specified the sample's length to diameter ratio in between 2:1 to 2.5:1. The minimum diameter of the specimen should be around 47 mm. Moreover, the specimen's diameter is required to be at least ten times the diameter of the largest mineral grain for the UCS test.

2.2.1. Correlation between UCS and Point Load Strength Index (PLSI)

Since the UCS testing requires exact measurements and precise preparations of the rock samples, sometimes, it becomes an expensive and time-consuming process to follow. Therefore, the point load strength index evaluation is considered for strength assessment for its simplified applicability. Similar to the UCS, the point load strength index also follows an ASTM standard for laboratory evaluation [51]. The ASTM standard for point load strength index (PLSI) test recommends any core specimen having the ratio of length to diameter between 1/3 to 1 should be suitable for axial loading test. Since the 1970s, several studies were performed and the subsequent correlations between the UCS and PLSI for different rock types were established. The correlation may vary depending on the textural, mineralogical factors as well as chemical composition and anisotropic behavior of the rocks [52]. The table summarizes several literatures that show correlations between UCS and PLSI.

Table 2.4. The correlations between UCS and PLSI.

Author (Year)	**Correlation**	**Rock Type**
Smith (1997)	$UCS = 14.3 \times PLSI$	Sedimentary
Broch & Franklin (1972)	$UCS = 23.7 \times PLSI$	Several

Agustawijaya (2007)	$UCS = 13.4 \times PLSI$	Several
Rusnak & Mark (1999)	$UCS = 20.6 \times PLSI$	Sandstone
Hassani et al. (1980)	$UCS = 29 \times PLSI$	Sedimentary
Bieniawski (1975)	$UCS = 23.9 \times PLSI$	Sandstone
Mishra & Basu (2012)	$UCS = 14.63 \times PLSI$	Several
V. K. Singh & Singh (1993)	$UCS = 23.4 \times PLSI$	Quartzite rock
Vallejo et al. (1989)	$UCS = 17.4 \times PLSI$	Sandstone
Hawkins & Oivert (1986)	$UCS = 26.5 \times PLSI$	Limestone
Das (1985)	$UCS = 18 \times PLSI$	Sandstone

From the table it is prominent that the conversion factor from PLSI to UCS may vary from one rock type to another depending on the variations in their geological formations. However, it will be inaccurate to use a single conversion factor to evaluate the UCS value from PLSI for different rock types. Therefore, a range of conversion factor of 14-16 is proposed for softer rocks and another range of 21-24 is suggested for harder rocks [52].

2.2.2. Correlation between UCS and Indirect Tensile Strength (ITS)

The tensile strength of the rock determines the load-bearing capability of the rock. In general, rocks tend to fail easily under tensile loading in comparison to compressive loading. The direct approach for tensile strength test is a tedious process for laboratory testing. Therefore, the indirect test of tensile strength is an acceptable and reliable approach to follow in the laboratory environment. Because of the simplicity of the experimental setup and specimen preparation, the Brazilian strength test (BTS) is broadly practiced. For an indirect tensile strength test, the ASTM standard recommends a circular disk of rock specimen with a thickness to diameter ratio between 0.2 and 0.75 [58]. In that case, the specimen's diameter should be at least ten times larger than the largest mineral grain. Several studies in finding the relation between UCS and indirect tensile strength have reported linear relationships. However, some investigations also suggested the non-linear relationships between BTS and UCS [59][60]. There is a common assumption, which refers that the UCS is nearly ten times tensile strength for rocks. However, the conversion factor may vary from 4 to 10 for roadmaking rocks [61]. Some correlations derived from the literatures are listed below in the summary table.

Table 2.5. The correlations between UCS and ITS.

Author	**Correlations**	**Rock Type**
Brook (1993)	$UCS = 15 \times ITS$	Sandstone
Kahraman et al. (2012)	$UCS = 10.61 \times ITS$	Different Rocks
Hosking (1955)	$UCS = (4\ to 10) \times ITS$	Roadmaking Rocks
Lumb (1982)	$UCS = 14 \times ITS$	Igneous Rock
Gupta and Rao (1988)	$UCS = 9.72 \times ITS$	Quartzite

Altindag & Guney (2010)	$UCS = 12.308 \times ITS^{1.073}$	Different Rocks
Nazir et al. (2013)	$UCS = 9.25 \times ITS^{0.947}$	Limestone

2.2.3. Ultrasonic Pulse Wave Velocity Measurement

Ultrasonic pulse wave velocity analysis can be utilized to evaluate dynamic rock properties. The non-destructive and simple analysis process make it suitable for various field applications. The measurement is performed based on the ASTM standard (ASTM D2845-08) for laboratory determination of pulse velocities and ultrasonic elastic constants of rock. The ultrasonic wave velocity provides necessary information regarding rock characterization process. Besides calculating elastic constants, the primary wave velocity (V_P) can be used to establish correlations with UCS of the correspond rocks. The developed relationships between UCS and V_P can be linear or power law. Some existing correlations from literature is summarized in the table below.

Table 2.6. The correlations between UCS and primary wave velocity of rocks.

Author (Year)	**Correlation**	**Rock Type**
Kahraman (2001)	$UCS = 9.95V_p^{1.21}$	several
Minaeian & Ahangari (2013)	$UCS = 0.005\, Vp$	sedimentary
Chary et al. (2006)	$UCS = 0.1564Vp - 692.41$	sandstone
Çobanoğlu & Çelik (2008)	$UCS = 56.71\, Vp - 192.93$	several

2.2.4. Technical Gap and Contribution of Current Work

Despite all the developed experimental facilities, researchers faced difficulties for in situ visualizations of cuttings transport. Literature addresses theoretical approaches to predict the flow behavior; however, defining flow regime and constructing the subsequent flow regime map is still a challenge to overcome with the help of theoretical models. Therefore, it is prominent that there is still room for experimental analysis regarding the flow mechanism in the annulus while transporting cuttings. This is precisely the area where the current study focused. The behavior of the flow pattern in multiphase flow has been addressed with comprehensive experimental investigations. Hundreds of frames captured by the high-speed camera were scrutinized for visualization purposes. The change in drilling parameters and constructing the subsequent flow regime maps while carrying solid particles is another unique aspect of the study that could be helpful to understand the complexity of multiphase flow. Moreover, inclusive numerical analysis is required to develop the fluid-solid interactive CFD model that can be validated with the existing empirical models. It also implies the industry demand in the reduction of tedious and expensive field experiments with the help of in-house numerical analyses. In this current study, these facts mentioned above have been considered while performing numerical investigations. On the other hand, literature also confirms that the strengths correlations for medium-strength rock-like material (RLM) are rare. To date, very few works have been done that reported both static and dynamic assessments on isotropic rock samples to develop strength correlations. However, these are essential information to evaluate drilling performance and subsequent cuttings size distribution while drilling such type of rock. The laboratory-based testing procedure reported in this thesis is a part of an investigation to predict cuttings size distribution from rock formation properties and drilling parameters. Future work will be hugely benefited from this current study.

References

[1] P. H. Tomren, A. W. Iyoho, and J. J. Azar, "EXPERIMENTAL STUDY OF CUTTINGS TRANSPORT IN DIRECTIONAL WELLS.," *SPE Drill. Eng.*, 1986, doi: 10.2118/12123-PA.

[2] S. S. Okrajni and J. J. Azar, "EFFECTS OF MUD RHEOLOGY ON ANNULAR HOLE CLEANING IN DIRECTIONAL WELLS.," *SPE Drill. Eng.*, 1986, doi: 10.2118/14178-PA.

[3] M. Zamora and P. Hanson, "More rules of thumb to improve high-angle hole cleaning," *Pet. Eng. Int.*, 1991.

[4] Y. Luo, P. A. Bern, and B. D. Chambers, "Flow-rate predictions for cleaning deviated wells," in *Drilling Conference - Proceedings*, 1992, doi: 10.2118/23884-ms.

[5] M. Martin, C. Georges, P. Bisson, and O. Konirsch, "Transport of cuttings in directional wells," in *SPE/IADC Drilling Conference, Proceedings*, 1987, doi: 10.2523/16083-ms.

[6] R. K. Clark and K. L. Bickham, "Mechanistic model for cuttings transport," in *Proceedings - SPE Annual Technical Conference and Exhibition*, 1994, doi: 10.2523/28306-ms.

[7] W. Campos, J. J. Azar, S. A. Shirazi, and A. A. Pilehvari, "Mechanistic modeling of cuttings transport in highly inclined wells," in *American Society of Mechanical Engineers, Fluids Engineering Division (Publication) FED*, 1994.

[8] H. G. Wang, X. S. Liu, H. Q. Li, and G. Ding, "An experimental study of transport of drilling cuttings in a horizontal well," *Acta Pet. Sin.*, vol. 16, no. 4, pp. 125–132, 1995.

[9] M. E. Ozbayoglu, A. Saasen, M. Sorgun, and K. Svanes, "Effect of pipe rotation on hole

cleaning for water-based drilling fluids in horizontal and deviated wells," in *Society of Petroleum Engineers - IADC/SPE Asia Pacific Drilling Technology Conference 2008 - "Drilling Technology to Access Future Energy Demand and Environmental Challenges,"* 2008, doi: 10.2118/114965-ms.

[10] B. V. Loureiro, R. S. De Paula, M. B. Serafim, and A. L. Martins, "Experimental evaluation of the effect of drillstring rotation in the suspension of a cuttings bed," in *SPE Latin American and Caribbean Petroleum Engineering Conference Proceedings*, 2010, doi: 10.2118/122071-ms.

[11] M. E. Ozbayoglu, M. Sorgun, A. Saasen, and K. Svanes, "Hole cleaning performance of light-weight drilling fluids during horizontal underbalanced drilling," *J. Can. Pet. Technol.*, 2010, doi: 10.2118/136689-PA.

[12] M. Duan, S. Miska, M. Yu, N. Takach, R. Ahmed, and C. Zettner, "Critical conditions for effective sand-sized-solids transport in horizontal and high-angle wells," *SPE Drill. Complet.*, 2009, doi: 10.2118/106707-PA.

[13] T. I. Larsen, A. A. Pilehvari, and J. J. Azar, "Development of a new cuttings-transport model for high-angle wellbores including horizontal wells," *SPE Drill. Complet.*, 1997, doi: 10.2118/25872-pa.

[14] J. M. Peden, J. T. Ford, and M. B. Oyeneyin, "Comprehensive experimental investigation of drilled cuttings transport in inclined wells including the effects of rotation and eccentricity," in *European Petroleum Conference*, 1990, doi: 10.2118/20925-ms.

[15] M. G. Gerritsen and L. J. Durlofsky, "Modeling fluid flow in oil reservoirs," *Annual Review of Fluid Mechanics*. 2005, doi: 10.1146/annurev.fluid.37.061903.175748.

[16] S. T. Munkejord, J. P. Jakobsen, A. Austegard, and M. J. Mølnvik, “Thermo- and fluid-dynamical modelling of two-phase multi-component carbon dioxide mixtures,” *Int. J. Greenh. Gas Control*, 2010, doi: 10.1016/j.ijggc.2010.02.003.

[17] P. L. Speeding, J. K. Watterson, S. R. Raghunathan, and M. E. G. Ferguson, “Two-phase co-current flow in inclined pipe,” *Int. J. Heat Mass Transf.*, 1998, doi: 10.1016/S0017-9310(98)00122-7.

[18] R. Rooki, F. D. Ardejani, A. Moradzadeh, and M. Norouzi, “CFD Simulation of Rheological Model Effect on Cuttings Transport,” *J. Dispers. Sci. Technol.*, 2015, doi: 10.1080/01932691.2014.896219.

[19] S. Mokhatab, W. A. Poe, and J. Y. Mak, *Handbook of natural gas transmission and processing: Principles and practices*. 2018.

[20] V. C. Kelessidis and G. E. Mpandelis, “Flow Patterns and Minimum Suspension Velocity for Efficient Cuttings Transport in Horizontal and Deviated Wells in Coiled-Tubing Drilling,” in *Proceedings of the SPE/ICoTA Coiled Tubing Roundtable Conf*, 2003, doi: 10.2523/81746-ms.

[21] A. A. Zahid, S. R. ur Rehman, S. Rushd, A. Hasan, and M. A. Rahman, “Experimental investigation of multiphase flow behavior in drilling annuli using high speed visualization technique,” *Front. Energy*, 2020, doi: 10.1007/s11708-018-0582-y.

[22] S. Miska, T. Reed, and E. Kuru, “Advanced Cuttings Transport Study,” University of Tulsa (US), 2004.

[23] S. Akhshik, M. Behzad, and M. Rajabi, “CFD-DEM approach to investigate the effect of

drill pipe rotation on cuttings transport behavior," *J. Pet. Sci. Eng.*, 2015, doi: 10.1016/j.petrol.2015.01.017.

[24] O. Anifowoshe and S. O. Osisanya, "The effect of equivalent diameter definitions on frictional pressure loss estimation in an annulus with pipe rotation," in *Society of Petroleum Engineers - SPE Deepwater Drilling and Completions Conference 2012*, 2012, doi: 10.2118/151176-ms.

[25] T. N. Ofei, S. Irawan, and W. Pao, "CFD Method for Predicting Annular Pressure Losses and Cuttings Concentration in Eccentric Horizontal Wells," *J. Pet. Eng.*, 2014, doi: 10.1155/2014/486423.

[26] E. M. Ozbayoglu and M. Sorgun, "Frictional pressure loss estimation of non-Newtonian fluids in realistic annulus with pipe rotation," in *Journal of Canadian Petroleum Technology*, 2010, doi: 10.2118/141518-PA.

[27] M. Sorgun, "Helical flow of non-Newtonian fluids in a concentric and fully eccentric annulus," *Energy Sources, Part A Recover. Util. Environ. Eff.*, 2012, doi: 10.1080/15567036.2011.567236.

[28] R. A. Sanchez, J. J. Azar, A. A. Bassal, and A. L. Martins, "The Effect of Drillpipe Rotation on Hole Cleaning During Directional Well Drilling," 1997, doi: 10.2118/37626-ms.

[29] R. J. Avila, E. Pereira, S. Miska, N. E. Takach, and A. Saasen, "Correlations and analysis of cuttings transport with aerated fluids in deviated wells," *SPE Drill. Complet.*, 2008, doi: 10.2118/87180-pa.

[30] H. Ferroudji, A. Hadjadj, M. A. Rahman, I. Hassan, T. N. Ofei, and A. Haddad, "The impact

of orbital motion of drill pipe on pressure drop of non-newtonian fluids in eccentric annulus," *J. Adv. Res. Fluid Mech. Therm. Sci.*, 2020.

[31] A. A. Bassal, "Thesis," University of Tulsa, 1996.

[32] T. R. Sifferman and T. E. Becker, "Hole cleaning in full-scale inclined wellbores," *SPE Drill. Eng.*, 1992, doi: 10.2118/20422-PA.

[33] M. Sorgun, "Thesis," Middle East Technical University, 2010.

[34] H. I. Bilgesu, N. Mishra, and S. Ameri, "Understanding the effects of drilling parameters on hole cleaning in horizontal and deviated wellbores using computational fluid dynamics," in *SPE Eastern Regional Meeting*, 2007, doi: 10.2523/111208-ms.

[35] M. Li, Y. F. Jv, Z. Q. Wang, B. Y. Hao, and Y. K. Hong, "Simulation on the effect of drillstring rotation on hole cleaning for extended reach well," *West-china Explor. Eng.*, vol. 5, pp. 51–54, 2010.

[36] O. Heydari, E. Sahraei, and P. Skalle, "Investigating the impact of drillpipe's rotation and eccentricity on cuttings transport phenomenon in various horizontal annuluses using computational fluid dynamics (CFD)," *J. Pet. Sci. Eng.*, 2017, doi: 10.1016/j.petrol.2017.06.059.

[37] M. Haciislamoglu and J. Langlinais, "Non-Newtonian Flow in Eccentric Annuli," *J. Energy Resour. Technol. Trans. ASME*, 1990, doi: 10.1115/1.2905753.

[38] M. Duan, S. Miska, Y. Mengjiao, N. Takach, R. Ahmed, and C. Zettner, "Transport of small cuttings in extended reach drilling," *Int. Oil Gas Conf. Exhib. China 2006 - Sustain. Growth oil Gas*, vol. 2, pp. 800–808, 2006, doi: 10.2523/104192-ms.

[39] M. Duan, S. Miska, M. Yu, N. Takach, R. Ahmed, and C. Zettner, “Transport of small cuttings in extended-reach drilling,” *SPE Drill. Complet.*, 2008, doi: 10.2118/104192-pa.

[40] N. Mishra, “Thesis,” West Virginia University, 2007.

[41] A. L. Martins, C. H. M. Sa, A. M. F. Lourenco, and W. Campos, “Optimizing cuttings circulation in horizontal well drilling,” in *Proceedings of the SPE International Petroleum Conference & Exhibition of Mexico*, 1996, doi: 10.2523/35341-ms.

[42] N. P. Ekberg, S. M. Ghiaasiaan, S. I. Abdel-Khalik, M. Yoda, and S. M. Jeter, “Gas - liquid two-phase flow in narrow horizontal annuli,” *Nucl. Eng. Des.*, 1999, doi: 10.1016/S0029-5493(99)00078-3.

[43] A. C. V. M. Lage, R. Rommetveit, and R. W. Time, “An Experimental and Theoretical Study of Two-Phase Flow in Horizontal or Slightly Deviated Fully Eccentric Annuli,” in *Proceedings of the IADC/SPE Asia Pacific Drilling Technology Conference, APDT*, 2000, doi: 10.2118/62793-ms.

[44] L. Zhou, R. M. Ahmed, S. Z. Miska, N. E. Takach, M. Yu, and M. B. Pickell, “Experimental study of aerated mud flows under horizontal borehole conditions,” in *Proceedings of the SPE/ICoTA Coiled Tubing Roundtable Conference*, 2004, doi: 10.2118/89531-ms.

[45] M. Salcudean, D. C. Groeneveld, and L. Leung, “Effect of flow-obstruction geometry on pressure drops in horizontal air-water flow,” *Int. J. Multiph. Flow*, 1983, doi: 10.1016/0301-9322(83)90007-1.

[46] C. Omurlu Metin and M. E. Ozbayoglu, “Two-phase fluid flow through fully eccentric horizontal annuli: A mechanistic approach,” in *Society of Petroleum Engineers Coiled*

Tubing and Well Intervention Conference and Exhibition 2007, 2007, doi: 10.2523/107076-ms.

[47] D. Moos, P. Peska, T. Finkbeiner, and M. Zoback, “Comprehensive wellbore stability analysis utilizing Quantitative Risk Assessment,” *J. Pet. Sci. Eng.*, 2003, doi: 10.1016/S0920-4105(03)00024-X.

[48] F. J. Santarelli, J. L. Dctienne, and J. P. Zundel, “Determination of the mechanical properties of deep reservoir sandstones to assess the likelyhood of sand production,” in *ISRM International Symposium, IS 1989*, 1990, doi: 10.1016/0148-9062(90)91096-p.

[49] R. A. Jaramillo, “Estudio geomecánico estadístico de l’estabilidad durante la perforación de pozos en el Piedemonte Llanero, campo Recetor,” Universidad Nacional de Colombia. Medellín, Colombia, 2004.

[50] ASTM D7012-14, “Standard test method for compressive strength and elastic moduli of intact rock core specimens under varying states of stress and temperatures,” *D7012-10*, 2017.

[51] ASTM D5731-08, “Standard Test Method for Determination of the Point Load Strength Index of Rock and Application to Rock Strength Classifications,” *ASTM Int. West Conshohocken, PA*, 2008.

[52] T. N. Singh, A. Kainthola, and A. Venkatesh, “Correlation between point load index and uniaxial compressive strength for different rock types,” *Rock Mech. Rock Eng.*, 2012, doi: 10.1007/s00603-011-0192-z.

[53] H. J. Smith, “The point load test for weak rock in dredging applications,” *Int. J. rock Mech.*

Min. Sci. Geomech. Abstr., 1997, doi: 10.1016/S1365-1609(97)00063-4.

[54] D. S. Agustawijaya, "The Uniaxial Compressive Strength of Soft Rock," *Civ. Eng. Dimens.*, 2007.

[55] D. A. Mishra and A. Basu, "Use of the block punch test to predict the compressive and tensile strengths of rocks," *Int. J. Rock Mech. Min. Sci.*, 2012, doi: 10.1016/j.ijrmms.2012.01.016.

[56] L. E. Vallejo, R. A. Welsh, and M. K. Robinson, "Correlation between unconfined compressive and point load strengths for appalachian rocks," in *30th U.S. Symposium on Rock Mechanics, USRMS 1989*, 1989, doi: 10.1016/0148-9062(90)94915-g.

[57] B. Das, "Evaluation of the Point Load Strength for Soft Rock Classification," in *Proceedings of the fourth international conference ground control in mining, Morgantown.*, 1985, p. WV, 220 226.

[58] ASTM, "Standard Test Method for Splitting Tensile Strength of Intact Rock Core Specimens 1 D3967-08," *ASTM Int. West Conshohocken, PA*, 2016.

[59] R. Altindag and A. Guney, "Predicting the relationships between brittleness and mechanical properties (UCS, TS and SH) of rocks," *Sci. Res. Essays*, 2010.

[60] R. Nazir, E. Momeni, D. J. Armaghani, and M. F. M. Amin, "Correlation between unconfined compressive strength and indirect tensile strength of limestone rock samples," *Electron. J. Geotech. Eng.*, 2013.

[61] J. R. Hosking, "A comparison of tensile strength, crushing strength and elastic properties of roadmaking rocks," *Quarr. Man. J.*, vol. 39, pp. 200–211, 1955.

[62] S. Kahraman, “Evaluation of simple methods for assessing the uniaxial compressive strength of rock,” *Int. J. Rock Mech. Min. Sci.*, 2001, doi: 10.1016/S1365-1609(01)00039-9.

[63] B. Minaeian and K. Ahangari, “Estimation of uniaxial compressive strength based on P-wave and Schmidt hammer rebound using statistical method,” *Arab. J. Geosci.*, 2013, doi: 10.1007/s12517-011-0460-y.

[64] K. B. Chary, L. P. Sarma, K. J. P. Lakshmi, N. A. Vijayakumar, V. N. Lakshmi, and M. V. M. S. Rao, “Evaluation of Engineering Properties of Rock Using Ultrasonic Pulse Velocity and Uniaxial Compressive Strength,” *Natl. Semin. Non-Destructive Eval.*, 2006.

[65] I. Çobanoğlu and S. B. Çelik, “Estimation of uniaxial compressive strength from point load strength, Schmidt hardness and P-wave velocity,” *Bull. Eng. Geol. Environ.*, 2008, doi: 10.1007/s10064-008-0158-x.

Chapter 3. Analysis of Cuttings Transport and Flow Pattern in Nearly Horizontal Extended Reach Well

Golam Rasul[1], M. Fahed Qureshi[1], Hicham Ferroudji[1], Stephen Butt[2], Rashid Hasan[3], Ibrahim Hassan[1], Mohammad Azizur Rahman[1]

Journal of Advanced Research in Fluid Mechanics and Thermal Sciences 71, Issue 2 (2020) 69-86.

Abstract

During the drilling activity, in an extended reach well, the deposition of cuttings (solids) in the annulus can lead to issues such as differential sticking and inefficient hole cleaning. This makes it essential to identify different multi-phase flow patterns and study the effect of drill pipe eccentricity and rotational speed on cutting transport in the annulus. Therefore, in this study, the experiments were conducted in a near-horizontal flow loop system, where the length of an annulus section was 6.16 m (20.2 ft) long and the outer and inner diameters were 4.5 in. (11.4 cm/0.37 ft) and 2.5 in. (6.4 cm/0.21 ft), respectively. A high-speed charge-coupled device (CCD) camera was used to perform the in-situ visualization of the multiphase-flow through the annulus. Then the recorded videos were used to investigate the cuttings transport for both 2 and 5 wt% solid concentrations. Glass beads having a diameter of 0.5-2 mm were used as cuttings for the experiments. The video recordings were used to scrutinize the flow behavior pattern which depicts the possible flow patterns for the gas-liquid-solid multiphase-flow through horizontal annuli. The effects of varying pipe eccentricity (0 to 75 %), drill pipe rotational speed (0- 120 RPM), air

[1]Texas A&M University at Qatar, Doha, Qatar

[2]Memorial University of Newfoundland, St. John’s Newfoundland and Labrador, Canada

[3]Texas A&M University, College Station, TX, USA

pressure (0.4-0.8 bar) and solid concentration on the cuttings transport through the annulus were investigated. It was observed that high rotational speed and eccentricity of the drill pipe lead to better hole cleaning. At 30% eccentricity, the solid bed height was found to vary from 8 to 20 times at different rotational speeds for changing the solid concentration form 2 wt% to 5 wt%. Moreover, while different drilling conditions were tested for cutting transport, six distinguishable flow patterns were observed. The findings also show that 75% of eccentricity may not be optimum drilling conditions because of the contact between cutting and the drill pipe. The novelty aspect of this work was the use of three phases (solid, liquid and gas) to investigate the flow pattern behavior and cutting transport phenomena in the annular flow loop system by varying drill pipe rotational speed and drill pipe eccentricity. The flow map of this work can be used to develop 3-phase models to figure out optimum conditions for cutting transport in horizontal wells for enhanced oil recovery.

Keywords: Cuttings transport; Flow pattern; Multiphase flow; Horizontal annulus; Eccentricity.

3.1. Introduction

Multiphase flow can take place through the whole production system intricate in fluids flowing across offshore oil and gas wells to the onshore facilities [1]. The multiphase flow can occur in the oil and gas reservoirs, the tubulars that link the reservoir to the surface and any flow lines that transport fluids from one facility to other processing facilities [2]. The multiphase flow encountered in the industry can be an amalgamation of a solid, liquid and gas phase [3]. The occurrence of multiphase flow in the petroleum industry forms complications, as the fluids involved are multicomponent mixtures whose phase behavior is extremely complex to determine [4]. This makes it difficult for engineers to predict the correlations between flow rates, pressure drop, and piping geometry (length, diameter, angle, etc.) for the multi-phase fluids produced across offshore fields and onshore processing facilities [5]. The study of multi-phase flow across annulus is also essential to determine the cuttings transport phenomena and ensure proper cleaning of the annulus [6]. As deposition of cuttings (solids) in the annulus can lead to issues such as differential sticking, loss of fluid circulation, blockages and inefficient hole cleaning.

3.1.1. Effects of Geometry

Earlier in the 1980s, Salcudean, Groeneveld [7] conducted experimental work to study the effect of flow impediment geometry on pressure drop in horizontal two-phase (water-air) system. In this work, a pipe of diameter 1 inch consisting of impediments positioned centrally and tangentially was used to evaluate pressure drop. The effect of the level of flow impediment and flow shape impediments on pressure drop was evaluated. However, no two-phase flow-regimes were reported in their work. Osamusali and Chang [8], investigated multiphase flow (water-air) regime alterations in horizontal annuli designed by concentrically positioning central rod, with variable radiuses in an acrylic tube of diameter 2 inches. The inner and outer diameters ratios varied from 0.375 to 0.675. The flow regimes observed by Osamusali and Chang [8], included stratified wavy, stratified-smooth, slug, plug and annular.

Ekberg, Ghiaasiaan [9], investigated two-phase flow regimes in thin horizontal annulus sections. They carried out experiments in two different annuli. The first annulus had the inner and outer diameters of 0.26 inch and 0.34 respectively, having an ID/OD ratio of 0.76. The second annulus had the inner and outer diameters of 1.30 inch and 1.38 correspondingly, providing an ID/OD ratio of 0.94. The two-phase flow regimes noted included some hybrid regimes and common flow regimes like a plug, slug, dispersed, bubble and churn flow. Lage, Rommetveit [10], carried out small scale experimental work to investigate the two-phase flow regimes in horizontal and marginally diverged fully eccentric annuli. The annulus had an inner and outer diameter of 2 inches and 4 inch and correspondingly, providing an ID/OD ratio of 0.5. The fluids tested in the annulus were the mixtures of water-air and nitrogen-diesel respectively. The flow regimes observed by Lage, Rommetveit [10], comprised of the stratified, dispersed bubble, annular and intermittent flows. But, the complete flow regime maps cannot be developed out of their experimental work due to a limited number of data points.

Zhou, Ahmed [11], conducted intensive two-phase (air-water) experiments in a larger size annulus with outer and inner diameters 8.34 inch and 3.50 inch correspondingly, providing ID/OD ratio of 0.42. The flow regimes identified included stratified wavy, stratified-smooth, stratified to slug, slug, slug to annular and slug to dispersed bubble. Zhou, Ahmed [11], also provided a theoretical explanation for the flow regime transitions in the two-phase system.

Omurlu and Ozbayoglu [12] and Metin and Ozbayoglu [13] investigated two-phase flow through a fully peculiar horizontal annulus. Their experimental loops involved variable outer diameters (3.67 inch, 4.5 inch) and variable inner diameters (1.92 inch, 2.25 inch) providing ID/OD ratios of 0.52 and 0.5 respectively. They observed flow regimes visually and mainly observed intermittent flow regime due to setup confinements. Based on their observation, they develop a mechanistic model that helps to predict a flow regime in annulus based on the reference diameter.

3.1.2. Effects of Eccentricity

Sorgun, Osgouei [14], examined gas-liquid flow inside horizontal eccentric annulus using an Eulerian CFD model for two-phase flow, using different flow patterns, such as dispersed bubble, dispersed annular, plug, slug and wavy annular. The results of Sorgun, Osgouei [14] simulations were compared with the experimental data and they were found to be in an agreement of ±20-30% error in estimates of gas-liquid pressure losses.

Ettehadi Osgouei, Ozbayoglu [15] examined the pressure loss differences among horizontal, inclined and nearly vertical positions for three-phase flow in eccentric annuli. It was observed that because of the increased gas velocity in the wellbore, the total pressure loss changes moderately in the horizontal section. However, in the case of inclined and nearly vertical sections, total pressure loss decreases considerably with increased gas velocity. They also indicated that the conformal mapping could also be useful to describe the impact of eccentricity in the three-phase flow system.

Gschnaidtner [16], carried out multiphase flow (air-water) experimental work in a concentric annulus with an outer diameter of 2 inch and an inner diameter of 1.3 inch, providing the ratio of 0.65. The flow regimes inside the annulus were observed using an HD video camera. The flow regimes reported were characterized as intermittent and bubble flow as only a minor range of gas and liquid superficial velocities were investigated.

Recently, another group [17], at Texas A & M University at Qatar (TAMUQ), observed flow regimes of two different multi-phase flow systems consisting of air-water and glass bead-water using a high-speed CCD camera in a horizontal annulus with a length of 240 inch and outer-inner diameters of 4.5 inch and 2.5 inch respectively, providing ID/OD ratio of 0.5. The flow regimes observed for the air-water system at different system pressure (0.2-0.4 bars) were characterized as bubbly and wavy. On the other hand, the flow regime observed for glass bead- water system at 0.3 bar was observed as a stationary bed. Moreover, the Computational fluid dynamics model work was also conducted by our group to develop correlations for pressure losses in annular geometries [18, 19].

Based on the literature review, it is evident that the study of cutting transport is essential for smooth drilling operation and flow assurance [20-22]. The majority of work in cuttings transport has been conducted using two-phase flow [23-27] and work using three-phase flow is limited [28-30]. Therefore, in this work, our group has used three phases (solid, liquid and gas) to investigate the flow pattern behavior and cutting transport phenomena in the same annular flow loop system by varying drill pipe rotational speed and drill pipe eccentricity. The group has used two different solid concentrations (2- 5wt %) and system operating pressure (0.4-0.8 bars) to visually observe the flow regimes within the system. In order to visualize the flow patterns, digital video recordings were collected and the image processing technique is applied for the corresponding videos. Different flow conditions and drilling parameters have been tested and subsequent analyses have also been performed to construct the desired flow map and flow regime.

3.2. Background

In the drilling activity, the fluid is pumped across the drilled pipe down to the hole. At that point, the fluid with cuttings flows back up to the surface via the annular space between the drilled pipe and the hole [31]. The hole cleaning is vital as it has a major influence on the drilling operations cost, time of operations and process safety. Insufficient hole cleaning can lead to issues such as differential sticking, premature wear out of drill bit, fracture formation and inducement of high torque or drag [32]. The type of fluid pumped and the other factors such as rotation of the drilled pipe affect the transport of cuttings. If cleaning of the annular hole is not carried out appropriately by the injection fluid, it may cause problems like pipe sticking, premature wear out of drill bit and lead to formation damages or issues in cementing or logging process [33]. It may also cause temporary hole blockages resulting in loss of circulation, excessive wear and tear in the pipe and more additives will be required in the drilling fluid which directly increases the cost of the drilling operation [34, 35]. Sometimes, the sticking of the solid particles at the lower annular section may also lead to a reduced penetration rate and also cause thickening of the pipeline [36].

The different elements which affect the efficiency of the hole cleaning process include the injection rate of the fluid stream, inclination of hole angle, rotation of drill, the rate of penetration (ROP), fluid properties and type of cuttings present in the hole [37]. These elements also rely on the mechanics of fluid transportation [33]. For instance, lower turbulence levels in the injection flow through the annulus may lead to inappropriate carrying up of the cuttings across the narrow zones of the annulus causing hole cleaning issues [38].

3.2.1. Effect of Multiphase Flow Regimes on Cuttings Transport

The transport of cuttings as a multiphase flow is essential for drilling operation, as it may help to reduce operation cost, reduce operation time, and improve the quality of well drilling and completion [39, 40]. The addition of the gas phase, into the flow system, helps to improve the cutting transport dynamics. The liquid phase of the blend provides cuttings moving capacity and assures that the cuttings move at the rate of fluid velocity, provided they are not present in the cuttings bed [41].

The most widely recognized flow regimes for effective cuttings transport are slug flow and dispersed-bubbly stream. The formation of cuttings beds occurs when the fluid flow rate in the annulus can't avoid cuttings deposition [42]. As the thickness of bed increases, the annular speed and the frictional pressure losses also increase due to restricted flow region, until equilibrium conditions or steady-state condition is achieved (rate of pumping and fluid properties, etc) [42]. The majority of cuttings transport models and correlations are also set up under equilibrium conditions or steady-state conditions. In order to ensure effective drilling operations and efficient transport of cuttings, it is essential to know about different types of multi-phase flow regimes patterns that occur in the horizontal or vertical systems.

3.2.2. Gas-liquid flow regimes

In a horizontal annulus, the gas-liquid flow regimes can be classified as the bubble flow, the plug flow, the slug flow, the wavy flow, stratified flow, disperse flow and the annular flow [Fig. 3.1]. The bubbly flow contains small-sized distributed bubbles in the liquid [43]. The plug flow involves a combination of liquids and large size bubbles with some small-sized bubbles. The slug flow consists of a mixture of liquids and large gas slugs which have random frequency [43]. In the wavy flow, the gas phase tends to flow distinctly on top of the liquid phase and depicts a wavy surface and in the annular flow, the liquid tends to flow as a narrow film adjacent to the pipe wall [44]. In the stratified flow both liquid and gas maintain moderate velocities and fluid surface remain flat, whereas in the case of dispersing flow, both velocities are very high and dispersed gas bubbles are scattered along the whole cross-section.

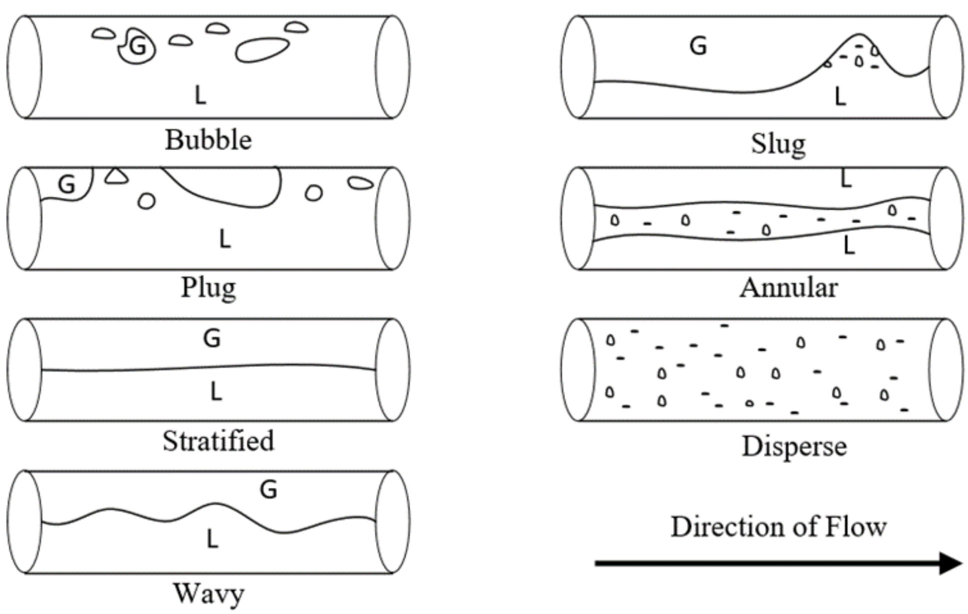

Figure 3.1. Flow regimes for gas-liquid two-phase flow in a horizontal pipe.

In vertical or discretely deviated pipes, the most widely recognized flow regime for gas-liquid mixtures are bubble flow, slug flow, mist flow, churn flow and annular flow [45]. In the bubble flow, the gas phase is circulated in the liquid phase and the fragile bubble moves upward in a zig-zag motion. The wall of the pipe is in touch with the liquid phase [45]. In the slug flow, the gas exists as large bullet-shaped air pockets with the area close to the area of the pipe. These air pockets, also known as Taylor bubbles, move consistently upward and are isolated by slugs of continuous liquid that connects with the pipe and contain small-sized gas bubbles. The speed of gas bubbles is higher compared to the liquid [46]. This oscillatory flow of the liquid is distinctive of churn flow and it may not take place in smaller size pipes.

In the Annular - Mist Flow, amid annular, the liquid phase flows consistently as an annular film on the wall with gas flowing as a central core. A portion of this liquid is entrained as small molecules in this gas core (mist flow) [47].

3.2.3. Solid-liquid flow regimes

In liquid-solid flow, the solid particles traveling through the annuli can form various patterns [48]. The term stationary bed relates to the flow regime where the liquid streams over a stationary solid bed molded at the bottom of an annulus. This type of phase scattering takes place when the liquid velocity varies from moderate to low [48]. As the flow rate of the liquid rises, the stationary bed separates into a pattern depicting moving dunes and as the flow rate of the liquid rises further the occurrence of a scouring regime may take place [48]. In that case, few particles tend to travel over the solid dune, while most of the particles gather in the lower portion of the dunes. This mechanism forces the solids towards the direction of flow. The dispersed flow regime takes place as a result of a high liquid flow rate in the annular horizontal portion [49].

There are different flow patterns like stratified, slug, plug and annular that can emerge as solid-liquid-gas multiphase move across an annulus. In the case of plug flow, the gas bubbles travel across the top portion of the annulus and have no significant effect on the solid. As the airflow rate rises the plug size increases and the formation of a slug flow regime occurs [49]. The carriage of cuttings in such multiphase flow tends to be complex as the particles tend to flow in the form of dispersed phase or tend to form a stationary bed. A liquid-gas interface is formed in the stratified flow as the liquid flows at the lower portion of the annulus [50]. The brief description of the flow regimes observed in this work is provided in the section below.

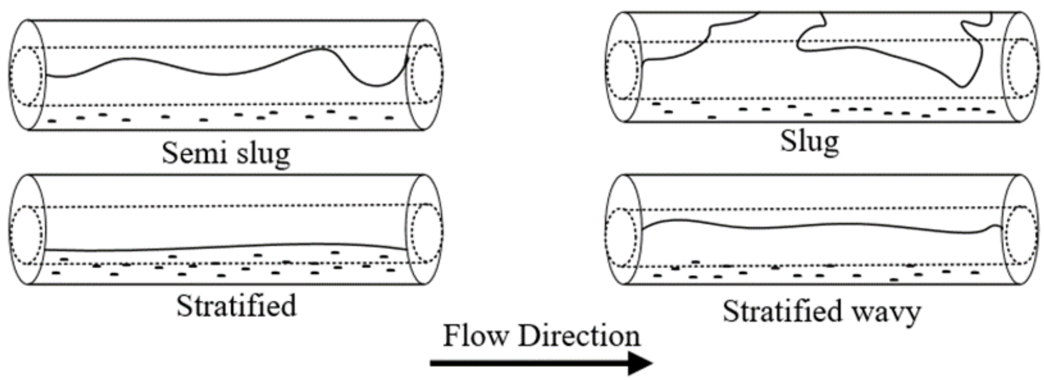

Figure 3.2. Flow regimes for solid-liquid-gas multiphase flow.

In Figure 3.2, Stratified flow is which the gas plugs tend to get lengthier till the gas and liquid flow discretely with a separate and comparatively smooth interface amid them. The gas flows in the top section and the liquid flows in the bottom section of the pipe. The Stratified wavy flow is that some waviness in the liquid is present although there is still an interface between air and water. The wavy pattern in the liquid is random and does not have any specific wave structure. The Slug flow is that when the flow rate of the gas is high, it shows the slug flow behavior in multiphase flow. It happens when the big gas pockets appear in the liquid in a random manner. Actually, the high flow rate and the high pressure of gas cause the accumulation of gas inside the annulus and show the slug behavior. While the Semi-slug flow, it is characterized as a flow where very large waves are present on the stratified layer.

3.3. Experimental Sections

In this section, the details of the experimental setup, procedure, and methodology have been discussed briefly.

3.3.1. Experimental setup

The existing flow loop in the petroleum department at Texas A&M University at Qatar (TAMUQ), shown in Figure 3, is 18.7 ft (6.16 m) long. The annulus consists of an acrylic outer pipe and a stainless steel inner pipe. The inner diameter of the outer pipe and the outer diameter of the inner pipe are 4.5 in (0.1143 m) and 2.5 in (0.0635 m) respectively. In order to perform visualization, a high-speed Photron Fastcam CCD camera was used. The system can be operated in both concentric and eccentric conditions where the inner drill pipe can go up to 80% eccentricity. Additionally, to check the inclination effect on the near-horizontal drilling, the annulus section can be tilted from 0° to -13°/+13°. The mixing tank having a capacity of 265 gal (1 m3) was used for mixing solid and liquid with the help of an agitator. This agitator was used to mix the solid beads homogeneously with the liquid. In order to keep the solid beads suspended, the agitator can be operated at different rotary speeds up to 200 RPM.

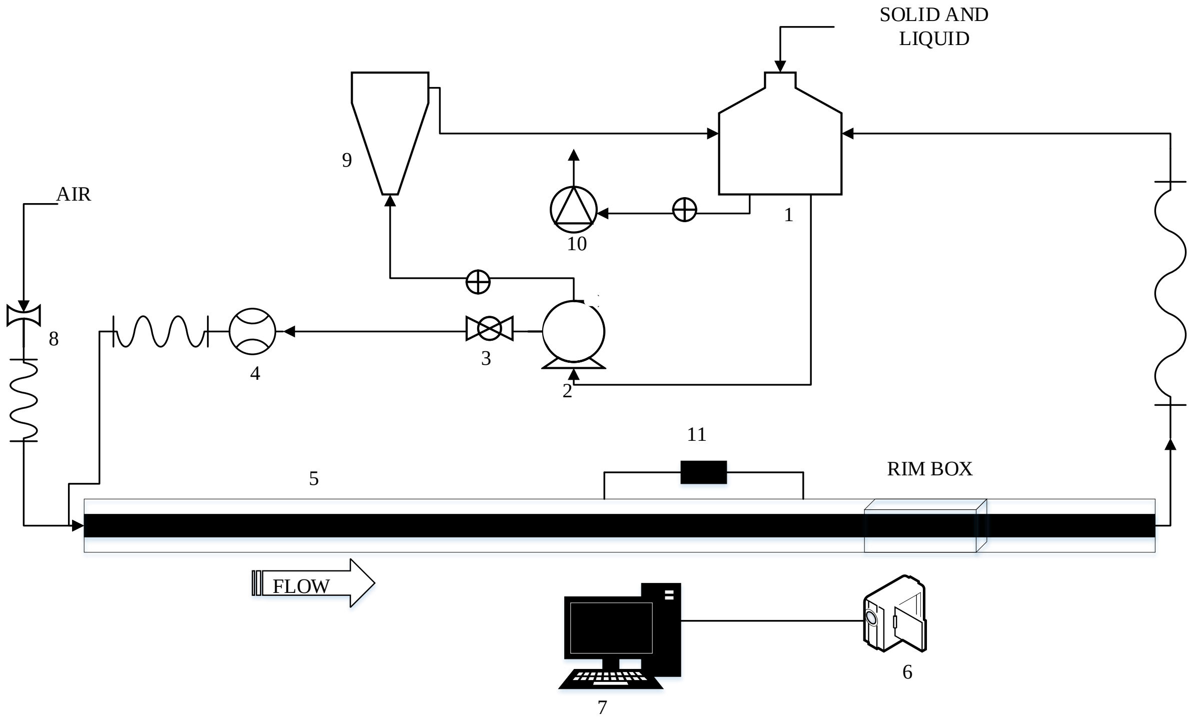

1. Tank; 2. Slurry pump; 3. Ball valve; 4. Slurry flow meter; 5. Annulus; 6. High speed camera; 7. Computer; 8. Air flow meter; 9. Hydro-cyclone; 10. Drain pump; 11. Pressure transducer.

Figure 3.3. Schematic of flow loop at Texas A&M University at Qatar.

The data acquisition system helps to acquire precise readings per second for each sensor integrated with the equipment of a flow loop system as shown in Figure 3.3. The data is displayed in the monitor containing the flow loop software. For aerated flow, air with variable pressure (0.4 bar and 0.8 bar) was injected inside the annulus along with water and solid mixture. Two different Coriolis flowmeters were used for measuring air and liquid flow rates. Both of them are Micro MotionTM branded having measurement accuracy of +/- 1.0%.

The robust flow loop system also contains pressure transducer, two flow meters (one for slurry another for air), hydro-cyclone, pressure relief valves, data acquisition system (DAS), electrical resistance tomography (ERT), and a highspeed charge-coupled device (CCD) camera with the computer display. A Toshiba branded slurry pump has a rating of 18.7 hp, 0.33 ft inlet and 0.166 ft outlet, which was used to maintain the desired flow of slurry. The multivariate pressure transmitter (MVT), two digital pressure sensors, and two Coriolis flowmeters are used in the system to make sure the measurement and control of the fluid flow through the loop.

3.3.2. Experimental procedure

Before the initiation of the experiments, the water volume of about 300 liters is added into the tank (Figure 3.3). After achieving the stable flow through the annulus the solid particles (glass beads) are added into the system. The flow loop can handle the maximum flow rate of 0.0213 m^3/s (21.3 l/s) which corresponds to the maximum angular velocity of 3 m/s (Re ~ 2×10^5). A slurry pump with a maximum capacity of 650 kg/min was employed to pump the slurry from tank to annulus. The solids weight of about 6 kg (2wt%) and 15 kg (5wt%) are added into the tank and then well agitated. These solids are spherical glass beads having a diameter of 0.5-2 mm and a density of 2650 kg/m^3.

The eccentricity of the inner pipe is controlled by a mechanical process built by the vendor (MARZOR LTD & CO) of the flow loop system. At first, the lock is released, and then the ratchet situated on top of the 3rd metallic flange is used to adjust the position of the inner pipe. The scale with an indicator on the same flange indicates the percentage of eccentricity. As the ratchet is turned, the indicator moves downward, and the eccentricity increases. While the indicator touches the halfway mark on the scale, it means 50% eccentricity is achieved. Similarly, the other values of eccentricity are measured based on the position of the indicator on the scale. Once the desired eccentricity is obtained, the locking system is engaged to ensure the inner pipe will not slip anymore. Moreover, there are several O-rings at the joints of the annulus section. Their internal mechanism also helps to minimize the chances of pipe sagging.

The solid dunes height, translational velocity, and type of flow pattern are visually observed by the help of the high-speed CCD camera (FASTCAM SA-X2) situated in front of the RIM (Refraction Index Matching) box, that records the images and videos of the solid dune across the RIM box. These recorded videos are used to investigate the cuttings transport for both 2 and 5 wt% solid concentrations. The video recordings help to scrutinize the flow behavior pattern which depicts the possible flow patterns for the gas-liquid-solid multiphase-flow through horizontal annuli. This helps to investigate the effects of varying pipe eccentricity (0 to 75 %), drill pipe rotational speed (0- 120 RPM), air pressure (0.4-0.8 bar) and solid concentration on the cuttings transport across the annulus.

3.4. Results and Discussions

The effects of drill pipe RPM (0-120) and eccentricity (0-75%) on the multiphase flow patterns in annulus were observed under different pressure conditions during the experiments. The purpose of these experiments was to visualize the type of flow and level of solid accumulation that occurs by varying the RPM and eccentricity parameters during the experiments. A high-speed CCD camera (Photron FastCam SA-X2) was used to visualize and conduct image analysis through the transparent section across the flow loop. The CCD camera recordings captured for each experimental condition were carefully examined and still, images were collected from these recordings as shown in the Tables below. These images were further enhanced to provide better visual illustrations of the type of flows, flow regimes and level of mixing occurring within the system.

3.4.1. Analysis for 2 wt% Solid Concentration

In order to investigate the effect of drilling parameters such as drill pipe eccentricity and rotational speed on cutting transport, experiments were performed at different gas pressure. The change in parameters also showed different flow patterns inside the annulus.

Table 3.1. Summary of the observation with 2 wt% solid at different drill pipe rotation, eccentricity and gas pressure.

Phase Component	Drill Pipe Rotational Speed (RPM)	Gas Pressure (bar)	Eccentricity (%)	Flow Type
Water, air and glass beads	0	0.4	30	Stratified wavy
Water, air and glass beads	40	0.4	30	Stratified wavy
Water, air and glass beads	120	0.4	30	Stratified wavy
Water, air and glass beads	0	0.8	75	Stratified wavy
Water, air and glass beads	40	0.8	75	Bubbly stratified
Water, air and glass beads	120	0.8	75	Bubbly slug

Overall analysis shows that at 0.4 bar gas pressure and 30% eccentricity of the drill pipe, the flow pattern remains as stratified wavy. For these cases, the contribution of air is not that high and liquid is the dominating phase inside the annulus [Table 3.1]. So, liquid may tend to compress the air at the top of the annulus while the weak airflow causes the waviness in the flow.

However, at elevated gas pressure (0.8 bar), rotational speed (40 and 120 RPM) and eccentricity (75%) bubbly stratified and slug flow were observed [Table 3.1]. The combined impact of those parameters may cause such transformation of flow patterns.

The dimensionless analysis was performed to calculate and compare the solid bed height at different drilling conditions. The dimensionless bed height was evaluated from the ratio between actual bed height and the considered standard height. In our case, the considered standard height was the casing diameter (4.5 in or 114.3 mm). During our observation, some drilling conditions displayed very efficient cutting transport and hence, the subsequent bed height was also very thin. However, to report the experimented values correctly, the captured images were scrutinized by the graphics editor tool. In our study, we utilized the pixel-based analysis method of the Microsoft Paint application. This method considered a vertical straight line on the captured image. The intersection points between that straight line and the horizontal lines generated by the casing and solid bed were notified. The corresponding pixels of those points were recorded. From that information, the distance between the lowest and highest points was calibrated as the casing diameter (114.3 mm). Based on this calibration, the distance between the lowest point and the point on the solid bed line provided the actual bed height. Furthermore, the dimensionless bed height was calculated by taking the ratio.

Figure 3.4 shows a clear decreasing trend of solid bed height with increasing rotational speed for different eccentricity. Higher the rotation better the agitation and that may increase shear stress too. This phenomenon does not allow the accumulation of the solid as a stationary bed. Moreover, when the eccentricity is enhanced the flow area reduces at the bottom of the annulus. Because of the rule of fluid dynamics (continuity equation for incompressible fluid), the corresponding flow velocity increases at the bottom at the same time and ensures less accumulation of solids. On top of that, our overall finding from visualization confirms that 2 wt% solid concentration is not high enough to get settled at the bottom of the annulus by superseding the liquid flow velocity.

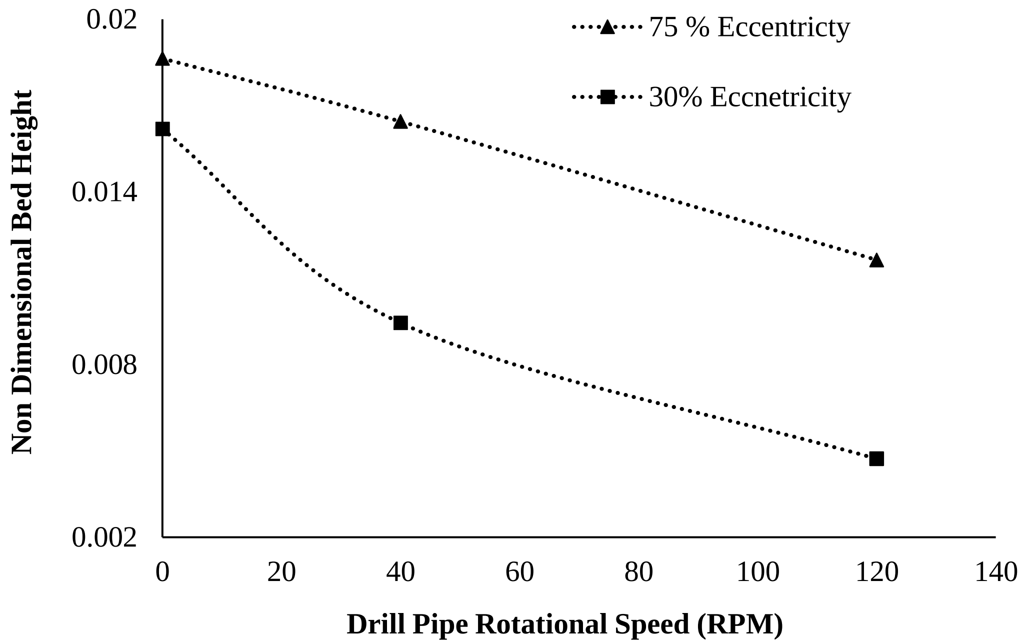

Figure 3.4. Change in solid bed height with different rotational speed and eccentricity for 2 wt% solid concentration.

However, 30% eccentricity with 0.4 bar gas pressure shows better hole cleaning than 75% eccentricity with 0.8 bar gas pressure. It clearly indicates that moderate eccentricity (30%) could be more desirable in the hole cleaning process than high eccentricity (75%). From the visualization, we also detected the contact between the drill pipe and cutting during high eccentricity. The friction between cutting and drill pipe due to the contact obstructs the cutting transport process through the annulus.

3.4.2. Analysis for 5 wt% Solid Concentration

The gas pressure was kept constant at 0.8 bar with the fixed liquid flow rate, whereas the eccentricity and the drill pipe rotational speed were varied to observe the solid accumulation and corresponding flow regime.

Table 3.2. Summary of visualization observed with 5 wt% solid at different drill pipe rotation and eccentricity at 0.8 bar gas pressure.

Phase Component	Drill Pipe Rotational Speed (RPM)	Eccentricity (%)	Flow Type	Visualized Image
Water, air and glass beads	0	0	Stratified wavy	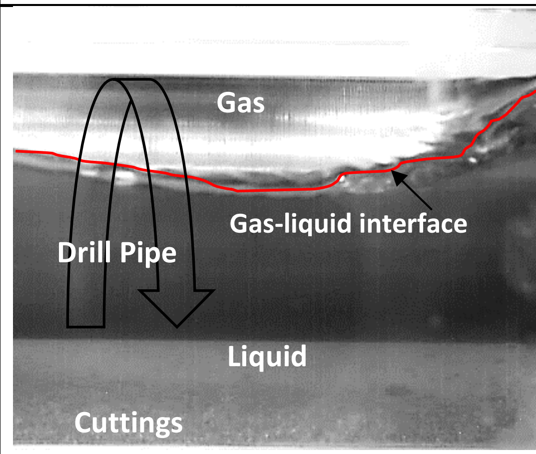
Water, air and glass beads	120	0	Bubbly wavy	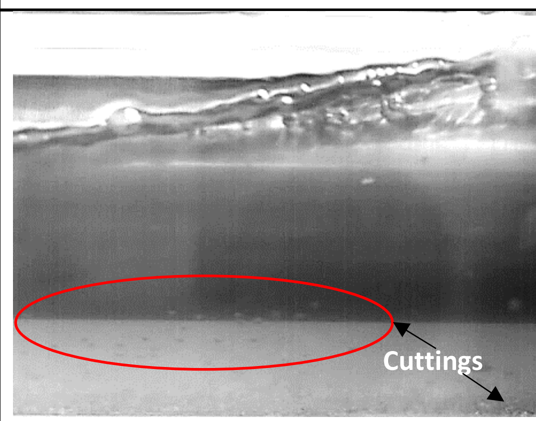

Table 3.3. Summary of visualization observed with 5 wt% solid at different drill pipe rotation and eccentricity at 0.8 bar gas pressure & eccentricity 30.

Phase Component	**Drill Pipe Rotational Speed (RPM)**	**Eccentricity (%)**	**Flow Type**	**Visualized Image**
Water, air and glass beads	0	30	Stratified	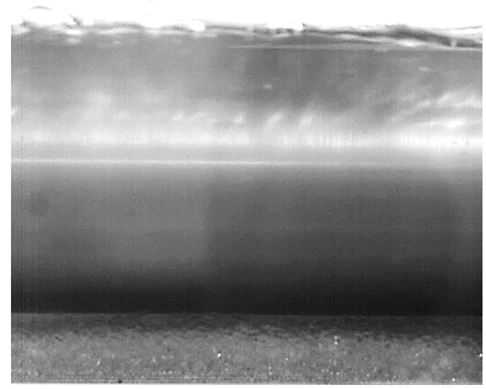
Water, air and glass beads	40	30	Stratified	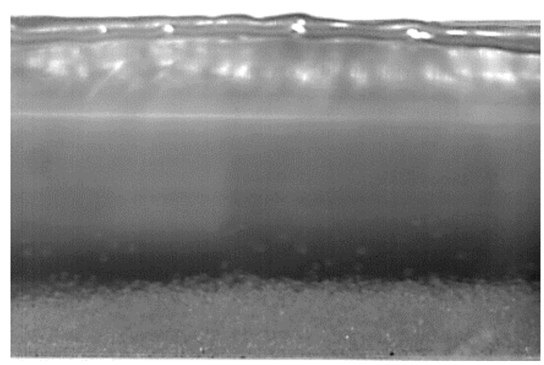
Water, air and glass beads	120	30	Slug	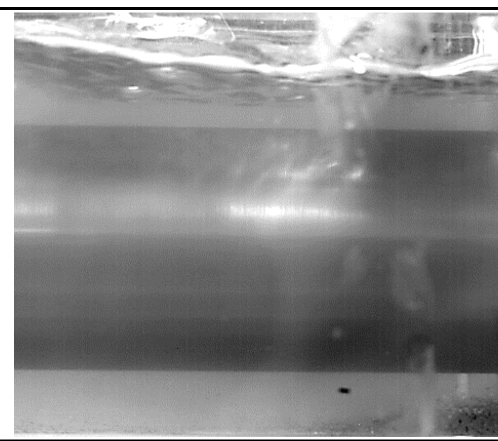

Without any eccentricity and rotational speed, we observed stratified wavy flow with a thick solid bed at the bottom of the annulus [Table 3.2]. However, if the rotational speed is increased to 120 RPM without any eccentricity, the solids are dispersed in the annulus while the wavy flow contains some bubbles at the top of the flow. In that case, high RPM provides more shear stress and agitation in the fluid which accelerates the particles and pushes them away from their stationary position [Table 3.2]. In order to check the eccentricity effect, similar experiments were carried out for 30% eccentricity of the drill pipe. The identical rotational speed effect is also noticed the same as previous experiments. Moreover, the combined impact of eccentricity and rotational speed is found to provide better hole cleaning conditions. At 30% eccentricity [Table 3.3], stratified flow is investigated for both 0 and 40 RPM of the drill pipe [Figure 3.5]. However, at 120 RPM slug flow is recorded with the least amount of solid in the annulus [Table 3.3]. As eccentricity is increased the flow area at the bottom part of the annulus is decreased that causes higher flow velocity in the same region which eventually pushes more solid out of the annulus.

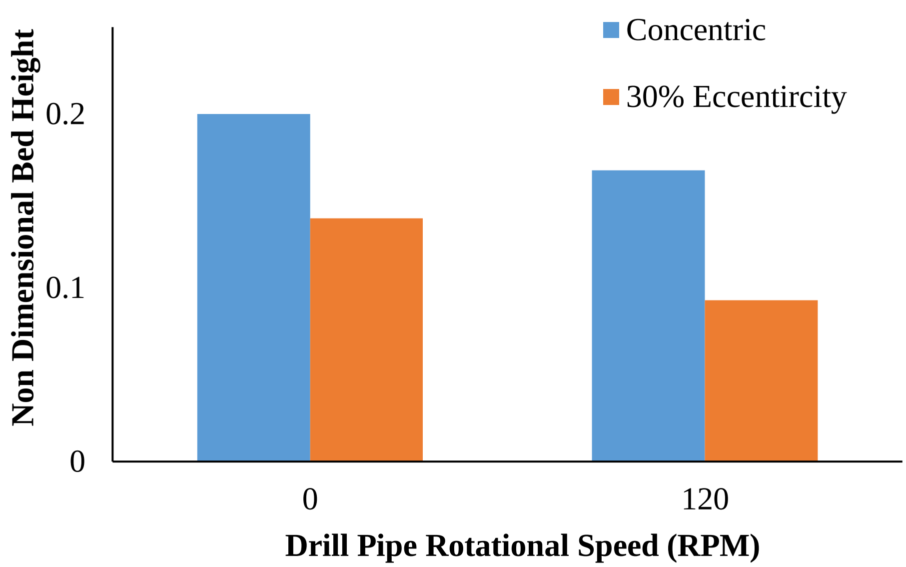

Figure 3.5. Effect of rotational speed and eccentricity on solid accumulation for 5 wt% solid concentration.

Figure 3.5 shows the impact of the rotational speed of the drill pipe on cutting accumulation for both concentric and eccentric situations. The analysis clearly represents that at higher eccentricity solid bed height is comparatively lower than the solid bed height found for the concentric situation. It also depicts that the increasing rotational speed helps the hole cleaning process irrespective of eccentricity.

From the aforementioned visualization Table 3.2 and Figure 3.5, it is clearly understandable that the drilling parameters like eccentricity and rotational speed of the drill pipe facilitate the cutting transport process for 5 wt% solid concentration.

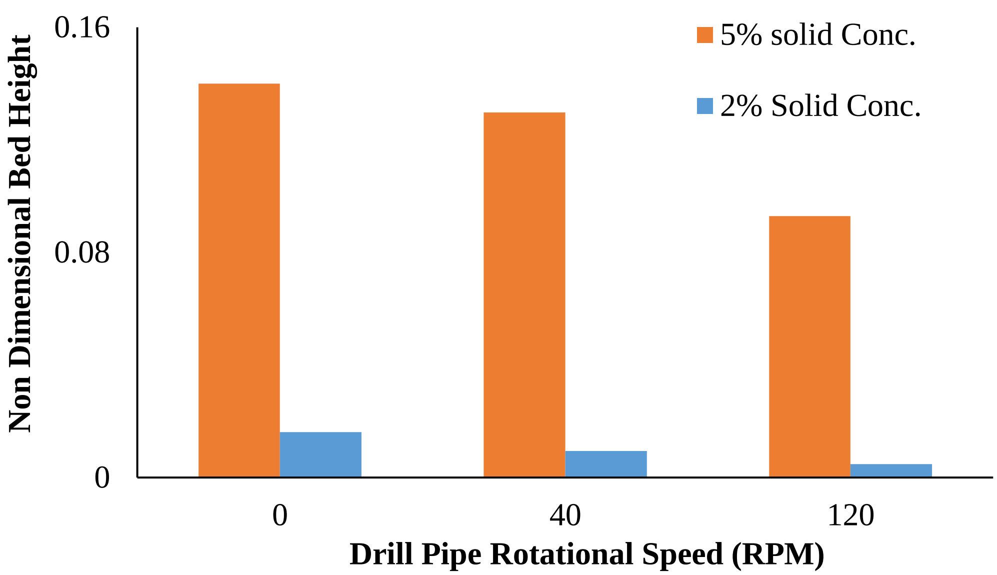

Figure 3.6. Variation in cutting accumulation for different concentrations of solid.

The solid concentration plays a vital role in cutting accumulation and transportation processes. Higher concentration causes a thicker bed of solid inside the annulus. Figure 3.6 displays this practical fact where the solid bed height for 5 wt% is clearly higher than the 2 wt% solid bed. With the variation of the rotational speed, the corresponding solid bed height varies from 8 to 20 times.

Although the low concentration is showing less accumulation of cutting, in reality, the general drilling process deals with higher concentration having more than 2 wt% of solid.

3.4.3. Flow Regime Maps

The dimensionless numbers are used either to scale up or to scale down the phenomenon to determine the influence of parameters in different scales. Froud number is a dimensionless number represented by the ratio of the flow inertia to the external field that implies the effect of gravity on fluid motion. On the contrary, Weber number is another dimensionless parameter that analyse the interface between two fluids. It provides essential information regarding multiphase flow having curved surface at the interface. The effect of the liquid and gas Froude numbers times Weber number on the flow regime map of multi-phase flow in terms of liquid and gas flow pattern and distribution of the solid phase in the annulus is presented in the Fig. 3.7. As can be seen in Fig. 3.7, a moving bed + slug wavy is stated at low values of liquid and gas Froude numbers times Weber number, however, the flow pattern is became moving/stationary bed + stratified wavy with an increase of the gas Froude numbers times Weber number.

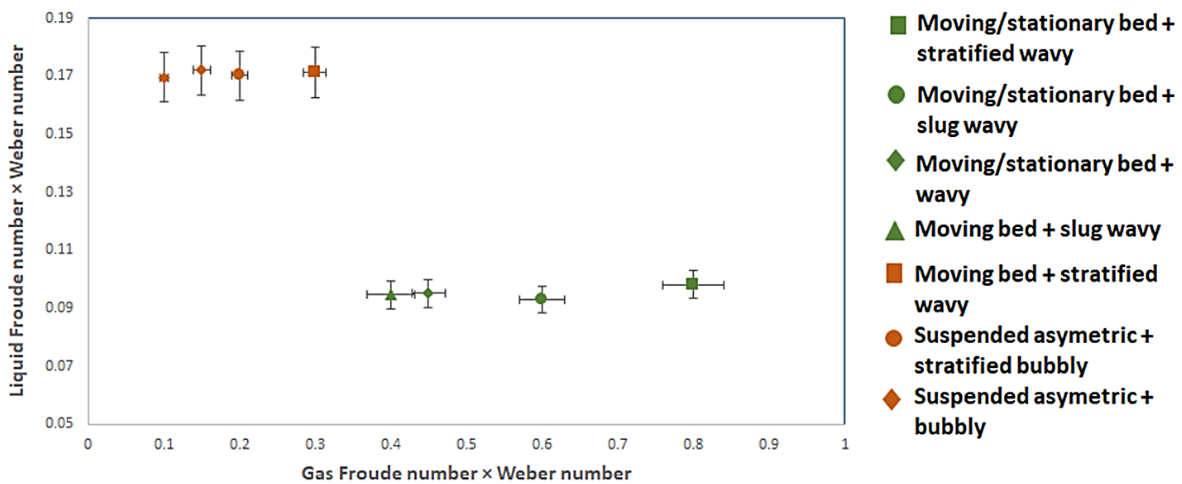

Figure 3.7. Three Phase Flow Regimes in the Horizontal Annulus.

Moreover, high values of liquid Froude numbers times Weber number results in moving bed and suspended asymmetric of the solid phase which allows achieving efficient cuttings transport and preventing the formation of the cuttings bed in the lower side of the annulus. Moreover, the orange color indicates an efficient cuttings transport process induced by the suitable parameters considered in this study, On the other hand, the dimensionless numbers adopted in this investigation may help to scale up findings of this study for comparison reasons.

A flow regime maps [Figure 3.7] are developed using the modified gas and liquid Froude numbers reported by Eyo and Lao [51]. The Froude number is an essential dimensionless parameter for identifying the flow regime and it provides an indication of the ratio of the inertial forces to the external field. The gas and liquid Froude numbers can be expressed as:

$$F_{r_G} = \sqrt{\frac{\rho_G v_{SG}}{(\rho_L - \rho_G) D_H g cos\theta}} \qquad (1)$$

$$F_{r_L} = \sqrt{\frac{\rho_G v_{SL}}{(\rho_L - \rho_G) D_H g cos\theta}} \qquad (2)$$

In the above expressions, V_{SL}, V_{SG}, g, D_H, are the liquid superficial velocity, gas superficial velocity, gravitational acceleration, and hydraulic diameter respectively; while ρ_L, ρ_G are the liquid and gas densities respectively. However, the Weber number is introduced to show the impact of a curved surface at the interface of multiphase flow and represented by the following equation:

$$W_e = \frac{\rho v^2 l}{\sigma} \qquad (3)$$

Here, ρ is the mixture of solid and liquid density, v is the velocity of the fluid, l is the characteristics length and σ is the surface tension.

Figure 3.8 outlines the development of the flow regime map with respect to the inner pipe rotation and liquid mass flow.

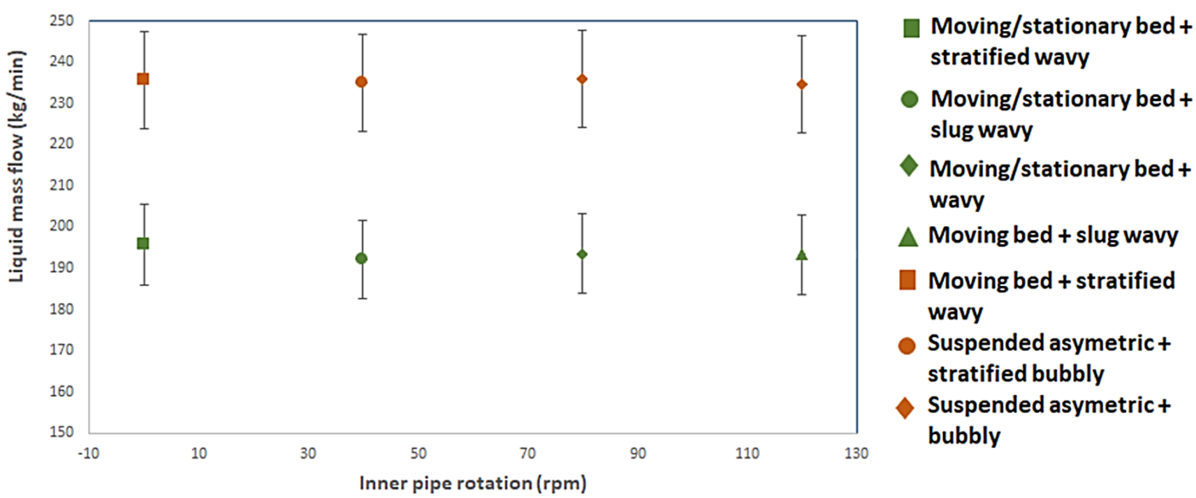

Figure 3.8. Liquid mass flow vs. Inner pipe rotation in the horizontal annulus.

As shown in Figure 3.8, high values of the inner pipe rotation has a positive effect on the accumulation of the solid particles where there is no formation of the stationary bed at 120 rpm even though for low liquid mass flow, however, for high liquid mass flow, suspended asymmetric + bubbly occurs in the annulus due to the agitation effect induced by the inner pipe rotation and high quantity of the liquid volume fraction (Holdup) in the annular space. Moreover, it can be concluded from this Figure that liquid mass flow is the dominant parameter to handle cuttings transport issue till a certain limit like drilling pump capacity, additional pressure drop induced by the increase of flow rate, drilling operating window, etc. On the other hand, from the present study, rotation of the drill pipe is considered as the second dominant parameter on cuttings transport, especially, for low liquid mass flow.

3.5. Conclusions

In this study, the impact of drilling parameters such as eccentricity and rotation of drill pipe on the cutting transport processes have been reported based on experimental analyses. The corresponding flow patterns of the multiphase flow for different drilling conditions have also been investigated. Two different concentrations of solids have been checked and their comparative analysis has been performed to find out the solid bed behavior inside the annulus.

Based on the analysis showed in the results and discussions section, we can conclude that drilling parameters like eccentricity and rotational speed of the drill pipe facilitate the cutting transport process for different solid concentrations. The 75% eccentricity may not be the optimum drilling condition because of the contact between cuttings and the drill pipe. Due to the friction generated from the contact, the cutting transport hampers and may result in higher solid bed formation than 30% eccentricity.

Six different flow patterns were observed during the experimental analysis. Most of the visualization results confirm the stratified wavy pattern, whereas slug flow was observed at elevated gas pressure and rotational speed condition. At 30% eccentricity, the solid bed height was found to vary from 8 to 20 times at different rotational speeds for changing the solid concentration from 2 wt% to 5 wt%.

References

1. Oliemans, R. *Multiphase science and technology for oil/gas production and transport*. in *University of Tulsa Centennial Petroleum Engineering Symposium*. 1994. Society of Petroleum Engineers.
2. Falcone, G., G. Hewitt, and C. Alimonti, *Multiphase flow metering: principles and applications*. 2009: Elsevier.
3. Gerritsen, M.G. and L.J. Durlofsky, *Modeling fluid flow in oil reservoirs.* Annu. Rev. Fluid Mech., 2005. **37**: p. 211-238.
4. Munkejord, S.T., et al., *Thermo-and fluid-dynamical modelling of two-phase multi-component carbon dioxide mixtures.* International Journal of Greenhouse Gas Control, 2010. **4**(4): p. 589-596.
5. Spedding, P., et al., *Two-phase co-current flow in inclined pipe.* International journal of heat and mass transfer, 1998. **41**(24): p. 4205-4228.
6. Rooki, R., et al., *CFD simulation of rheological model effect on cuttings transport.* Journal of Dispersion Science and Technology, 2015. **36**(3): p. 402-410.
7. Salcudean, M., D.C. Groeneveld, and L. Leung, *Effect of flow-obstruction geometry on pressure drops in horizontal air-water flow.* International Journal of Multiphase Flow, 1983. **9**(1): p. 73-85.
8. Osamusali, S. and J. Chang, *Two-phase flow regime transition in a horizontal pipe and annulus flow under gas–liquid two-phase flow.* ASME FED, 1988. **72**: p. 63-69.
9. Ekberg, N., et al., *Gas–liquid two-phase flow in narrow horizontal annuli.* Nuclear engineering and design, 1999. **192**(1): p. 59-80.

10. Lage, A., R. Rommetveit, and R. Time. *An experimental and theoretical study of two-phase flow in horizontal or slightly deviated fully eccentric annuli*. in *IADC/SPE Asia Pacific Drilling Technology*. 2000. Society of Petroleum Engineers.

11. Zhou, L., et al. *Experimental study of aerated mud flows under horizontal borehole conditions*. in *SPE/ICoTA Coiled Tubing Conference and Exhibition*. 2004. Society of Petroleum Engineers.

12. Omurlu, C. and M.E. Ozbayoglu. *A new mechanistic model for two-phase flow through eccentric horizontal annulus*. in *SPE Europec/EAGE Annual Conference and Exhibition*. 2006. Society of Petroleum Engineers.

13. Metin, C.O. and M.E. Ozbayoglu. *Two-Phase Fluid Flow Through Fully Eccentric Horizontal Annuli: A Mechanistic Approach*. in *SPE/ICoTA Coiled Tubing and Well Intervention Conference and Exhibition*. 2007. Society of Petroleum Engineers.

14. Sorgun, M., et al., *An experimental and numerical study of two-phase flow in horizontal eccentric annuli.* Energy Sources, Part A: Recovery, Utilization, and Environmental Effects, 2013. **35**(10): p. 891-899.

15. Ettehadi Osgouei, R., et al., *Three Phase Flow Characteristics in Inclined Eccentric Annuli*, in *SPE/IADC Middle East Drilling Technology Conference & Exhibition*. 2013, Society of Petroleum Engineers: Dubai, UAE. p. 23.

16. Gschnaidtner, T., *Two-phase Flow (Air-water) Characteristics in Annulus*. 2014, Cranfield University.

17. Zahid, A.A., et al., *Experimental investigation of multiphase flow behavior in drilling annuli using high speed visualization technique.* Frontiers in Energy, 2018: p. 1-9.

18. Sultan, R.A., et al., *Validation of CFD model of multiphase flow through pipeline and annular geometries.* Particulate Science and Technology, 2019. **37**(6): p. 681-693.

19. Dall'Acqua, D., et al., *A new tool for modelling the decompression behaviour of CO2 with impurities using the Peng-Robinson equation of state.* Applied Energy, 2017. **206**: p. 1432-1445.

20. Qureshi, M.F., et al., *Gas Hydrate Prevention and Flow Assurance by Using Mixtures of Ionic Liquids and Synergent Compounds: Combined Kinetics and Thermodynamic Approach.* Energy & Fuels, 2016. **30**(4): p. 3541-3548.

21. Altamash, T., et al., *Gas hydrates inhibition via combined biomolecules and synergistic materials at wide process conditions.* Journal of Natural Gas Science and Engineering, 2017. **46**: p. 873-883.

22. Tang, C., et al., *Investigation of the Flow Characteristics of Methane Hydrate Slurries with Low Flow Rates.* Energies, 2017. **10**(1): p. 145.

23. Mokhtari Moghari, R., et al., *Two phase mixed convection Al2O3–water nanofluid flow in an annulus.* International Journal of Multiphase Flow, 2011. **37**(6): p. 585-595.

24. Mao, K. and T. Hibiki, *Drift-flux model for upward two-phase cross-flow in horizontal tube bundles.* International Journal of Multiphase Flow, 2017. **91**: p. 170-183.

25. Baghernejad, Y., et al., *Effect of pipe rotation on flow pattern and pressure drop of horizontal two-phase flow.* International Journal of Multiphase Flow, 2019. **111**: p. 101-111.

26. Ahammad, M.J., et al., *Numerical investigation of two-phase fluid flow in a perforation tunnel.* Journal of Natural Gas Science and Engineering, 2018. **55**: p. 606-611.

27. Frank, M., et al., *Multiphase Flow Effects in a Horizontal Oil and Gas Separator*. Energies, 2019. **12**(11): p. 2116.

28. Jose, E., *Experimental Study of Hole Cleaning Win an Aerated Fluid at Intermediate Hole Angles*. 2003, University of Tulsa.

29. Sunthankar, A., *Study of the flow of aerated drilling fluids in annulus under ambient temperature and pressure coditions*. 2000, University of Tulsa.

30. Kelessidis, V., G. Bandelis, and J. Li, *Flow of dilute solid-liquid mixtures in horizontal concentric and eccentric annuli*. Journal of Canadian Petroleum Technology, 2007. **46**(05).

31. Zhou, L., *Finding ways to improve UBD hole cleaning.* Drilling contractor, 2006.

32. Ndeda, R., et al. *Review of thermal surface drilling technologies*. in *Proceedings of Sustainable Research and Innovation Conference*. 2015.

33. Dewangan, S.K. and S.L. Sinha, *Exploring the hole cleaning parameters of horizontal wellbore using two-phase Eulerian CFD approach.* The Journal of Computational Multiphase Flows, 2016. **8**(1): p. 15-39.

34. Kelessidis, V. and A. Dukler, *Modeling flow pattern transitions for upward gas-liquid flow in vertical concentric and eccentric annuli.* International Journal of Multiphase Flow, 1989. **15**(2): p. 173-191.

35. Altamash, T., et al., *Cost-effective alkylammonium formate-based protic ionic liquids for methane hydrate inhibition.* Journal of Natural Gas Science and Engineering, 2018. **58**: p. 59-68.

36. Masuda, Y., et al. *Critical cuttings transport velocity in inclined annulus: experimental studies and numerical simulation*. in *SPE/CIM International Conference on Horizontal Well Technology*. 2000. Society of Petroleum Engineers.

37. Al-Haleem, A.A., et al., *Optimization of Hole Cleaning In Iraqi Directional Oil Wells.* Journal of Engineering, 2016. **22**(7): p. 108-117.

38. Kristensen, A., *Flow properties of water-based drilling fluids*. 2013, Institutt for petroleumsteknologi og anvendt geofysikk.

39. Rooki, R., et al., *Simulation of cuttings transport with foam in deviated wellbores using computational fluid dynamics.* Journal of Petroleum Exploration and Production Technology, 2014. **4**(3): p. 263-273.

40. Ferroudji, H., et al., *The Impact of Orbital Motion of Drill Pipe on Pressure Drop of Non-Newtonian Fluids in Eccentric Annulus.*

41. Osgouei, R.E., *Determination of cuttings transport properties of gasified drilling fluids.* Middle East Technical University, 2010. **1**.

42. Miska, S., T. Reed, and E. Kuru, *Advanced Cuttings Transport Study*. 2004, University of Tulsa (US).

43. Sharaf, S., et al., *Structures in gas–liquid churn flow in a large diameter vertical pipe.* International Journal of Multiphase Flow, 2016. **78**: p. 88-103.

44. Brauner, N., *Liquid-liquid two-phase flow systems*, in *Modelling and Experimentation in Two-Phase Flow*. 2003, Springer. p. 221-279.

45. Zhu, W., *An Investigation of Two-Phase Flow Regime Transition in Large Diameter Pipes*. 2003.

46. Street, J.R. and M.R. Tek, *Dynamics of bullet shaped bubbles encountered in vertical gas liquid slug flow.* AIChE Journal, 1965. **11**(4): p. 644-650.

47. Mokhatab, S., W.A. Poe, and J.Y. Mak, *Handbook of natural gas transmission and processing: principles and practices*. 2018: Gulf professional publishing.

48. Kelessidis, V. and G. Mpandelis. *Flow patterns and minimum suspension velocity for efficient cuttings transport in horizontal and deviated wells in coiled-tubing drilling*. in *SPE/ICoTA Coiled Tubing Conference and Exhibition*. 2003. Society of Petroleum Engineers.

49. Zahid, A.A., et al., *Experimental investigation of multiphase flow behavior in drilling annuli using high speed visualization technique.* Frontiers in Energy: p. 1-9.

50. Sommerfeld, M., *Numerical Methods for Dispersed Multiphase Flows*. 2017. p. 327-396.

51. Eyo, E.N. and L. Lao, *Gas-liquid flow regimes in horizontal annulus.* Journal of Petroleum Science and Engineering, 2019. **175**: p. 573-586.

Chapter 4. Drilling Cuttings Transport in Horizontal Wells While Aerated Drilling

Golam Rasul[1], Rashid Hasan[2], Ibrahim Hassan[1], Stephen Butt[3], Mohammad Azizur Rahman[1]

4th Thermal and Fluids Engineering Conference (TFEC), April 14–17, 2019, Las Vegas, NV, USA

Abstract

The design and application of a drilling operation rely highly on the hole cleaning process. When the fluid velocity is not enough for removing thick drilling cuttings bed, it might cause countless problems including high drag, increased probability of stuck pipe and greater hydraulic requirements. In this study, cuttings transport in aerated water drilling is investigated for horizontal and slightly inclined annulus. Numerous flow conditions were tested using a 6.16-m long test section with 4.5-in. casing (CSG) and 2.5-in. drill pipe (DP) having both concentric and eccentric annulus geometry. Findings indicate that the air injection considerably reduces the cuttings bed height and enhances cuttings transport efficiency in both horizontal and slightly inclined annulus as found in the visualization. Development in the cuttings transport efficiency by DP rotation is also distinctive even at the low range of angular velocity (40 RPM) resulting in making cuttings dispersed in the annulus.

Keywords: Cutting Transport, Flow Loop, Aerated Fluid, Bed Height, DP Rotation.

[1]Texas A&M University at Qatar, Doha, Qatar

[2]Texas A&M University, College Station, TX, USA

[3]Memorial University of Newfoundland, St. John's Newfoundland and Labrador, Canada

4.1. Introduction

The economics of the drilling process is greatly influenced by the cutting transport. Inadequate hole cleaning can cause stuck pipe, reduced weight on bit results in reduced ROP, transient hole blockage leads to lost circulation conditions, extreme drill pipe wear, additional cost for mud additives, and wasted time by wiper-trip schemes [1]. One of the most common cleanout options is circulating the cuttings out with an appropriate fluid or a mixture of fluids. For designing this cleanout operation, circulation fluid and proper range selection of flow rate should be considered. These factors need to be optimized to transport the drilling cuttings to surface in a cost-effective way.

Cuttings transport in horizontal and deviated wells with a single-phase flow has been tested with considerable effort. Researchers have conducted experiments of effects of various parameters on drilling cuttings-bed formation using the University of Tulsa's flow loop. Depending on the test results, they established correlations to predict critical velocity and pressure loss. The correlations provide a means of analyzing cuttings transport as a function of operating conditions, mud properties, well configuration and cuttings size [2, 3, 4, 5].

For cuttings transport with two-phase flow in annulus, some experiments with aerated mud have been conducted by few researchers [6, 7, 8, 9]. Li et al. measured the bed height with different flowrate of gas/liquid mixed fluid. In this study, they stated the most significant factor for determining the hole cleaning performance is liquid volume fraction in the mixed fluid with air and water [10]. Also, they stated the need for optimization for circulation strategy because of the nonlinearity between the fluid flow rate and hole cleaning time. Naganawa et al. conducted over 300 experiments about measuring hole cleaning performance and critical flow rate avoiding formation of cuttings bed [11]. They concluded the aerated fluid affected the cutting transport significantly, its efficiency is better in horizontal or relatively low inclination wellbore. Additionally, the cutting transport behavior in highly inclined geometry heavily depended on the gas/liquid two phase flow pattern. However, their air injection experiments seem somewhat vague in terms of quantification such as flow rate or amount injection. Moreover, the linkage between two-phase flow pattern and cutting transport has not been stated specifically. For the recent years, many researchers have been studying the sand transport with aerated fluid in the pipe [12, 13, 14, 15, 16]. Their studies mainly focused on the complex and unique sand flow patterns with various liquid and gas flow rate, however; those experiments were conducted with extremely low sand concentration. Due to complexity and the incomplete understanding of solid transport, it is challenging to utilize these data on the annulus in hole cleaning situations that should be handled with more solids. In this study, we conducted using 5% wt. of drilling cuttings concentration over 100 combinations of various drilling parameters.

4.2. Experimental Section

The flow loop, shown in Fig. 4.1, consists of a 6.16m (18.7ft) long transparent acrylic pipe having an inner diameter of 11.4 cm (4.5in) and a concentric stainless-steel pipe simulating the drilling pipe with an outer diameter of 6.4 cm (2.5in). For visualization and image analysis through the transparent section, a high-speed CCD camera (PHOTRON FASTCAM SA-X2) recording system is equipped. The range of image recording speed was 1000-120000 frames per second (fps). The test section can simulate a concentric/eccentric annulus with DP maximum eccentricity of 80%. The loop is mounted on an aluminum rail and can be inclined in the range of -12 to 12o from horizontal. Cuttings particles and liquid is mixing and stored in a 1m3 (265gal) tank. The slurry is agitated with a mixer driven by a hydraulic motor. The slurry pump with a maximum capacity of approximately 650kg/min can pump slurry into the annulus. In order to make sure the aerated flow, air is injected into the slurry flow before entering the test section varying the pressure from 0.35 bar to 0.8 bar. The flow rates, liquid and gas, are measured by two Micro Motion™ Coriolis type flow meters. The accuracy of the flow-rate measurement is +/- 1.0%. For drilling cuttings, we used glass beads with a diameter of 1 mm and a density of 2650 kg/m3. We made the agitator speed 130 and 160 RPM, but we only analyzed data sets with 160 RPM. Each experimental analysis consists of the following procedures:

i) Ensure the circulation of fluid.

ii) Start the mixing of cuttings.

iii) After having a steady state, record 5 seconds with a high-speed camera

iv) For the next stage, reduce the flow rate and repeat from step 3.

v) Stop the cutting mixing process as well as the fluid circulation.

A single experimental run comprises 5 stages of steady-state conditions with different fluid flow rates. From an initial high flow rate, the fluid flow rate was reduced to the subsequent flow rate after finishing the required evaluation for the stage. The reduction of fluid flow rate between the stages can cause the accumulation of cuttings in the test section which might require few minutes to achieve steady state. The flow phenomena and the flow patterns were observed visually and recorded with a digital camera. The flow rate, temperature, pressure, and density were monitored and recorded using a computer data acquisition system.

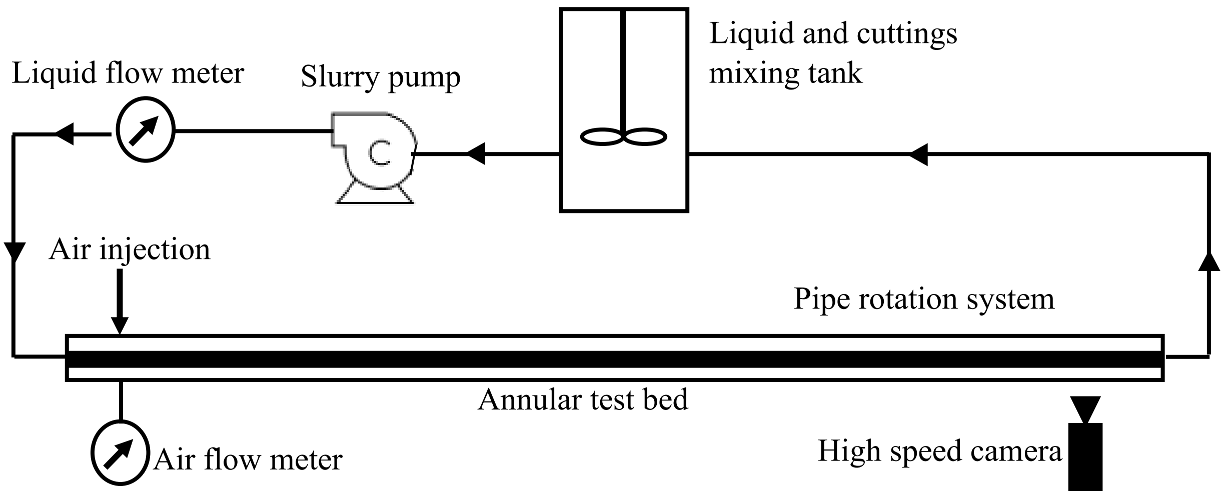

Figure 4.1. Schematic of TAMUQ flow loop.

Table 4.1. Experimental conditions for the tests performed in the laboratory.

	S.I Unit		English Unit	
Hole OD	11.4	cm	4.5	in.
Inner-pipe OD	6.4	cm	2.5	in.
Water amount	300	ℓ	79.4	gal.
Water flow rate	200~500	kg/min	53~132	gal/min
Air pressure	0.25~0.75	bar	3.63~10.88	psi
Cuttings amount	15	kg	33.1	lb
Cuttings concentration	5	%wt.	Same	
Cuttings size	1	mm	0.04	in.
Cuttings density	2650	kg/m^3	165.7	Lb/ft^3
DP Rotation Speed	0,40,120	RPM	Same	
DP Eccentricity	0,50	%	Same	
Test bed inclination	0˚,4˚,12˚		Same	
Fluid temperature	23~28	℃	73~82	℉

4.3. Results and Discussions

4.3.1. Stationary Bed Height with Aerated Water

Every bed height shown in this paper is converted to a dimensionless bed height, h/D, which is defined as the equilibrium bed height, h, divided by the wellbore diameter, D. We measure the bed height using high speed camera, its axial length of test bed section is 5.5 m from the inlet. We first measured the dimensionless bed height variation with different flow rate of single-phase fluid, water, in Figure 4.2 Intuitively, the bed height is decreasing with higher superficial liquid velocity, this trend is distinct when the velocity is relatively low, below than 0.7m/s. Comprehensive finding from previous studies indicates that fluid flow velocity is the dominant variable on hole cleaning because of its direct relation to shear stress acting on the cuttings [10, 11, 17]. Even though some outliers that are suspected to be experimental error, air injection significantly decreases the bed height compared the same superficial liquid velocity. We stated the reason of experimental error due to complex and unique flow pattern of cuttings in the last part of this section. Specifically, this trend is distinct in relatively low superficial liquid velocity below 0.7m/s. For the superficial liquid velocity over 0.83m/s, the amount of reduction in bed height is less than the data sets below 0.83m/s of superficial liquid velocity. This is the reason that we did not conduct the experiment regarding air injection with high superficial liquid velocity over 0.83m/s.

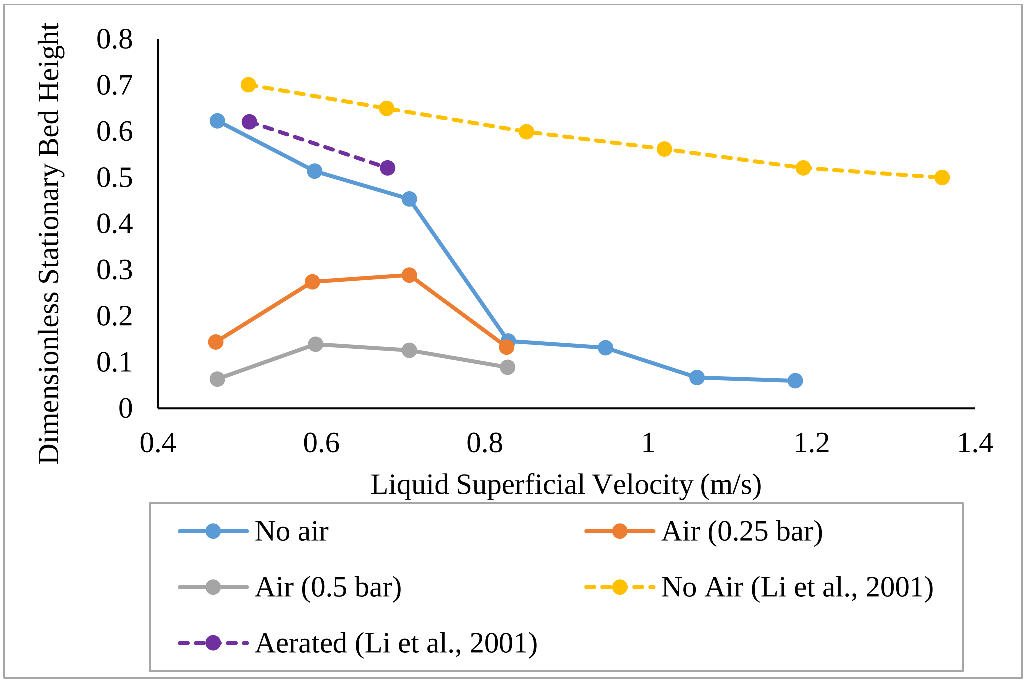

Figure 4.2. Variation of bed height for aerated water.

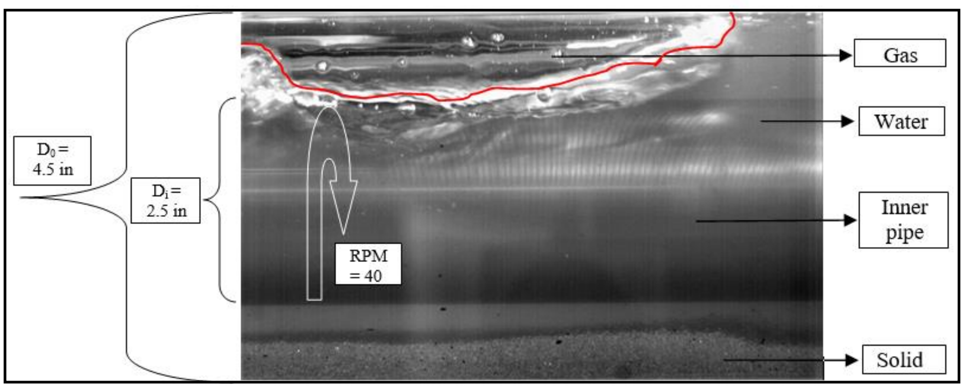

a

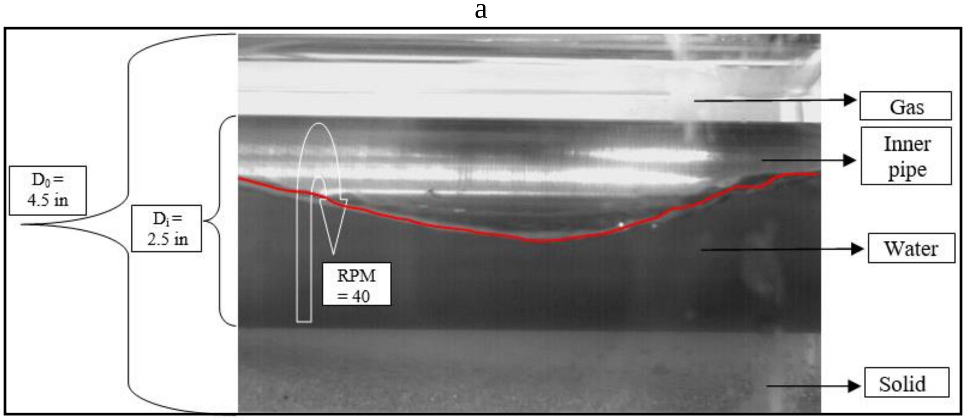

b

Figure 4.3. Impact of air injection on reduction of bed height.

For the comparison of bed height decreasing trend, we presented the result of Li et al. [10] in the Fig. 4.2 by dashed straight lines. The data from the study was not collected in a consistent manner especially among different group, therefore, should not be compared straightforward. However, the comparison of the decreasing trend is still meaningful. The trend that injecting air decrease the cuttings bed height, but the extent of this effect is less than our result. Their values, 0.5 or 0.7m/s, are far higher than ours, relatively higher superficial gas velocity might cause lower liquid hold-up in the wellbore. Reduced liquid hold-up gives rise to impose insufficient shear stress acting on cuttings. However, our findings also indicate that the injection of air causes the reduction of bed height and the images in Fig. 4.3 approve this statement. The image at the top of Fig. 4.3 shows the accumulation of solids which formed the thick bed at the bottom of the outer pipe. In that case the amount of air was less represented by a small gas pocket at the top of the gas-water interface and the corresponding gas pressure was 0.35 bar. On the other hand, image at the bottom, displays a big portion of gas at the top of the interface where the gas pressure was 0.8 bar. Moreover, the thick solid bed is converted into dispersed solids in the same image because of the increased air injection.

As cuttings enter the annulus, they move over the stationary/moving bed and start accumulating behind the bed. Also, cuttings that eroded from the bed by fluid flowing are also accumulating and create a sizeable ‘dune’ of cuttings. When increasing superficial liquid velocities, these dunes start moving as a caterpillar. These dunes consist of a large amount of cuttings, have a distinct belly shape and random length, height and occurrence interval. These phenomena extremely make the reliable measurement of bed height and hole cleaning performance. When we start measuring the stationary bed height, it gradually changed the moving dune. The result can be varied depending on which bed we choose to measure, this is one of the reasons for inconsistent results. Previous study pointed out this feature of cuttings moving behavior, when the fluid is faster than a “critical” velocity, the cuttings form dune and move on and off [18]. For reliable observation of bed height, finding the boundaries of cuttings flow pattern should be the first step. For this reason, each experiment should be conducted with smaller interval of fluid velocity in the next experiment.

4.3.2. Stationary Bed Height with Different Drill Pipe RPM

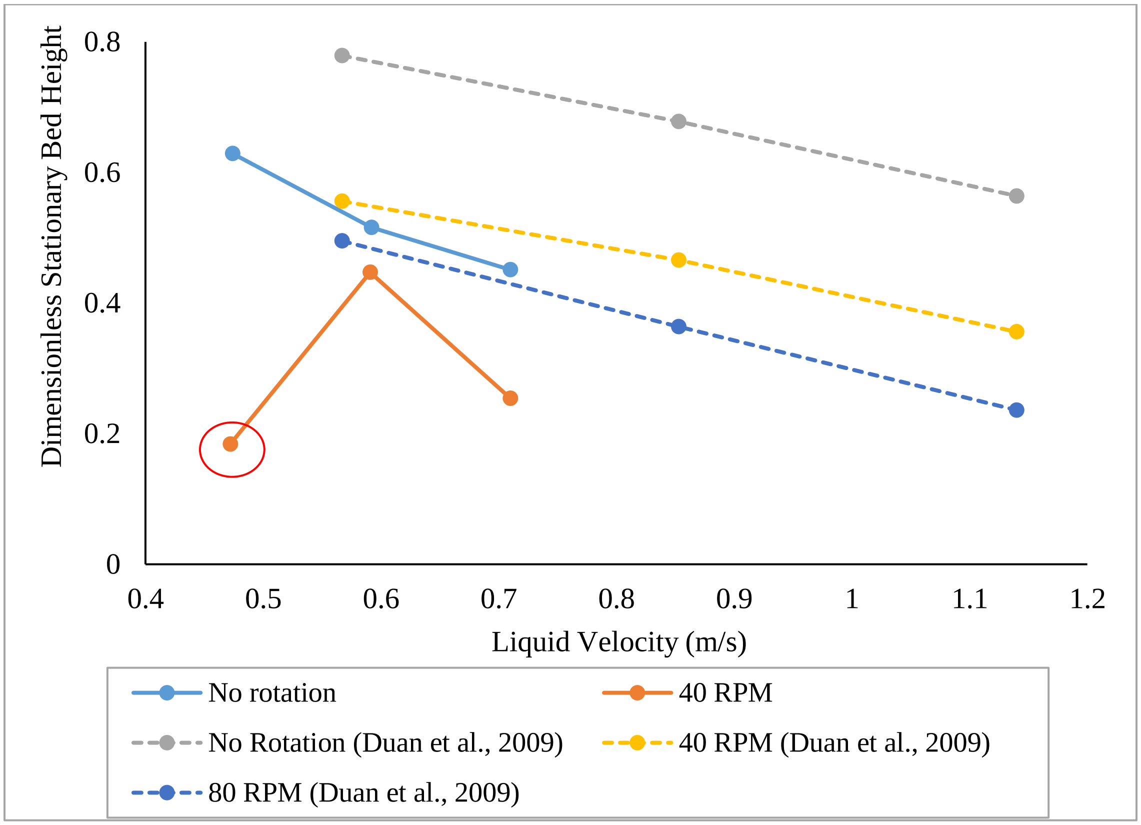

Figure 4.4. Variations of bed height for DP rotational speed.

As shown in Fig. 4.4, two solid lines indicate that DP rotation helps to reduce the bed height in spite of one outlier which was marked with the red-colored circle. The outlier is suspected for the experimental error stated in the previous section. The dashed straight lines of Fig. 4.4 also indicate that the higher RPM reduces the amount of bed height [3] which can be compared with our obtained result. It is noteworthy that the amount of reduction between 0 RPM to 40RPM is more than that from 40 to 80 RPM, further increasing pipe rotation only slightly reduces the bed height. Once the pipe is rotated, even at a low speed, a large amount of cuttings are agitated and moved up to a suspension layer. Increasing pipe rotation to 120 RPM brings more cuttings into suspension but not as many as when the pipe is rotated from 0 to 40 RPM. This explains why pipe rotation from 0 to 40 RPM makes a big difference for bed heights [3].

4.4. Conclusions

In this study, experiments have been carried out at different flow conditions and observations are made for cuttings transport in aerated water drilling. The key findings are as follows:

- Air injection significantly reduces the bed height and improves hole cleaning performance, especially in relatively low superficial liquid velocity.
- The drill pipe’s rotation can reduce the bed height by agitating the cuttings and keeping them dispersed even at low angular velocity.
- Cuttings enter into the annulus, they move over the stationary/moving bed and start accumulating as sand dune. The cuttings dune changes the shape in a random manner along with the flow.

However, these were the outcomes of the initial experiments. The future comprehensive study will focus on providing more conclusive results.

References

[1] Li, Jeff and Walker, Scott. 2001. Sensitivity analysis of hole cleaning parameters in directional wells. SPE Journal 6 (04): 356-363.

[2] Ahmed, Ramadan Mohammed and Miska, Stefan Z. 2008. Experimental Study and Modeling of Yield Power-Law Fluid Flow in Annuli with Drillpipe Rotation. Proc., IADC/SPE Drilling Conference, Orlando, Florida, USA, 4-6 March.

[3] Duan, Mingqin, Miska, Stefan Z, Yu, Mengjiao et al. 2009. Critical conditions for effective sand-sized solids transport in horizontal and high-angle wells. SPE Drilling & Completion 24 (02): 229-238.

[4] Ozbayoglu, E.M. 2010. Frictional Pressure Loss Estimation of Non-Newtonian Fluids in Realistic Annulus With Pipe Rotation. Journal of Canadian Petroleum Technology 49 (12).

[5] Zhang, Feifei, Miska, Stefan, Yu, Mengjiao et al. 2015. Pressure Profile in Annulus: Solids Play a Significant Role. Journal of Energy Resources Technology 137 (6): 064502.

[6] Vieira, P, Miska, S, Reed, T et al. 2002. Minimum air and water flow rates required for effective cuttings transport in high angle and horizontal wells. Proc., IADC/SPE drilling conference, Dallas, Texas, 26-28 February.

[7] Avila, Ricardo J, Pereira, Edgar J, Miska, Stefan Z et al. 2008. Correlations and analysis of cuttings transport with aerated fluids in deviated wells. SPE Drilling & Completion 23 (02): 132-141.

[8] Sorgun, M, Osgouei, RE, Ozbayoglu, ME et al. 2013. An experimental and numerical study of two-phase flow in horizontal eccentric annuli. Energy Sources, Part A: Recovery, Utilization, and Environmental Effects 35 (10): 891-899.

[9] Gul, Sercan, Kuru, Ergun, and Parlaktuna, Mahmut. 2017. Experimental Investigation of Cuttings Transport in Horizontal Wells Using Aerated Drilling Fluids. Proc., SPE Abu Dhabi International Petroleum Exhibition & Conference, Abu Dhabi, UAE, 13-16 November.

[10] Li, J. and Walker, S. 2001. Article. Sensitivity analysis of hole cleaning parameters in directional wells (in English). SPE Journal 6 (4): 356-363.

[11] Naganawa, Shigemi. 2002. Cuttings Transport in Directional and Horizontal Wells While Aerated Mud Drilling. Proc., IADC/SPE Asia Pacific Drilling Technology, Jakarta, Indonesia, 8-11 September.

[12] Al-lababidi, S., Yan, W., and Yeung, H. 2012. Sand Transportations and Deposition Characteristics in Multiphase Flows in Pipelines. Journal of Energy Resources Technology 134 (3): 034501.

[13] Najmi, Kamyar, Hill, Alan L., McLaury, Brenton S. et al. 2015. Experimental Study of Low Concentration Sand Transport in Multiphase Air–Water Horizontal Pipelines. Journal of Energy Resources Technology 137 (3): 032908.

[14] Ibarra, Roberto, Mohan, Ram S, and Shoham, Ovadia. 2017. Investigation of critical sand-deposition velocity in horizontal gas/liquid stratified flow. SPE Production & Operations 32 (03): 218-227.

[15] Dabirian, Ramin, Mohan, Ram, Shoham, Ovadia et al. 2018. Sand Transport in Slightly Upward Inclined Multiphase Flow. Journal of Energy Resources Technology 140 (7): 072901.

[16] Dabirian, Ramin, Padsalgikar, Ashwin, Mohan, Ram S. et al. 2018. Four-layer model for prediction of sand bed height in horizontal gas-liquid stratified flow. Journal of Petroleum Science and Engineering 165: 151-160.

[17] Ozbayoglu, M.E. 2010. Hole Cleaning Performance of Light-Weight Drilling Fluids During Horizontal Underbalanced Drilling. Journal of Canadian Petroleum Technology 49 (04).

[18] Kelessidis, VC, Bandelis, GE, and Li, J. 2007. Flow of dilute solid-liquid mixtures in horizontal concentric and eccentric annuli. Journal of Canadian Petroleum Technology 46 (05).

Chapter 5. Numerical Analysis of Cuttings Accumulation Tendency in Horizontal Annulus at Different Drilling Conditions

Golam Rasul[1], Mohammad Azizur Rahman[2], Stephen Butt[1]

Proceedings of the ASME 2021 40th International Conference on Ocean, Offshore and Arctic Engineering OMAE2021, June 21-30, 2021, Virtual, Online.

(*Presented and accepted for publication in the proceedings*)

Abstract

The influence of rotational speed and eccentricity of the drill pipe as well as the effect of fluid flow rate on the accumulation of cuttings in the horizontal annulus are the focus of this study. Computational Fluid Dynamics (CFD) is utilized to model a horizontal annulus section which conveys solid-liquid two-phase flow at different drilling conditions. In this numerical study, the Eulerian multiphase flow model has been adopted for solid-liquid characteristics analysis. Here the basic continuity and momentum equations have been considered, which have further been reduced to solve the conservation of mass and momentum equations with appropriate boundary and initial conditions. The study has considered the transient, turbulent model (k-epsilon) with no-slip conditions at pipe walls as well as velocity inlet and pressure outlet at the boundaries. The result indicates the clear impact of rotational speed on the cuttings removal process in the horizontal annulus section. As the rotational speed of the drill pipe increases, the cuttings concentration drops down significantly in the annulus section. Around 20% less accumulation is

[1]Memorial University of Newfoundland, St. John's Newfoundland and Labrador, Canada

[2]Texas A&M University at Qatar, Doha, Qatar

noticed if the drill pipe rotation is increased from 0 RPM to 120 RPM, which happens due to momentum created by the rotation that does not allow the particles to be accumulated. The eccentricity has a significant impact on solid accumulation as well. However, with increased flow rate and eccentricity, the pressure across the annulus section drops substantially. The difference in pressure drop is noticed as much as around 61 Pa/m with the flow rate change. Consequently, a higher pressure drop per length for the higher velocity of fluid implies higher pumping power consumption. The findings from this study may help to understand the optimum operating conditions for horizontal drilling. The effects of drilling conditions are identified and the complex multiphase flow in the annulus is modeled that could be extended to further related studies.

Keywords: Horizontal drilling, annulus, multiphase flow, cuttings accumulation, drill pipe rotation, eccentricity.

5.1. Introduction

Cuttings in horizontal drilling tends to form a bed instead of remaining distributed in the hole because of the gravitational effect of the solid particles. Therefore, in horizontal drilling or extended-reach well drilling, cuttings transport is considered a vital issue. The key factors that dominate the cuttings transport process include drill pipe rotational speed, diameter of the pipe, inclination angle and fluid velocity.

Due to the rotational impact of the drill pipe, the cuttings remain distributed in a non-symmetric way that reduces cuttings accumulation in the hole at medium and high fluid velocities, and once the critical value of high fluid velocity is achieved, there is no impact of drill pipe rotation [1]. Observations derived from the high-speed camera visualization and electric resistance tomography (ERT) also agreed on the positive effect of drill pipe rotation till 120 RPM on the cuttings transport process during horizontal drilling at a moderate fluid velocity range [2–5]. Moreover, finding for extended reach drilling declares the pipe rotation as one of the key factors, which improves the small cuttings transport efficiency up to twofold compared to large cuttings [6]. On the contrary, studies have reported the effect of change in RPM on the pressure drop across the annulus while confirming both increase and decrease in pressure drop with the change in rotational speed of the drill pipe [7–10].

The rotational impact of drill pipe on hole cleaning is also examined in deviated wells, where the rotational speed with orbital motion is found effective for cuttings transport [11]. The drill pipe's orbital motion may appear during the rotational speed range of 80 – 110 RPM [12]. Another study on non-Newtonian fluid confirms a significant change in frictional pressure drop in the annulus for the drill pipe’s orbital motion with increasing Reynolds number [13].

In order to find out the impact of eccentricity, sensitivity analysis on cuttings transport has been reported by experimental studies, where the cases from concentric to 75% eccentric positions were analyzed with the change of drill pipe rotational speed, ROP and fluid flow rate [14]. The analysis concluded that the cuttings tend to accumulate after a certain point of eccentricity is achieved and the impact of the drill pipe’s rotational speed is also negligible after a certain RPM. Based on the experimental findings regarding the pressure drop in the annulus section, one of the studies argued that the pressure drop may completely disappear with increasing eccentricity [15].

In this study, a numerical method is considered to determine the impact of drilling parameters, such as RPM, eccentricity, and fluid velocity on cuttings accumulation tendency in a horizontal annulus of 4.5 in. OD and 2.5 in. ID. Moreover, the overall impact of these parameters on pressure drop in the annulus is also reported. Although numerous experimental research is performed in this field, there is still room for the numerical investigation that would address these critical features of horizontal drilling with the help of CFD software.

5.2. Model and Method

5.2.1. Mathematical Equation

Computational Fluid Dynamics (CFD) is utilized to model a horizontal annulus (4.5 in. OD and 2.5 in. ID) which conveys solid-liquid two-phase flow at different drilling conditions. In this numerical study, the Eulerian-Eulerian multiphase flow model has been adopted for solid-liquid characteristics analysis. The turbulent flow inside the annulus is considered fully developed and the governing equations are as follows.

The mass conservation equation for the liquid phase is expressed as

$$\frac{\partial}{\partial t}(\alpha_l \rho_l) + \nabla .(\alpha_l \rho_l \bar{v}_l) = \Delta m_{sl} \tag{1}$$

The mass conservation equation for the solid phase is expressed as

$$\frac{\partial}{\partial t}(\alpha_s \rho_s) + \nabla .(\alpha_s \rho_s \bar{v}_s) = \Delta m_{ls} \tag{2}$$

The momentum conservation equation for the liquid phase can be expressed as

$$\frac{\partial}{\partial t}(\alpha_l \rho_l \bar{v}_l) + \nabla .(\alpha_l \rho_l \bar{v}_l \bar{v}_l) + \rho_l (2\bar{\omega} \times \bar{v}_l + \bar{\omega} \times \bar{\omega} \times \bar{r}) \\ = -\alpha_l \nabla \mathrm{P} + \mu \nabla^2 \bar{v}_l + \alpha_l \rho_l \bar{g} + K_{sl}(\bar{v}_s - \bar{v}_l) + \Delta m_{sl} \bar{v}_{sl} - \Delta m_{ls} \bar{v}_{ls} \tag{3}$$

Similarly, the momentum conservation equation for the solid phase can be expressed as

$$\frac{\partial}{\partial t}(\alpha_s \rho_s \bar{v}_s) + \nabla .(\alpha_s \rho_s \bar{v}_s \bar{v}_s) + \rho_s (2\bar{\omega} \times \bar{v}_s + \bar{\omega} \times \bar{\omega} \times \bar{r}) \\ = -\alpha_s \nabla \mathrm{P} + \mu \nabla^2 \bar{v}_s + \alpha_s \rho_s \bar{g} + K_{ls}(\bar{v}_l - \bar{v}_s) - \Delta m_{sl} \bar{v}_{sl} + \Delta m_{ls} \bar{v}_{ls} \tag{4}$$

Based on the considered Eulerian-Eulerian model, the particles and the liquid are assumed as continuous phases. The fluid and particles behaviors can be estimated by the differential equations stated above, which imply that the particles pass through the control volume, where the mass and momentum are conserved. Here, Δm_{sl} denotes the mass transfer from solid to liquid phase and the Δm_{ls} refers the mass transfer in the opposite direction. Therefore, due to the mass conservation, $\Delta m_{sl} = -\Delta m_{ls}$. α indicates the volume fraction of the corresponding phase, K_{ls} is the liquid-solid momentum interchange coefficient and in this study, $K_{ls} = K_{sl}$.

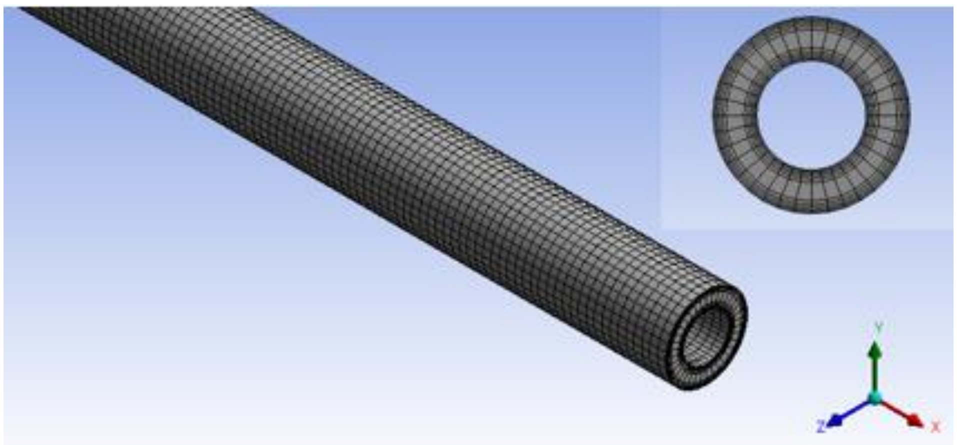

Figure 5.1. Meshed domain for the annulus.

5.2.2. Boundary Conditions and Mesh Sensitivity

The study has considered the transient, turbulent model (Realizable k-ε) with no-slip conditions at pipe walls and velocity inlet and pressure outlet at the boundaries. The solid phase is defined by 3 mm diameter silicon spheres with a density of 2600 kg/m^3 and water is considered as the liquid phase. The inlet volume fraction of the cuttings is 1.17%. To ensure that the result of the present study is independent of the mesh adopted, a mesh sensitivity analysis is carried out to investigate the threshold value of the number of the elements in which the numerical results are no longer influenced. The sensitivity analysis shows that the pressure gradient roughly gets constant when the elements number reaches at 107316. For the numerical analysis, SIMPLE algorithm from ANSYS-Fluent platform has been adopted.

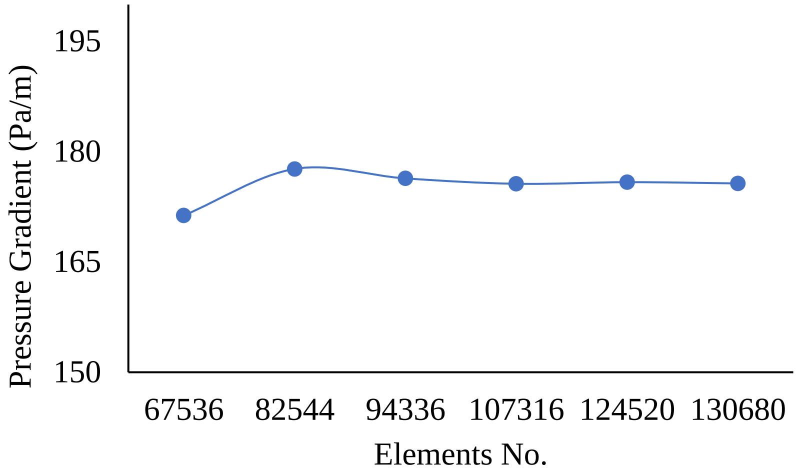

Figure 5.2. Mesh sensitivity analysis.

5.2.3. Model Validation

To validate the developed CFD model, an experimental analysis performed by Duan et al. [6] is considered, where a horizontal annulus section is experimentally tested to observe the cuttings concentration for different water velocities (0.57 m/s, 0.85 m/s and 1.14 m/s) at 0 RPM of drill pipe.

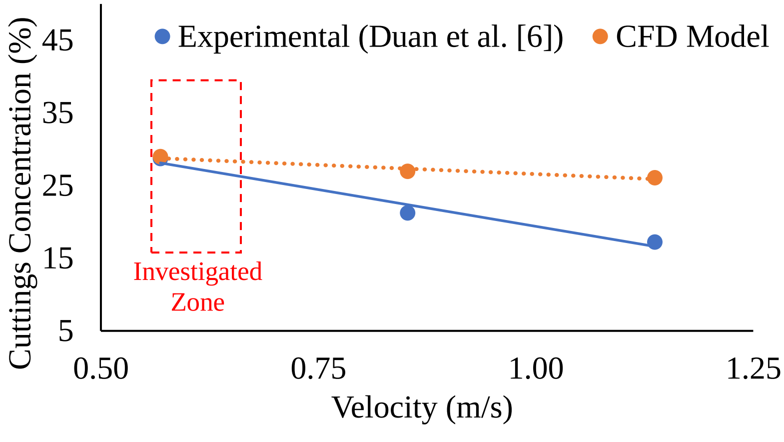

Figure 5.3. Model validation with experimental result of Duan et al. [6].

As depicted in Figure 5.3, a good agreement between the CFD model and the experimental results is clearly observed while both showing a similar decreasing trend of cuttings concentration with increasing water velocity. The results are very close at lower velocity and a substantial difference is noticed at higher velocity. The percentage of errors between the results are 1%, 27% and 52% for 0.57 m/s, 0.85 m/s and 1.14 m/s velocities, respectively. The difference occurs because the CFD model always considers assumptions for numerical solutions, unlike real experimental analysis. These assumptions may cause the deviation in the results in a significant way at higher velocity and turbulence. Moreover, any geometrical dissimilarities between the CFD and experimental model might influence the results as well. However, the investigated zone (denoted by red box in Figure 5.3) in this study is restricted between 0.55 m/s to 0.65 m/s, where the CFD model is closely following experimental results with a minimal difference. Therefore, the model satisfies the validation and provides the confidence for further study.

5.3. Results and Discussion

As the drill pipe's rotational speed increases, the cuttings concentration drops significantly in the annulus section. At any given fluid velocity, the cuttings accumulation is much less at 120 RPM than that of 0 RPM, which happens due to the momentum created by the rotation that does not allow the particles to be accumulated at the bottom of the annulus.

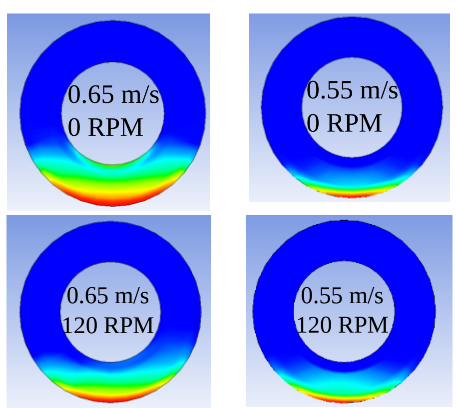

Figure 5.4. Solid volume fraction contours at different fluid velocity and rotational speed.

As shown in Figure 5.5, around 20% less accumulation is noticed if the drill pipe rotation increases from 0 RPM to 120 RPM at 0.65 m/s fluid velocity. Initially, without rotation, a big difference in concentrations is noticed for two fluid velocities. However, the gap between the concentrations minimizes with increasing RPM while both are showing a decreasing trend. It also signifies that at higher RPM of drill pipe, the effect of fluid velocity on the cuttings accumulation reduces. Here, the annulus geometry plays a vital role in the cuttings concentrations as the ratio of radius is as less as 0.56. Annulus having a higher ratio of radius may behave in a different manner with increasing fluid velocity.

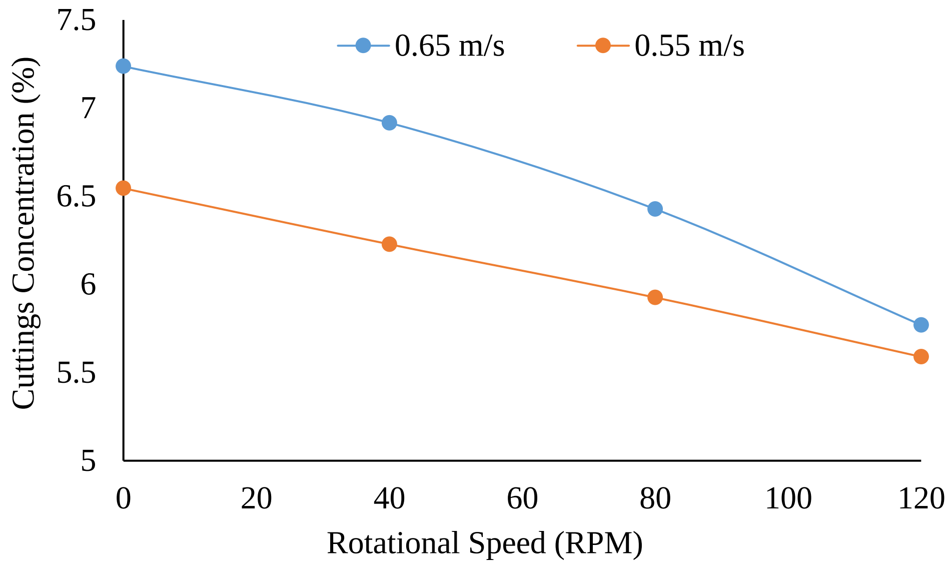

Figure 5.5. Effect of rotational speed on cuttings accumulation.

The statement is justified by the experimental results obtained from the similar annular geometry. Huque et al. (2021) illustrate with high-speed camera images that the increasing fluid velocity can cause higher amount of suspended solids in the annulus [16]. The experiments were performed in a 4.5×2.5-in annulus, which is exactly same as the developed model of current study.

However, with increased fluid velocity, the pressure across the annulus section drops substantially. The difference in pressure gradient is noticed as much as around 61 Pa/m with the flow rate change at 120 RPM. Unlike cuttings concentrations, the pressure gradients for two different fluid velocities always maintain a significant gap with increasing RPM while showing an increasing trend. A higher fluid flow rate results in a higher friction loss. In the case of turbulent flow, the friction loss is proportional to the square of fluid velocity. Consequently, a higher pressure drop per length is also obvious at higher velocity as demonstrated in Figure 5.6.

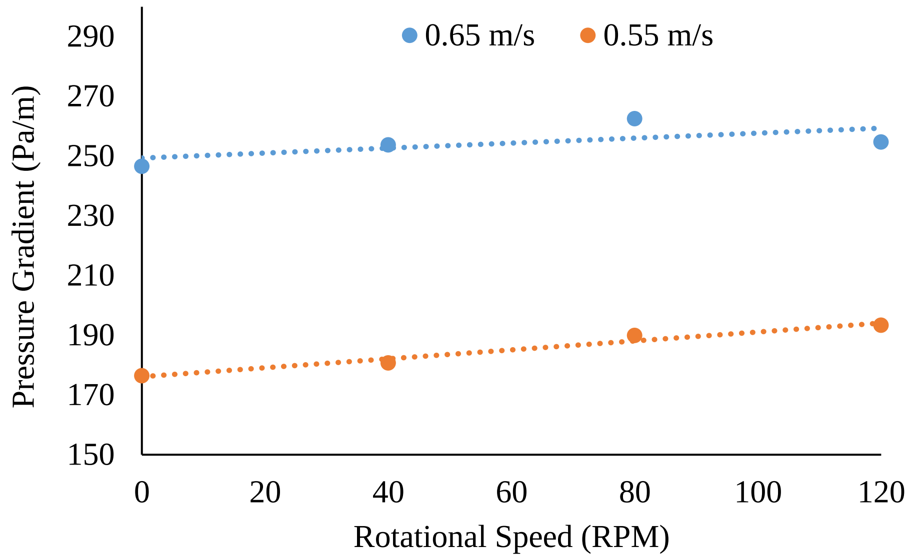

Figure 5.6. Effect of rotational speed on pressure drop.

Moreover, the agitation generated by the drill pipe rotation facilitates the turbulence of the multiphase flow in the annulus. Hence, a higher pressure gradient is observed for higher rotational speed as well. Therefore, it is prominent that RPM helps cuttings removal with a cost of higher pressure drop.

The cuttings accumulation tendency is clearly distinguishable at different eccentricities of the inner pipe in the annulus. As shown in the figure below, the concept of eccentricity is illustrated. Here, E signifies the offset from the concentric situation. E = 0.5 indicates that the inner pipe has moved halfway radially towards the outer pipe. At a specific section of the annulus, the cuttings concentration drops significantly at 0.50 eccentricity compared to 0.25. It happens because the annulus's bottom area reduces with increasing eccentricity, which results in higher flow velocity that does not allow the solids to be accumulated at the bottom region of the annulus section.

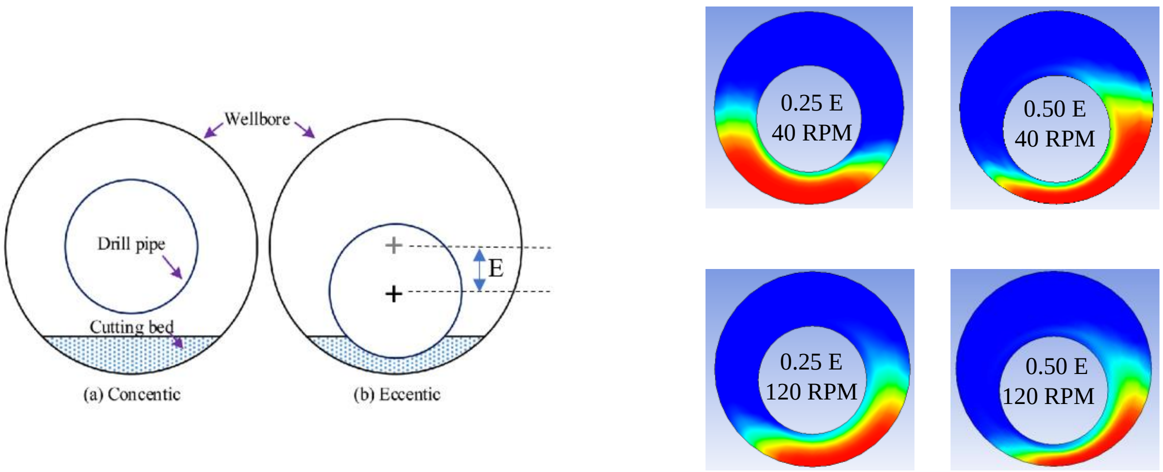

Figure 5.7. Solid volume fraction contours at different eccentricity and rotational speed.

The eccentricity becomes more effective with higher rotational speed. As shown in Figure 5.8, around 7% less cuttings accumulation occurs at higher RPM (120 RPM) and higher eccentricity (0.50) than that of lower RPM (40 RPM) and lower eccentricity (0.25) configuration.

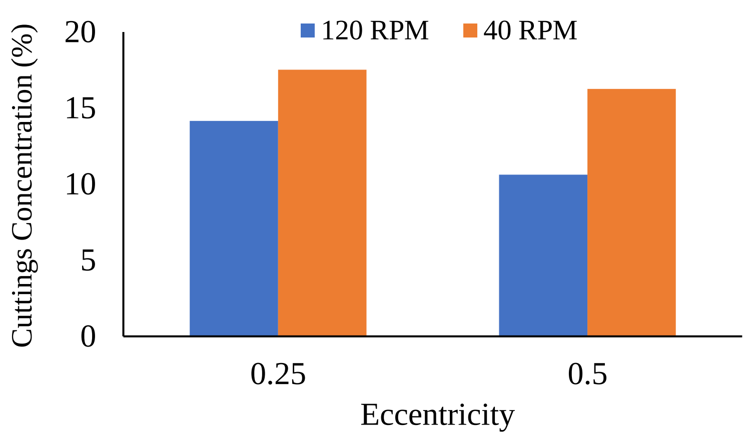

Figure 5.8. Change in cuttings concentration with eccentricity.

The change in pressure gradient with eccentricity shows different trends at different rotational speeds. As Figure 5.9 depicts, at a lower rotational speed (40 RPM), the pressure drop decreases with increasing eccentricity. However, the opposite trend is noticed at high rotational speed (120 RPM). The pressure gradient difference is detected more than 50 Pa/m at the 0.50 eccentricity for two different rotational speeds. The two-phase flow inside the annulus is influenced by the agitation generated from the rotational speed. Additionally, the high eccentricity reduces the flow area at the bottom part of the annulus. The combined effect of high rotation and high eccentricity leads to higher friction loss as well as higher pressure drop.

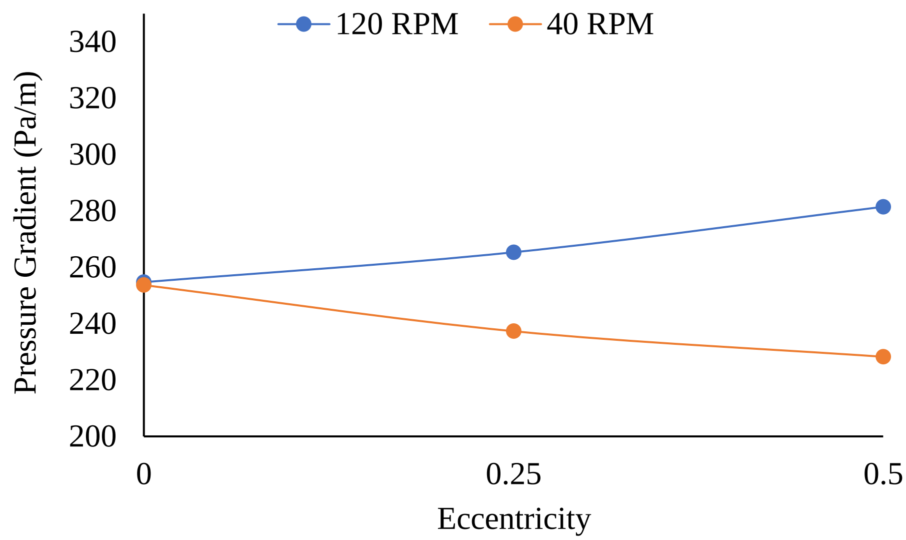

Figure 5.9. Variation in pressure drop with eccentricity.

On the contrary, low ration (40 RPM) does not deliver significant agitational impact on multiphase flow in the annulus compared to high rotation (120 RPM). Therefore, for a certain fluid velocity, the combination of high eccentricity (0.5) and high RPM (120 RPM) shows significant improvement in cuttings removal at the cost of a bigger pressure drop per unit length.

5.4. Conclusions

Based on the analyses performed in this study the summary can be drawn as

- The rotational speed of the inner pipe (drill pipe) reduces the chances of cuttings accumulation in the annulus. Increasing RPM decreases cuttings concentration.
- At higher RPM, the effect of fluid velocity is not so significant as without rotation for cuttings removal.
- Eccentricity enhancement from 0.25 to 0.5 reduces the tendency of cuttings accumulation in the annulus. However, the desired combination of high eccentricity and high RPM leads to a higher pressure drop per unit length.

This study may contribute to future numerical analysis on cuttings distribution in the annulus where the reported drilling parameters could be considered for further investigation.

References

[1] S. Akhshik, M. Behzad, and M. Rajabi, “CFD-DEM approach to investigate the effect of drill pipe rotation on cuttings transport behavior,” *J. Pet. Sci. Eng.*, 2015, doi: 10.1016/j.petrol.2015.01.017.

[2] M. F. Qureshi, M. Ali, M. A. Rahman, I. Hassan, G. Rasul, and R. Hassan, “Experimental Investigation of Multi-Phase Flow in an Annulus Using Electric Resistance Tomography,” 2019, doi: 10.2118/198011-ms.

[3] G. Rasul *et al.*, “Analysis of Cuttings Transport and Flow Pattern in Nearly Horizontal Extended Reach Well,” *J. Adv. Res. Fluid Mech. Therm. Sci.*, vol. 71, no. 2, pp. 69–86, 2020, doi: 10.37934/arfmts.71.2.6986.

[4] G. Rasul, R. Hasan, I. Hassan, S. Butt, and M. A. Rahman, “DRILLING CUTTINGS TRANSPORT IN HORIZONTAL WELLS WHILE AERATED DRILLING,” 2019, doi: 10.1615/tfec2019.emt.028527.

[5] M. F. Qureshi *et al.*, “Measuring solid cuttings transport in Newtonian fluid across horizontal annulus using electrical resistance tomography (ERT),” *Flow Meas. Instrum.*, vol. 77, no. October 2019, p. 101841, 2021, doi: 10.1016/j.flowmeasinst.2020.101841.

[6] M. Duan, S. Miska, Y. Mengjiao, N. Takach, R. Ahmed, and C. Zettner, “Transport of small cuttings in extended reach drilling,” *Int. Oil Gas Conf. Exhib. China 2006 - Sustain. Growth oil Gas*, vol. 2, pp. 800–808, 2006, doi: 10.2523/104192-ms.

[7] O. Anifowoshe and S. O. Osisanya, “The effect of equivalent diameter definitions on frictional pressure loss estimation in an annulus with pipe rotation,” in *Society of Petroleum Engineers - SPE Deepwater Drilling and Completions Conference 2012*, 2012, doi: 10.2118/151176-ms.

[8] T. N. Ofei, S. Irawan, and W. Pao, “CFD Method for Predicting Annular Pressure Losses and Cuttings Concentration in Eccentric Horizontal Wells,” *J. Pet. Eng.*, 2014, doi: 10.1155/2014/486423.

[9] E. M. Ozbayoglu and M. Sorgun, “Frictional pressure loss estimation of non-Newtonian fluids in realistic annulus with pipe rotation,” in *Journal of Canadian Petroleum Technology*, 2010, doi: 10.2118/141518-PA.

[10] M. Sorgun, “Helical flow of non-Newtonian fluids in a concentric and fully eccentric annulus,” *Energy Sources, Part A Recover. Util. Environ. Eff.*, 2012, doi: 10.1080/15567036.2011.567236.

[11] R. A. Sanchez, J. J. Azar, A. A. Bassal, and A. L. Martins, “The Effect of Drillpipe Rotation on Hole Cleaning During Directional Well Drilling,” 1997, doi: 10.2118/37626-ms.

[12] R. J. Avila, E. Pereira, S. Miska, N. E. Takach, and A. Saasen, “Correlations and analysis of cuttings transport with aerated fluids in deviated wells,” *SPE Drill. Complet.*, 2008, doi: 10.2118/87180-pa.

[13] H. Ferroudji, A. Hadjadj, M. A. Rahman, I. Hassan, T. N. Ofei, and A. Haddad, “The impact of orbital motion of drill pipe on pressure drop of non-newtonian fluids in eccentric annulus,” *J. Adv. Res. Fluid Mech. Therm. Sci.*, 2020.

[14] O. Heydari, E. Sahraei, and P. Skalle, “Investigating the impact of drillpipe’s rotation and eccentricity on cuttings transport phenomenon in various horizontal annuluses using computational fluid dynamics (CFD),” *J. Pet. Sci. Eng.*, 2017, doi: 10.1016/j.petrol.2017.06.059.

[15] M. Haciislamoglu and J. Langlinais, “Non-Newtonian Flow in Eccentric Annuli,” *J. Energy Resour. Technol. Trans. ASME*, 1990, doi: 10.1115/1.2905753.

[16] M. M. Huque, M. A. Rahman, S. Zendehboudi, S. Butt, and S. Imtiaz, “Investigation of cuttings transport in a horizontal well with high-speed visualization and electrical resistance tomography technique,” J. Nat. Gas Sci. Eng., 2021, doi: 10.1016/j.jngse.2021.103968.

Chapter 6. Tensile and Shear Fracture Examination for Optimal Drilling Performance Evaluation

Golam Rasul[1], Weizhou Quan[1], Abdelsalam Abugharara[1], Yahui Zhang[1], Mohammad Azizur Rahman[2], Stephen Butt[1]

Proceedings of 74th Canadian Geotechnical Conference, GeoNiagara 2021, Niagara Falls, ON, Canada, Sept. 26 - 29, 2021.

(Accepted for publication in the proceedings)

ABSTRACT

Rock strength is an important parameter to evaluate rotary drilling performance in the petroleum industry. It also determines the drill bit type (such as Roller Cone (RC) bit or polycrystalline diamond compact (PDC) bit) used most efficiently for maximizing the drilling rate of penetration (ROP). This research concentrates on studying multiple rock strengths and establishing correlations among them to provide necessary information that could be explored to enhance drilling performance afterward. The study was conducted by applying several strength tests, utilizing a calibrated geomechanics loading frame. The applied loads and corresponding displacements were recorded and analyzed for strength determination in all tests. Two main rock types were tested, including natural isotropic sandstone and synthetic isotropic rock like material (RLM). The strength tests that were conducted on the NQ cores included indirect tensile strength (ITS) performed on disk samples, unconfined compressive strength (UCS) performed on standard

[1]Memorial University of Newfoundland, St. John's Newfoundland and Labrador, Canada

[2]Texas A&M University at Qatar, Doha, Qatar

samples and point load strength index (PLSI) performed on core samples following axial PLSI tests. Moreover, acoustic analysis based on ultra-sound wave velocity measurement was adopted for the rock samples. The subsequent correlation between the UCS and primary wave velocity (V_P) is developed as well as strength data correlations between UCS and ITS, UCS and PLSI were constructed. Hence, fitting relationships were obtained, and a comparative study with published correlations was conducted for detailed analysis.

Keywords: Isotropic rocks, rock like material (RLM), tensile & shear strength, point load strength index, P-wave velocity.

6.1. Introduction

Evaluation of rock strength is an essential parameter for designing mining, geotechnical and petroleum engineering projects. The unconfined compressive strength (UCS) is required to evaluate several geomechanical factors that influence wellbore instability as well as sand production capability (Moos et al., 2003; Santarelli et al., 1990). The UCS of formation has been reported more influential than the mud weight or azimuth angle for drilling activity (Jaramillo, 2004). The standard method for determining the UCS has been proposed by the scientific agency, such as ASTM and this standard is followed universally for the preparation and testing of rock specimens.

However, the UCS test requires exact measurement and specimen preparation, which is a time-consuming and expensive procedure to follow. Sometimes, it is impossible to get the core specimen's desired dimension, especially in highly jointed rock masses. Therefore, the point load strength index is considered for estimating the UCS of rocks considering its simplicity and flexibility of testing specimens in both field and laboratory applications.

Since the 1970s, researchers have developed several correlations between the UCS and PLSI for different rocks. The correlation may vary depending on the textural, mineralogical factors as well as chemical composition and anisotropic behavior of the rocks (T. N. Singh et al., 2012). A group of researchers investigated different rocks and reported that the value of UCS is nearly 24 times the PLSI value (Broch & Franklin, 1972). However, for sandstones, the conversion factor may vary from 20 to 23 according to different studies (Bieniawski, 1975; Rusnak & Mark, 1999). In the case of sedimentary rock, the UCS has found 29 times of point load index (Hassani et al., 1980). In contrast, for the quartzite rock, the conversion factor is reported at 23.4 (V. K. Singh & Singh, 1993). Another study on limestone confirmed the conversion factor as much as 26.5 (Hawkins & Oivert, 1986). However, it will be inaccurate to use a single conversion factor to evaluate the UCS value from PLSI for different rock types. Therefore, a range of conversion factor of 14-16 is proposed for softer rocks and another range of 21-24 is suggested for harder rocks (T. N. Singh et al., 2012).

On the other hand, the tensile strength of the rock determines the load-bearing capability of the rock. In general, rocks tend to fail easily under tensile loading in comparison to compressive loading. The direct approach for tensile strength test is a tedious process for laboratory testing. Therefore, the indirect test of tensile strength is an acceptable and reliable approach to follow in the laboratory environment. Because of the simplicity of the experimental setup and specimen preparation, the Brazilian strength test (BTS) is broadly practiced.

The UCS and indirect tensile strength correlation is helpful to determine essential rock characteristics. This type of relationship has been utilized to report sandstone isotropy (Abugharara et al., 2019a). Several studies in finding the relation between UCS and indirect tensile strength have reported linear relationships. However, some investigations also suggested the non-linear relationships between BTS and UCS (Altindag & Guney, 2010; Nazir et al., 2013). There is a common assumption, which refers that the UCS is nearly ten times tensile strength for rocks. However, the conversion factor may vary from 4 to 10 for roadmaking rocks (Hosking, 1955). Moreover, another study has reported that the compressive strength could be up to 20 times tensile strength for granite and 15 times for sandstones (Brook, 1993).

On the other hand, ultrasonic wave velocity analysis is a well-established geo-engineering tool to evaluate dynamic rock properties. The non-destructive nature and simplicity of testing make it suitable for field and laboratory applications. The ultrasound wave analysis has been studied for sandstone characterization applied on different sample orientations (Abugharara et al., 2019b). Moreover, the circular ultrasonic wave velocity measurement approach has been adopted to investigate rock anisotropy (Abugharara et al., 2017). However, studies have confirmed the relationships between rock strength and P-wave velocity. Some of them have reported correlations between UCS and V_P (Chary et al., 2006; Çobanoğlu & Çelik, 2008; Kahraman, 2001; Minaeian & Ahangari, 2013), whereas different study also confirms the relationship between indirect tensile strength (ITS) and V_P (Khandelwal, 2013).

In this study, UCS, PLSI and ITS have been reported for two types of isotropic rocks, including sandstone and medium strength rock like material (RLM). Furthermore, the correlations between UCS and ITS, UCS and PLSI have been determined. Moreover, the dynamic rock properties have been evaluated based on standard ultrasonic wave velocity analysis. Consequently, the evaluated primary-wave (P-wave) velocity has been utilized to establish the correlation between UCS and V_P.

6.2. Experimental Equipment and Procedure

6.2.1. Geomechanics Loading Frame

The geomechanics loading frame at Drilling Technology Laboratory (DTL) has the capability of performing different strength tests, including compressive strength (both UCS and CCS) test, Indirect tensile strength (ITS) test, point load strength index (PLSI) test. The loading frame can provide a maximum of 450 KN. The corresponding linear displacement is recorded with the help of an LVDT sensor. The data acquisition (DAQ) system can record the data from all the sensors at different sampling rates. The data was recorded at 100 Hz sampling rate for all the samples tested in the loading frame in this study. Before the tests, calibration was performed to ensure the reliability of the geomechanics loading frame. Figure 6.1 shows the different parts of the geomechanics loading frame located at the DTL.

Figure 6.1. Geomechanics loading frame equipped with data acquisition (DAQ) system at DTL.

[1-Axial compression pressure piston, 2-Bottom compression plate, 3-Manual compression hydraulic pump, 4-Top fixed compression plate, 5-Control valves, 6-Safety bypass valve, 7-Hydraulic fluid reservoir, 8-Data Acquisition System (DAQ-Sys)]

6.2.2. Standard Test Procedure

Two Different types of rock: sandstones and medium strength RLM were tested for different strength tests. For each type of rock, unconfined compressive strength (UCS), indirect tensile strength (ITS), point load strength index (PLSI) and compressive and shear wave velocity (Vp and Vs) have been measured and further correlation have been developed. Standard testing procedures have been followed for each type of test. The ASTM standards for rock characterization were mainly adopted for the testing process.

6.2.2.1. UCS Test Procedure

The UCS of the rock samples was performed based on the ASTM standard (ASTM D7012-14, 2017) for 12 specimens of sandstone and medium strength RLM. The average length of the specimens was 105.32 mm and the average diameter was 47.16 mm, which ensured the height to diameter ratio (2.23:1) within the ASTM standard range of 2:1 to 2.5:1. Moreover, the specimens were ground by a grinder before the tests to ensure flat and parallel faces. As shown in Figure 6.2, the specimens were placed between the plates of the geomechanics loading frame, where the load was applied at a constant rate. Once the test is performed, the maximum load is recorded by the load sensor as the failure load, which is then used for UCS calculation according to Eq. [1].

$$\sigma_u = \frac{P}{A} \qquad [1]$$

Where, σ_u = unconfined compressive strength (MPa); P = failure load (N); A = cross-sectional area (mm^2).

Figure 6.2. Rock sample before and after UCS test.

6.2.2.2. Indirect Tensile Strength (ITS) Test Procedure

An indirect test of tensile strength is an acceptable and reliable approach to follow in a laboratory environment because of the experimental setup and specimen preparation simplicity. In this study, a total of 38 sandstone and RLM specimens were examined for the ITS test. The tested circular disk specimens had the thickness to diameter ratio between 0.29 to 0.36, which satisfies the standard range of 0.2 - 0.75 (ASTM D3967-08, 2016). As shown in Figure 6.3, the specimens were placed between the flat plates of loading frame and because of the nature of tensile fracture, the crack propagated along the diameter as soon as the highest tensile stress point was achieved. The required tensile strength is calculated by Eq. [2].

$$\sigma_t = \frac{2P}{\pi t D} \qquad [2]$$

Where, σ_t = splitting tensile strength, (MPa)

P = maximum applied load N (or lbf)

t = thickness of the specimen, mm (or in.)

D = diameter of the specimen, mm (or in.)

Figure 6.3. Rock sample before and after indirect tensile strength test.

6.2.2.3. Point Load Strength Index Test Procedure

In this current study, axial point load strength index was performed for 27 sandstone and RLM specimens. The samples maintained the length-diameter ratio between 0.5 to 0.53, within the recommended range (1/3 to 1) of the ASTM standard (ASTM D5731-16, 2016). As shown in Figure 6.4, the specimens were placed between the conical platens and the axial load was applied steadily at a constant rate. After testing, the specimens should be divided into equal pieces (Figure 6.4) to ensure the valid test according to ASTM standard. The equation that measures the uncorrected point load strength index (I_s) is

$$P = \frac{P}{D_e^2} \qquad [3]$$

P = failure load, N

D_e = Equivalent core diameter, mm and it is represented as

$D_e^2 = D^2$ for diametral core test (without penetration), mm^2, or

$D_e^2 = \frac{4A}{\pi}$, mm^2

A = WD = minimum cross-sectional area, mm^2

Figure 6.4. Rock sample before and after point load index test.

Since, the average core diameter (47.14 mm) was less than 50 mm, the size correction was applied by the below equation

$$I_{s(50)} = F \times I_s \qquad [4]$$

Therefore, the size corrected point load strength index can be evaluated by Eq. [4], which is denoted by PLSI throughout this current study.

The "size correlation factor" can be calculated as

$$F = (D_e/50)^{0.45} \qquad [5]$$

However, for the samples close to 50 mm diameter, the approximation below provides very negligible error

$$F = \sqrt{\frac{D_e}{50}} \qquad [6]$$

6.2.2.4. Ultrasonic Wave Velocity Measurement and Analysis Procedure for Rock

The measurement was performed based on the ASTM Standard (ASTM D2845-08, 2008) for laboratory determination of pulse velocities and ultrasonic elastic constants of rock. As shown in Figure 6.5, Pulse is transmitted through the rock sample by one transducer and received by the other one. The pulse and received wave are displayed in the oscilloscope screen. Both primary (P-wave) and secondary (S-wave) wave information are received at the same time. However, the primary wave or P-wave is the fastest wave that travels through the rock. The relationship between P-wave and UCS is an important aspect of this study. The P and S-wave velocities (V_P and V_S) are calculated by following equation

$$V_p = \frac{L}{T_p} \quad [7]$$

$$V_s = \frac{L}{T_s} \quad [8]$$

Where, L = Core length or pulse propagation distance, m; T_P = P-wave travel time, s; T_S = S-wave travel time, s

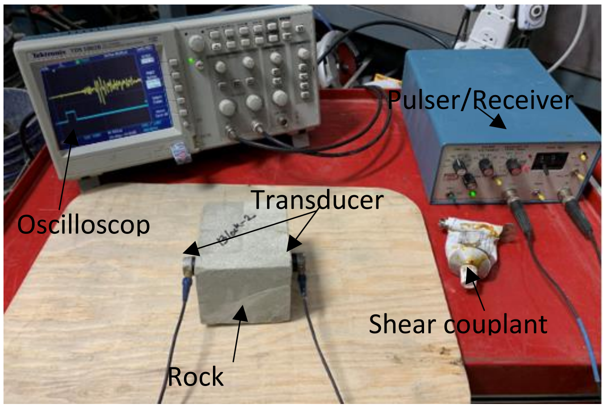

Figure 6.5. Ultrasonic wave velocity measurement setup.

Moreover, dynamic elastic constants (dynamic elastic modulus, E and Poison's ratio, μ) of rock can be evaluated form the density (ρ) and the ultrasonic wave velocities (V_P and V_S) by the following equations

$$E = [\rho v_s^2(3v_p^2 - 4v_s^2)]/(v_p^2 - v_s^2) \quad [9]$$

$$\mu = (v_p^2 - 2v_s^2)]/[2(v_p^2 - v_s^2)] \quad [10]$$

6.3. Results and Discussions

Different strength tests, including unconfined compressive strength (UCS), indirect tensile strength (ITS) and point load strength index (PLSI) have been carried out for two types of isotropic rock: sandstone and medium strength RLM. Here, all sandstone samples were collected from the same source of two big blocks of rock. They were initially cored for 6-inch samples and then all specimens for strength tests were collected from these 6-inch cylinders. However, for medium strength RLM, the same recipe and ingredients were used to cast several 6-inch cylinders, which were further cored to collect RLM specimens for the tests. The main goal was to determine the correlation between UCS and ITS and UCS and PLSI for rocks. Additionally, the acoustic measurements done for the samples provided valuable information about rock's dynamic elastic constants. The subsequent correlation between UCS and V_P is another aspect of the study. The table below provide the UCS values determined from the current study.

Table 6.1. Determined UCS values of different rock types.

Rock Type	Density (Kg/m^3)	Average core diameter (mm)	Average UCS (MPa)
Sandstone	2270	47.1	59.72
Medium Strength RLM	2300	47.2	69.30

6.3.1. Correlations for Sandstone

The data represented in the figure below shows the distribution of indirect tensile strength tests performed on sandstone samples. There were 16 samples and the average ITS value of samples was found 6.11 MPa as shown in Figure 6.6.

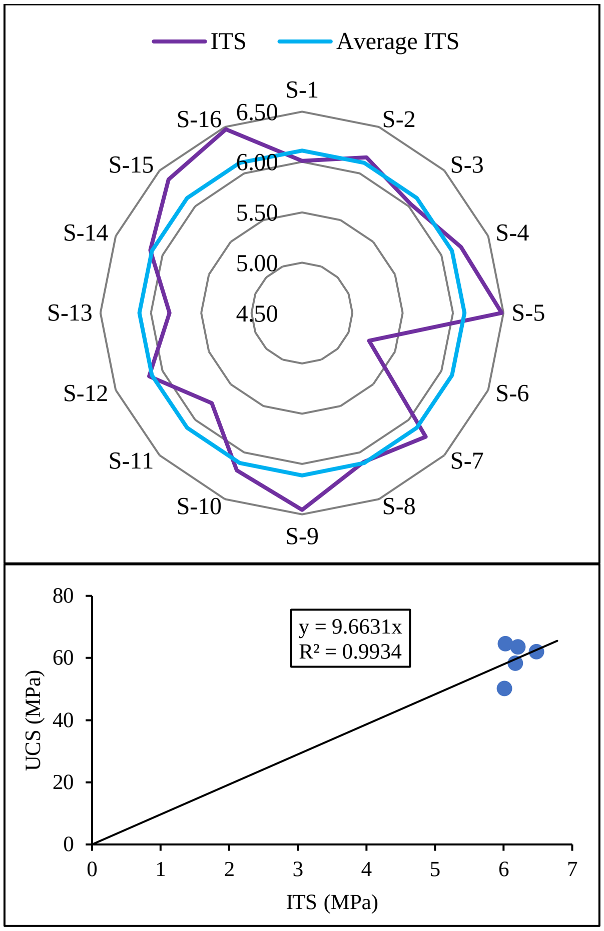

Figure 6.6. Distribution of indirect tensile strength data (top) for samples (S-1 to S-16) and correlation between UCS and ITS for sandstone (bottom).

When the UCS data is plotted against the ITS values with zero intercept, a fitted correlation of $y = 9.6631x$ is spotted with the correlation coefficient (R^2) value of 0.9934. That infers the conversion factor of 9.6631 between UCS and ITS. Hence, the evaluated value shows good agreement with the commonly considered conversion factor value of 10. In that regard, it can be said that the determined correlation behaved as per expectation.

On the other hand, the distribution of point load strength data and subsequent UCS and PLSI relationship has been developed through a fitted correlation in Figure 6.7. As depicted in the figure, the average point load strength value is 4.32 MPa. The correlation of $y = 13.652x$ is determined from a zero intercepted linear relationship with a correlation coefficient (R^2) of 0.9932.

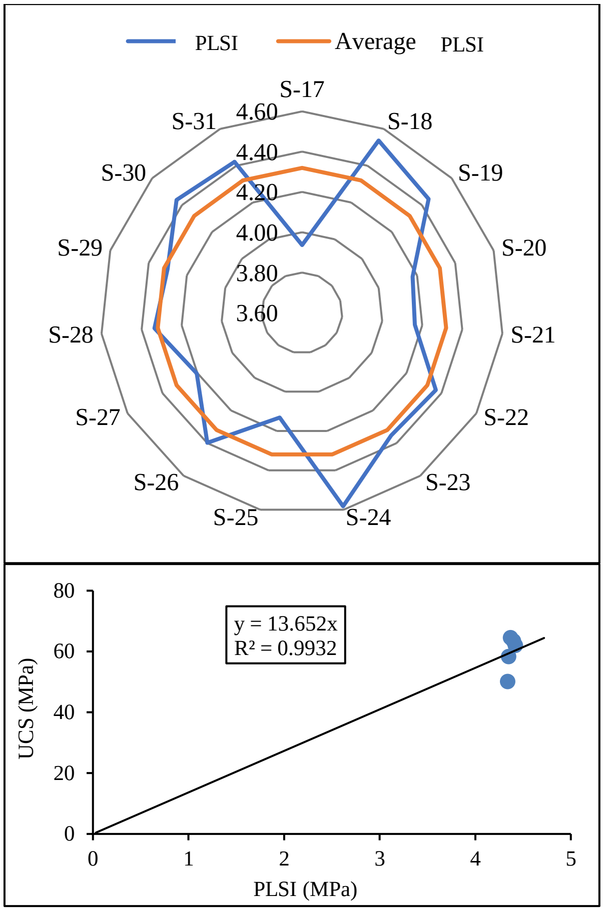

Figure 6.7. Distribution of point load index strength data (top) for samples (S-17 to S-31) and correlation between UCS and PLSI for sandstone (bottom).

Table 6.2 shows some developed relationships between UCS and PLSI for different rock samples. The reported correlation in this study is comparable with the table for having the identical linear relationship with a conversion factor of 13.652. Hence, this study can be considered as an approved method to perform indirect strength evaluation for sandstone.

Table 6.2. Correlations between UCS and point load strength index (PLSI) from different studies.

Author (Year)	Correlation	Rock Type
Smith (1997)	$UCS = 14.3 \times PLSI$	Sedimentary
Agustawijaya (2007)	$UCS = 13.4 \times PLSI$	Several
Mishra & Basu (2012)	$UCS = 14.6 \times PLSI$	Several
Vallejo et al. (1989)	$UCS = 17.4 \times PLSI$	Sandstone
Das (1985)	$UCS = 18 \times PLSI$	Sandstone

6.3.2. Correlations for Medium Strength RLM

The analysis performed on medium strength rock like material (RLM) has been represented in the figure below. Here as shown in Figure 6.8, the average tensile strength value is 6.90 MPa. On the other hand, the subsequent UCS and ITS correlation has been developed. A linear relationship with zero intercept provides the correlation of $y = 9.7624x$. This relationship indicates a conversion factor of 9.7624, comparable with the commonly assumed conversion factor, 10.

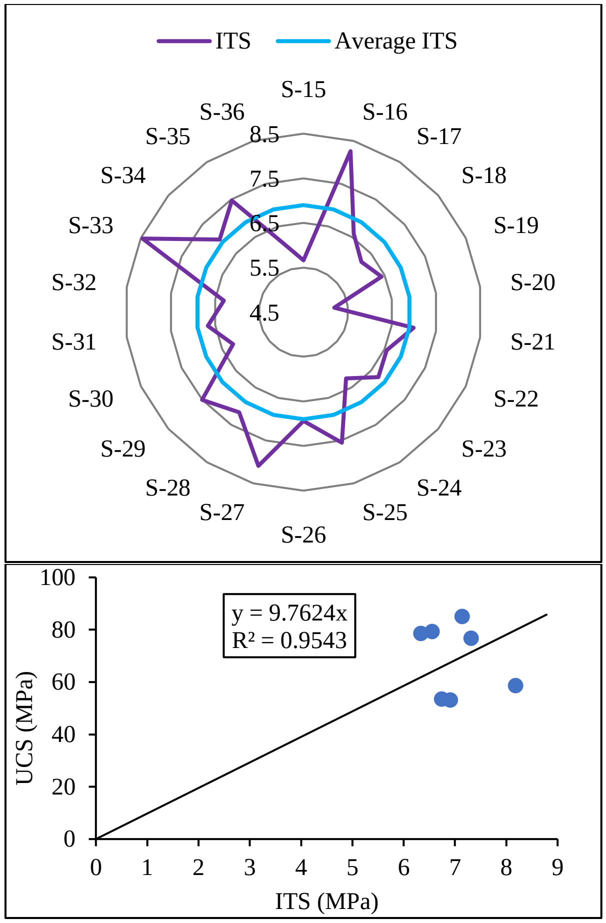

Figure 6.8. Representation of indirect tensile strength data (top) for samples (S-15 to S-36) and subsequent UCS-ITS correlation (bottom) for medium strength RLM.

The point load strength tests performed for the medium strength RLM indicate an average value of 5.79 MPa. The developed correlation between UCS and PLSI for medium strength RLM shows a fitted straight line with an R^2 value of 0.9549. From this correlation, a conversion factor of 12.273 is found between UCS and PLSI for the medium strength RLM. To date, no study has reported the correlation for medium strength RLM. Therefore, the derived correlation can be helpful to determine the strength of such rock like materials during drilling application. However, as shown in Table 6.2, equations derived from the literature offer a range of correlation factors comparable to this current study.

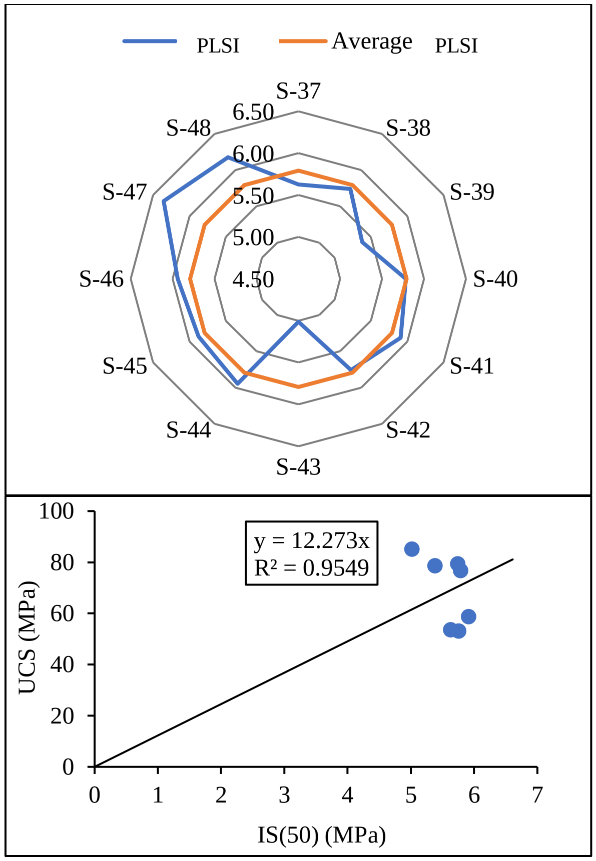

Figure 6.9. Representation of point load index data (top) for samples (S-37 to S-48) and subsequent UCS-PLSI correlation (bottom) for medium strength RLM.

6.3.3. Ultrasonic Wave Velocity Analysis for Specimens

The acoustic measurement of rock provides essential information regarding dynamic elastic properties and can be utilized for developing correlations with rock strength. Table 6.3 shows the measured elastic constants determined from the tests performed at the Drilling Technology Laboratory (DTL) for sandstone and medium strength RLM.

Table 6.3. Rocks elastic constants measured by acoustic analysis.

Rock Type	Dynamic Elastic Modulus, E (GPa)	Poison's Ratio, μ
Sandstone	23.31	0.10
Medium Strength RLM	44.98	0.21

Figures 6.10 and 6.11 depict the linear correlations between UCS and P-wave velocity for the tested rocks. However, published research on acoustic analyses for rocks concluded with different correlations, as shown in Table 6.4. The correlations vary with the rock types as well as geological origin of the rock samples.

Table 6.4. Developed correlations between UCS and P-wave velocity (V_P) reported in different studies.

Author (Year)	Correlation	Rocks
Kahraman (2001)	$UCS = 9.95V_p^{1.21}$	several
Minaeian & Ahangari (2013)	$UCS = 0.005\,Vp$	sedimentary
Chary et al. (2006)	$UCS = 0.1564Vp - 692.41$	sandstone
Çobanoğlu & Çelik (2008)	$UCS = 56.71\,Vp - 192.93$	several

In Figure 6.10, the UCS values of sandstone samples are plotted against the primary wave velocities. A fitted line plot with a correlation coefficient (R^2) of 0.9882 is determined. As it appears, the relationship between UCS and V_P is linear, having a conversion factor of 0.0179.

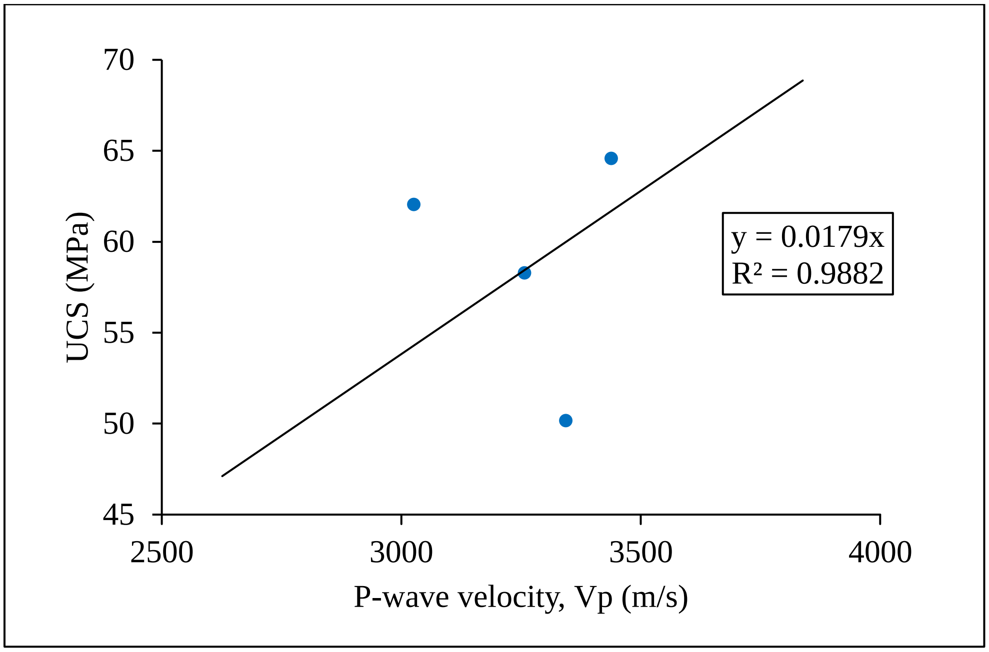

Figure 6.10. Relationship between UCS and P-wave velocity (V_P) for sandstone.

On the other hand, a similar relationship for RLM samples is demonstrated in Figure 6.11. To date, no study has reported such relationship for medium strength RLM. The evaluated correlation factor is 0.017 ensuring a correlation coefficient (R^2) of 0.9985. Hence, the derived correlation can be considered to determine the strength of such rock like materials.

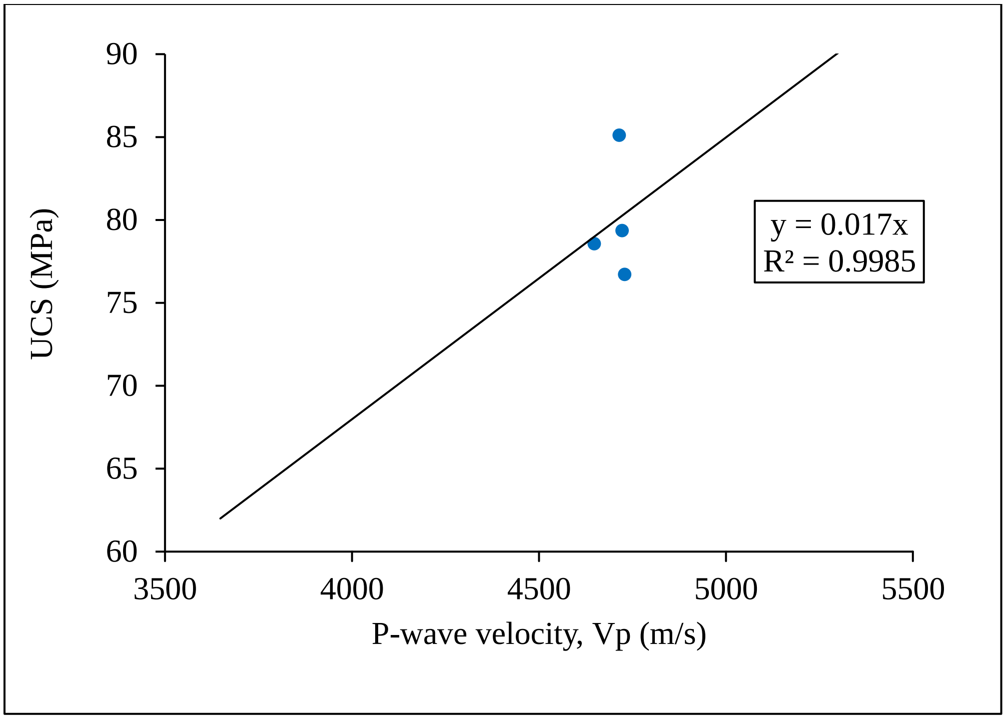

Figure 6.11. Relationship between UCS and P-wave velocity (V_P) for medium strength RLM.

Since the acoustic data can be obtained by non-destructive tests (NDT), such correlations may offer faster and easier way to evaluate rock strengths during field applications while dealing with isotropic rocks. However, a wider range of data may provide a better conclusive result.

6.4. Conclusions

This research is the first part of a comprehensive study, where several rock strengths have been reported and their mutual correlations have been determined. Moreover, the dynamic measurement through ultrasonic wave velocity measurement and subsequent correlation with rock strength have been reported. The findings can be summarized as follows:

- The indirect tensile strengths (ITS) for tested isotropic rock samples indicate an average value of 6.11 MPa for sandstone and 6.90 MPa for medium strength RLM. Moreover, in both cases, the subsequent relationships between UCS and ITS derived from fitted plots provide the confidence to utilize the correlations for future studies.
- Moreover, the average point load strength index (PLSI) value for sandstone is determined 4.32 MPa and 5.79 MPa for medium strength RLM. The fitted relationships with UCS have been developed for both cases, which may offer another way to determine rock strength from PLSI with less effort and cost-effective manner.
- The acoustic analyses for the tested samples determine the dynamic elastic constants for isotropic rock specimens. Moreover, the developed correlations between UCS and V_P can be utilized to evaluate rock strength from the acoustic measurement, which may offer a faster, cheaper and non-destructive way of rock strength analysis.

The second part, "Tensile and Shear Fracture Examination for Optimal Drilling Performance Evaluation: Part – II," is conducted by a different author (Quan et al., 2021) and is not included in this thesis. Part - II contains the drilling test and reports the drilling performance for different drill bit types (RC and PDC). However, the present study's limitations consist of lacking a variety of rock sources and a limited collection of acoustic data. Future investigations will consider these aspects to support the findings of the current study.

References

Abugharara, A. N., Hurich, C. A., Molgaard, J., & Butt, S. D. (2017). Implementation of circular wave measurements and multiple drilling parameter analysis in rock anisotropy evaluation. *Proceedings of the International Conference on Offshore Mechanics and Arctic Engineering - OMAE*. https://doi.org/10.1115/OMAE2017-62088

Abugharara, A. N., Hurich, C. A., Molgaard, J., & Butt, S. D. (2019a). Empirical Procedure Investigation For Sandstone Anisotropy Evaluation: Part I. *Canadian Geotechnical Society / GEO ST. JOHN'S-2019*.

Abugharara, A. N., Hurich, C. A., Molgaard, J., & Butt, S. D. (2019b). Empirical Procedure Investigation For Sandstone Anisotropy Evaluation: Part II. *Canadian Geotechnical Society / GEO ST. JOHN'S-2019*.

Altindag, R., & Guney, A. (2010). Predicting the relationships between brittleness and mechanical properties (UCS, TS and SH) of rocks. *Scientific Research and Essays*.

ASTM D2845-08. (2008). *Standard Test Method for Laboratory Determination of Pulse Velocities and Ultrasonic Elastic Constants of Rock*.

ASTM D3967-08. (2016). Standard Test Method for Splitting Tensile Strength of Intact Rock Core Specimens 1 D3967-08. *ASTM International, West Conshohocken, PA,*.

ASTM D5731-16. (2016). Standard Test Method for Determination of the Point Load Strength Index of Rock and Application to Rock Strength Classifications. *ASTM International, West Conshohocken, PA,*.

ASTM D7012-14. (2017). Standard test method for compressive strength and elastic moduli of intact rock core specimens under varying states of stress and temperatures. *D7012-10*.

Bieniawski, Z. T. (1975). The point-load test in geotechnical practice. *Engineering Geology*. https://doi.org/10.1016/0013-7952(75)90024-1

Broch, E., & Franklin, J. A. (1972). The point-load strength test. *International Journal of Rock Mechanics and Mining Sciences And*. https://doi.org/10.1016/0148-9062(72)90030-7

Brook, N. (1993). The measurement and estimation of basic rock strength. *Comprehensive Rock Engineering. Vol. 3*. https://doi.org/10.1016/b978-0-08-042066-0.50009-4

Chary, K. B., Sarma, L. P., Lakshmi, K. J. P., Vijayakumar, N. A., Lakshmi, V. N., & Rao, M. V. M. S. (2006). Evaluation of Engineering Properties of Rock Using Ultrasonic Pulse Velocity and Uniaxial Compressive Strength. *National Seminar on Non-Destructive Evaluation*.

Çobanoğlu, I., & Çelik, S. B. (2008). Estimation of uniaxial compressive strength from point load strength, Schmidt hardness and P-wave velocity. *Bulletin of Engineering Geology and the Environment*. https://doi.org/10.1007/s10064-008-0158-x

D. S. Agustawijaya. (2007). The Uniaxial Compressive Strength of Soft Rock. *Civil Engineering Dimension*.

Das, B. (1985). Evaluation of the Point Load Strength for Soft Rock Classification. *Proceedings of the Fourth International Conference Ground Control in Mining, Morgantown.*, WV, 220 226.

Hassani, F. P., Scoble, M. J., & Whittaker, B. N. (1980). Application of the point load index test to strength determination of rock and proposals for a new size-correction chart. *21st U.S. Symposium on Rock Mechanics, USRMS 1980*. https://doi.org/10.1016/0148-9062(81)90070-x

Hawkins, A. B., & Oivert, J. A. G. (1986). Point Load Tests: Correlation factors and contractual use. An example from the Corallian at Weymouth. *Geological Society Engineering Geology Special Publication*. https://doi.org/10.1144/GSL.1986.002.01.48

Hosking, J. R. (1955). A comparison of tensile strength, crushing strength and elastic properties of roadmaking rocks. *Quarry Man. J.*, *39*, 200–211.

Jaramillo, R. A. (2004). *Estudio geomecánico estadístico de l'estabilidad durante la perforación de pozos en el Piedemonte Llanero, campo Recetor*. Universidad Nacional de Colombia. Medellín, Colombia.

Kahraman, S. (2001). Evaluation of simple methods for assessing the uniaxial compressive strength of rock. *International Journal of Rock Mechanics and Mining Sciences*. https://doi.org/10.1016/S1365-1609(01)00039-9

Khandelwal, M. (2013). Correlating P-wave Velocity with the Physico-Mechanical Properties of Different Rocks. *Pure and Applied Geophysics*. https://doi.org/10.1007/s00024-012-0556-7

Minaeian, B., & Ahangari, K. (2013). Estimation of uniaxial compressive strength based on P-wave and Schmidt hammer rebound using statistical method. *Arabian Journal of Geosciences*. https://doi.org/10.1007/s12517-011-0460-y

Mishra, D. A., & Basu, A. (2012). Use of the block punch test to predict the compressive and tensile strengths of rocks. *International Journal of Rock Mechanics and Mining Sciences*. https://doi.org/10.1016/j.ijrmms.2012.01.016

Moos, D., Peska, P., Finkbeiner, T., & Zoback, M. (2003). Comprehensive wellbore stability analysis utilizing Quantitative Risk Assessment. *Journal of Petroleum Science and Engineering*. https://doi.org/10.1016/S0920-4105(03)00024-X

Nazir, R., Momeni, E., Armaghani, D. J., & Amin, M. F. M. (2013). Correlation between unconfined compressive strength and indirect tensile strength of limestone rock samples. *Electronic Journal of Geotechnical Engineering*.

Quan, W., Rasul, G., Abugharara, A., Rahman, M. A., Zhang, Y., & Butt, S. (2021). Tensile and Shear Fracture Examination for Optimal Drilling Performance Evaluation: Part - II. *GeoNiagara 2021, the 74th Canadian Geotechnical Conference*.

Rusnak, J., & Mark, C. (1999). Using the point load to determine the uniaxial compressive strength of coal measure rock. *18th Internationl Conference on Ground Control in Mining*.

Santarelli, F. J., Dctienne, J. L., & Zundel, J. P. (1990). Determination of the mechanical properties of deep reservoir sandstones to assess the likelyhood of sand production. *ISRM International Symposium, IS 1989*. https://doi.org/10.1016/0148-9062(90)91096-p

Singh, T. N., Kainthola, A., & Venkatesh, A. (2012). Correlation between point load index and uniaxial compressive strength for different rock types. *Rock Mechanics and Rock Engineering*. https://doi.org/10.1007/s00603-011-0192-z

Singh, V. K., & Singh, D. P. (1993). Correlation between point load index and compressive strength for quartzite rocks. *Geotechnical and Geological Engineering*. https://doi.org/10.1007/BF00466369

Smith, H. J. (1997). The point load test for weak rock in dredging applications. *International Journal of Rock Mechanics and Mining Sciences & Geomechanics Abstracts*. https://doi.org/10.1016/S1365-1609(97)00063-4

Vallejo, L. E., Welsh, R. A., & Robinson, M. K. (1989). Correlation between unconfined compressive and point load strengths for appalachian rocks. *30th U.S. Symposium on Rock Mechanics, USRMS 1989*. https://doi.org/10.1016/0148-9062(90)94915-g

Chapter 7. Conclusions and Future Recommendations

This thesis dealt with cuttings transport mechanism in the horizontal annulus and reported isotropic rock strengths analysis to investigate cuttings size distribution from rock formation properties and drilling parameters. A comprehensive analysis of the cuttings transport process, including experimental and numerical investigations, has been reported. On the other hand, isotropic rock strengths evaluation is a part of ongoing research; additional parts and future study will lead from this thesis's findings.

7.1. Cuttings Transport in Horizontal Annulus

The cuttings transport mechanism has been analyzed broadly in several chapters of the thesis containing three manuscripts out of four, including experimental and numerical assessments.

- The experimental analysis in the flow loop tried to find out the optimum drilling parameters depicting the flow regime maps at different flow conditions during the horizontal drilling process.
- The experimental findings conclude that the drilling parameters like eccentricity and rotational speed of the drill pipe facilitate the cutting transport process for different solid concentrations. The 75% eccentricity may not be the optimum drilling condition because of the contact between cuttings and the drill pipe. Due to the friction generated from the contact, the cutting transport hampers and may result in higher solid bed formation than 30% eccentricity.
- Six different flow patterns were observed during the experimental analysis. Most of the visualization results confirmed the stratified wavy pattern, whereas slug flow was observed at elevated gas pressure and rotational speed condition.

- At 30% eccentricity, the solid bed height was found to vary from 8 to 20 times at different rotational speeds for changing the solid concentration from 2 wt% to 5 wt%.
- Observations from the visualizations confirmed that the cuttings enter into the annulus, they move over the stationary/moving bed and start accumulating as sand dune. The cuttings dune changes the shape in a random manner along with the flow.
- On the other hand, the numerical assessment utilized a CFD commercial package (ANSYS-Fluent) to simulate the cuttings-fluid interaction in a suitable fluid domain. The analysis was performed after confirming mesh sensitivity and model validation.
- The numerical assessments indicate the impact of several drilling parameters, including RPM, eccentricity and fluid velocity on cuttings accumulation and report the subsequent pressure drop in the annulus section. The study concludes that efficient cuttings transport may occur at higher RPM and eccentricity; however, it comes with a price of higher pressure drop.

This study may contribute to future analysis on cuttings distribution in the annulus, where the reported drilling parameters could be considered for further investigation.

7.2. Isotropic Rock Strength Analysis

The last portion of the thesis comprises the strength tests of isotropic rocks as part of an ongoing investigation to predict cuttings size distribution from drilling performance.

- Tests are performed in a fully calibrated geomechanics frame. The UCS-ITS and UCS-PLSI correlations are developed from the collected data, representing linear relationships with reliable correlation coefficients.
- The indirect tensile strengths (ITS) for tested isotropic rock samples indicate an average value of 6.11 MPa for sandstone and 6.90 MPa for medium strength RLM. On the other hand, the PLSI value for sandstone was found 4.32 MPa and 5.79 MPa for medium strength RLM.
- The acoustic analyses for the tested samples determine the dynamic elastic constants for isotropic rock specimens. Moreover, the developed correlations between UCS and V_P can be utilized to evaluate rock strength from the acoustic measurement, offering a faster, cheaper and non-destructive way of rock strength analysis.
- Eventually, all fitted relationships have been analyzed through a comparative study with published correlations.

The second part, "Tensile and Shear Fracture Examination for Optimal Drilling Performance Evaluation: Part – II," is conducted by a different author (Quan et al., 2021) and is not included in this thesis. Part - II contains the drilling test and reports the drilling performance for different drill bit types (RC and PDC). However, the findings from the current study will play a significant role in the future evaluation of cuttings size distribution while drilling such type of rock.